Development of planar filters and diplexers for wireless transceiver front ends.

Damir Zayniyev

School of Electronics and Computer Science

DEVELOPMENT OF PLANAR FILTERS AND DIPLEXERS FOR WIRELESS TRANSCEIVER FRONT ENDS

DAMIR ZAYNIYEV

A thesis submitted in partial fulfilment of the requirements of the University of Westminster for degree of Doctor of Philosophy

May 2010

ABSTRACT

The central theme of this work is the design of compact microstrip bandpass filters and diplexers and the investigation of applications of these circuits in integrated transceiver RF front-end. The core of this thesis therefore presents the following stages of the work:

- Analysis of coupled pseudo-interdigital resonators and lines; formulation of approximate transmission zero conditions and the investigation of coupling between these two resonators and related structures.

- Development of compact, low loss and high selectivity microstrip pseudo-interdigital bandpass filters. The design procedure of the filter consists of three simple steps, starting from the design of a parallel-coupled bandpass filter using the image parameter method applied to coupled microstrip lines. The development of compact microstrip diplexers composed of these filters uses the optimized common-transformer diplexing technique. An experimental verification of the developed filters and diplexers is made.

- Investigation of the use of stepped impedance resonators (SIR) for the design of pseudo-interdigital bandpass filters with advanced characteristics. The design of compact dual-band filter using SIR. The investigation of possible improvement of the stopband of bandpass filters using bandstop generating structures. The application of SIR, defected ground structures (DGS), spur-lines, and open-circuited stubs in the design of compact bandpass filters with improved stopband.

- The application of the proposed filters and diplexers in the design of integrated antenna filters and antenna diplexers. Improvement of performance of patch antennas, such as suppression of spurious harmonics of single-band antenna and improvement of bandwidth and selectivity of dual-band antenna, as a result of integration with filters. Separation of antennas' bands and reduction of component count in integrated antenna diplexers

ACKNOWELEDGEMENTS

I would like to give my particular thanks to my director of studies, Dr. D. Budimir for his supervision, encouragement and guidelines throughout this research work. I would also like to thank my supervisor Dr. A. Tarczynski for his useful advice and support.

The financial support provided by School of Electronics and Computer Science, University of Westminster is gratefully acknowledged.

Also I would like to thank my mother Raisa and my brother Rashid for their faith in me, support and encouragement thought all four years of studying and working towards this degree.

CONTENTS

LIST OF ACRONYMS

ABCD	Transfer matrix
BPF	Bandpass filter
CAD	Computer-Aided Design
dB	Decibel
DGS	Defected ground structures
DSS	Dumbbell-shaped slot
EBG	Electromagnetic bandgap
EM	Electromagnetic
FBW	Fractional bandwidth
GHz	Gigahertz
HTS	High Temperature Superconductor
IEEE	Institute of Electrical and Electronics Engineers
IF	Intermediate frequency
IPM	Image parameter method
LCP	Liquid Crystal Polymers
LNA	Low noise amplifier
LTCC	Low-Temperature Cofired Ceramics
MEMS	Microelectromechanic Systems
MIC	Microwave Integrated Circuits
MMIC	Monolithic Microwave Integrated Circuits
PA	Power amplifier
RF	Radio frequency
SAW	Surface acoustic waves
SIR	Stepped impedance resonator
SSS	Spiral-shaped slot
TEM	Transverse electromagnetic propagation mode
TZ	Transmission zero
UIR	Uniform impedance resonator
WLAN	Wireless local area network
WiMAX	Worldwide Interoperability for Microwave Access
UWB	Ultra wide band

LIST OF FIGURES AND TABLES

Chapter 1

Chapter 2

Chapter 3

Chapter 4

Chapter 5

Chapter 6

Chapter 7

Chapter 3

1. INTRODUCTION

1.1. Filters for Wireless Applications

Electronic filters are circuits that have signal processing functions. i.e. they transform an input signal to obtain an output signal with the required characteristics. In the frequency domain filters are used to reject unwanted signal frequencies and to pass signals of desired frequencies. Filters are indispensable devices, in many systems and applications including wireless broadband, mobile, and satellite communications, radar, navigation, sensing and other systems [1-1]-[1-5]. With the development of these systems, mostly induced by great commercial interests, limited electromagnetic spectrum has to be shared among more and more systems. Thus, there is an increasing demand for RF, microwave, and millimetre wave filters with more stringent requirements. These filters are employed in various systems to select or confine signals within specified spectral limits.

Typical application of filters and variety of function performed by them can be illustrated in conventional superheterodyne transceiver. The block diagram of full-duplex superheterodyne transceiver with single conversion stage is shown in Figure 1-1 [1-6]-[1-8].

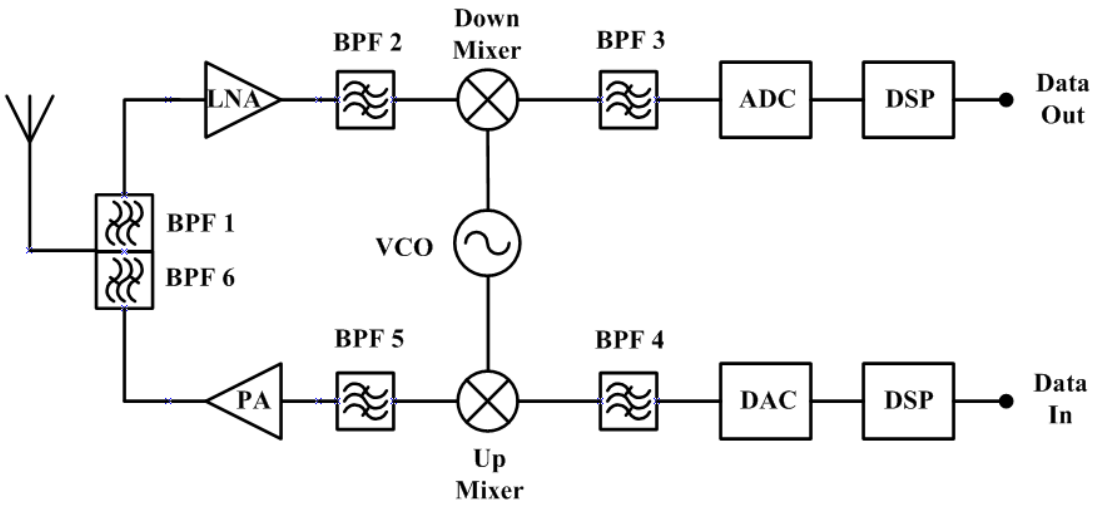

Figure 1-1: Block diagram of full-duplex superheterodyne transceiver with single conversion stage.

The block diagram of the receiver is on the top and block diagram of the transmitter is on the bottom of the scheme. Both these systems share antenna, voltage-controlled oscillator, and duplexer which consists of two bandpass filters (BPF). BPF 1 has a passband at the receiver band and it is used to select signal for the receiver and to remove interference caused by them leakage of the output signal from transmitter. It should have low insertion loss, which affects the sensitivity of receiver, and high attenuation, especially at the transmitter band. BPF 6, the second filters of duplexer, is employed to reduce spurious radiation power from transmitter. It also should attenuate noise at the receiver band. Therefore, a bandpass filter with low insertion loss and wide stopband is required. At the receiver part, BPF 2, placed after low noise amplifier (LNA), is an image rejection filter. It is used to suppress the signal at the image frequency, which after down-conversion will appear at the same intermediate frequency (IF) as the main signal and will degrade signal-to-noise ratio. The channel selection filter BPF 3 is a narrow band filter with steep attenuation which operates at IF frequency. In the transmitter part, BPF 5, is placed before power amplifier (PA) to select the required signal and to reject mixing products generated by up-converter. The baseband signal is filtered by BPF 4 before upconversion. For particular applications, the number and type of employed filters can vary, but still filters are essential components in these systems.

The advancement in the design of microwave filters was influenced by the requirements of different systems they were developed for. Mainly these are military systems, satellite communications systems, cellular communication base-stations, and cellular radio handsets [1-3]. The main frequency bands used by these and other wireless communication systems are spread throughout a wide range, from several tens of MHz to several tens of GHz. Hence a wide range of resonators and filters can be applied to these frequency bands in order to provide the most optimal solution to the various application requirements. For example at the frequencies below 1 GHz, surface acoustic wave (SAW) and helical resonators are used [1-4]. SAW filters have extremely sharp selectivity and they are used in cases when miniaturisation and low loss are required. Moreover, SAW resonators show outstanding temperature characteristics satisfying conditions for applications of narrow band filters. Helical resonator filters are used when a high level of power handling is required.

For the frequency range from RF to microwave, various types of filters are employed, including coaxial, dielectric, waveguide, and stripline/microstrip resonator filters [1-4]. Coaxial filters are very attractive filters with low insertion loss and compact size, but fabrication of these filters for high frequency bands is difficult. Dielectric resonator filters also have small size and low insertion loss. However, their application is limited by cost and complexity of the processing techniques. Waveguide filters, which have been used in this frequency range for a long time, have low insertion loss, high power capability, and practical application feasibility up to 100 GHz. The size of waveguide filters is much larger than the size of others types of filters.

Stripline/microstrip resonators and filters are commonly used in wireless communications due to their small size, low cost of production, and possibility to integrate with other lumped passive and active microwave devices. These filters can be used on wide range of frequency bands by employing various kinds of substrate materials. The main disadvantage of this type of filter is high insertion loss, due to significantly lower Q factor of stripline/microstrip resonators, compared to other types of resonators. The rapid development of microstrip and other planar filters is mainly driven by two factors. First is the recent advance of new materials and fabrications technologies, such as high-temperature superconductors (HTS), low-temperature cofired ceramics (LTCC), monolithic microwave integrated circuits (MMIC) and others. The second factor is the improvement and further development of computer-aided design (CAD) tools. Full-wave electromagnetic simulators (EM) are frequently used in the design and optimisation of novel microwave filters with advanced filtering performance [1-2].

1.2. Filters Design

The basic concept of filters was proposed in 1915 independently by Campbell and Wagner. Their results were obtained from earlier work on loaded transmission lines and classical theory of vibrating systems. Afterwards, two different filter theories were developed, known as image parameter theory and insertion loss theory [1-9], [1-10].

The image parameter method was developed in the 1920s by Campbell, Zobel, and some others. This method involves specification of the passband and stopband characteristics for a cascade of 2-port networks. The image viewpoint, used in this method is similar to the wave viewpoint used in the analysis of transmission lines. Hence, this method provides a link between practical filters and infinite periodic structures [1-11]. Simple filters can be designed without requiring a computer. However, sometimes impractical component values can be obtained using image parameter method [1-12]. This approximate technique was the only practical filter design method untill computers become widespread.

The insertion loss theory, also known as modern filter theory, is far more complex but accurate design technique. It owns its origin to the work of Cauer and Darlington who put forward a theory that involves a set of problems relating to modern network synthesis [1-13]. This design method consists of two basic steps: determination of a transfer function that approximates required filter specification and synthesis of electrical circuit using frequency response estimated by the previous transfer function. Although this method was very efficient, it had become widely used only since high-speed computers, used to make all necessary complex calculations, became widely available.

Nowadays, lowpass prototype network with angular cutoff frequency of 1 rad/s terminated by in 1-Ω impedances is normally used as a starting point in the design of microwave filters. The final design of lumped-element lowpass, bandpass, bandstop and highpass filters can be obtained from lowpass prototype using frequency and impedance transformation. Modern filter theory is expanded from lumped-element (LC) resonators to distributed resonators, such as waveguide, coaxial and

microstrip/stripline. In the design of many distributed resonator filters values of elements of lowpass prototype network are used to determine important transmission characteristic of filters using formula derived for each type of filters [1-5].

1.3. Microstrip Bandpass Filters

According to their frequency response, electronic filters are categorised into four groups: lowpass, highpass, bandpass, and bandstop filters. In wireless communications bandpass filters are the most widely used. For the design of microstrip bandpass filters, several various techniques exist and most of proposed novel filters with advanced characteristics are based on these several structures [1-2].

Combline bandpass filters consist of array of parallel resonators which are short circuited at one end with a loading capacitor at the other end [1-14]. These are very compact filters with the length of resonators equal to $\lambda_g/8$ at fundamental passband frequency f_0 and spurious response centered at about $4f_0$. Combline filters are widely implemented using coaxial resonators. The design of these filters in microstrip includes optimisation and computer aided design tools [1-15], [1-16].

Interdigital filters consist of parallel coupled quarter-wavelength lines which are short-circuited at one end and open-circuited at another end [1-17]. Interdigital filters have the first spurious harmonic at $3f_0$. Coupling between interdigital lines is stronger then between comblines and gap between resonators can be larger, making interdigital filters simpler to fabricate for high frequency and wide bandwidth applications, when dimensions of filters are quite small [1-18]. Accurate design of interdigital filters in microstrip also involves optimization techniques, such as for example aggressive space mapping optimization [1-19] or optimization that uses an accurate computer aided design method which is based on the identification of direct and parasitic coupling of each resonator [1-20].

Parallel-coupled-line filters, initially proposed for stripline [1-21], are the most popular microstrip filters. They are composed of half-wavelength resonators that are coupled to each other along half of their full length. For all types of microstrip filters in which coupling is arranged by parallel coupled lines different phase velocities between even and odd mode in coupled-line region should be taken into account. Thus, for the design of microstrip parallel-coupled-line filters, special design curves or optimization techniques are used [1-22], [1-23]. Parallel-coupled-line filters in which folded

resonators are used, are known as hairpin-line filters [1-24], [1-25], in which half-wavelength resonators have U-shaped form. The introduction of this modification substantially decreased the size of filters. Miniaturized hairpin resonators [1-26], in which arms of resonator are bent inside to form coupled lines region, are frequently used in the design of compact cross-coupled bandpass filters [1-27], [1-28].

Miniaturized hairpin resonators have some similarity with square open-loop resonators [1-29, 1-30], which are used to obtain capacitive and inductive coupling by only proximity coupling through fringing fields. This type of resonators can be used to build microstrip cascaded quadruplet and other types of cross-coupled bandpass filters. Another type of resonators and filters employed for compact size bandpass filter are dual-mode patch and ring microstrip resonators [1-31], [1-32]. Both, open-loop and dual-mode resonators have been employed in the design of a huge variety of microstrip bandpass filters.

Due to the development of wireless communications and the appearance of new systems there is high demand in small size, low cost filters with high performance. Therefore, miniaturization of bandpass filters with improvement of their characteristics is a big challenge in modern filters design. This is achieved by improvement of conventional concepts and approaches, as well as by introduction of new topologies and designs. For example, size of parallel-coupled-line filters can be reduced by bending coupled microstrip lines, while suppression of spurious harmonic [1-33] or dual-band operation is achieved by the use of SIR [1-34]. Implementation of bandstop generating spur-lines inside resonators can also result in size reduction and spurious harmonics suppression [1-35].

For miniaturized hairpin resonator filters, further size reduction with rejection of spurious harmonic has been achieved by employing either interdigital capacitors embedded in resonators [1-36], or sections with different characteristic impedances, i.e. SIR hairpin resonators [1-37]. Implementation of SIR also can be used in the design of compact dual-band hairpin resonators filters, with these resonators employed on top [1-38], as well as on both, top and ground layer [1-39].

1.4. Aims and Objectives of this Thesis.

The aims and objectives of this work are the development of compact, low cost, high performance, microstrip filters and diplexers for wireless applications.

The first aim of the work is the development of simple design procedure that can be used for design of compact, high selectivity bandpass filters. As the first objective, coupled pseudo-interdigital lines and resonators need to be analysed; approximate conditions of transmission zeros (TZs), the nature and range of coupling, and the effects of physical dimensions of resonators on both these characteristics are to be determined. The feasibility to design pseudo-interdigital bandpass filters using a procedure based on classical design approaches is then investigated, followed by an attempt to incorporate technological constraints and to achieve maximum possible improvement and miniaturization. Additionally, the possibility to design compact microstrip diplexer composed of developed filters is investigated. Different diplexing techniques and circuits need to be studied to find the most optimal way to combine bandpass filters in diplexer in order to achieve small size and high performance.

The second aim of this work is to extend and apply developed design approach in order to design bandpass filters with advanced performance, such as dual-band bandpass filters and bandpass filters with improved stopband. At first, a study of the various techniques available in literature is carried out in order to find the ones most appropriate for implementation. Then the possibility to design compact dual-band filter is investigated. Various approaches, used for the suppression of spurious harmonics and improvement of stopband, are investigated and then applied in the design of pseudo-interdigital bandpass filters with improved stopband.

Finally, integration of the designed filters and diplexers with patch antennas, as one of the applications of these circuits, is investigated. The purpose of such integration can be the suppression of spurious harmonics, the reduction of the number of elements in the RF front end, size reduction, and improvement of performance of subsystem. Single-band, multi-band, and wideband antennas can be used.

1.5. Outline of the Thesis

This thesis is organized into eight chapters.

Chapter 1 gives a brief introduction to electronic filters in wireless applications and an overview of the main types of RF/microwave filters and two main approaches in the design of filters. It briefly reviews key types of microstrip bandpass filters and a few approaches employed to achieve size reduction and improvement of performance simultaneously. It also outlines the aims and objectives of this works.

Chapter 2 provides a review of the basic theory used in the design of filters, presented in next chapters. It starts with description of main parameters of microstrip and coupled microstrip transmission lines. Then it presents analysis and physical properties of quarter- and half-wavelength microstrip transmission-line resonators. Coupling of resonators, analysed using RLC resonant circuits, is presented at the end of this chapter.

Chapter 3 focuses on the analysis of coupled microstrip pseudo-interdigital lines and resonators. Approximate TZ conditions of coupled lines are derived. These conditions describe frequencies at which transmission through coupled lines is zero, i.e. coupling between coupled pseudo-interdigital lines is zero as well. Coupling between pseudo-interdigital resonators and dependence of the coupling coefficient and transmission-zero frequencies on the main dimensions of resonators are investigated.

Chapter 4 is devoted to the development of compact pseudo-interdigital bandpass filters. Design of these filters is based on the second order microstrip parallel-coupled transmission-line-resonator filter designed using image parameter method, applied directly to coupled microstrip lines. Parallel-coupled transmission-line-resonator filter has been transformed into hairpin bandpass filter and subsequently into pseudo-interdigital bandpass filter. This is very compact bandpass filter with high selectivity improved by TZs occurred below and above the passband.

Chapter 5 presents the designs of dual-band bandpass filters and bandpass filters with improved stopband. Quarter-wavelength SIR are implemented in both kinds of filters to

control the first spurious harmonic of filters. An SIR with an impedance ratio bigger than one is used in dual-band bandpass filter designed to shift second harmonic closer to the fundamental passband, whereas SIR with impedance ratio smaller than one are used to extend the stopband of filter by pushing the second harmonic to the higher frequencies. Further improvement of stopband is achieved by generating bandstops at harmonic frequencies. Two types of circuits are used for this: spur-lines and open-circuited stubs connected in cascade with filter, and defected ground structures (DGS), etched in ground plane under the feeding line of bandpass filter. Suppression of the second and third harmonics using this approach is demonstrated.

Chapter 6 illustrates application of bandpass filters in designs of compact microstrip diplexers. Two different approaches of combining filters in diplexers are used: Y-junction and modified common-transformer diplexer. Degradation of the passband of the low frequency channel is observed when the Y-junction is used. The use of the common-transformer diplexing technique provides a very compact solution with minimal degradation of passbands of both filters. Compact diplexers designed using this technique, composed of single-band and dual-band bandpass filters, are presented.

Chapter 7 demonstrates the application of bandpass filters and diplexers in integrated antenna filters and antenna diplexers. The integration of inset-fed rectangular patch antenna with single-band bandpass filter with extended stopband is proposed to suppress the first and the second spurious harmonics of the antenna. A dual-band antenna is integrated with a dual-band filter in order to improve selectivity and bandwidth of the antenna. Diplexers are integrated with dual- and multiband antennas to reduce component count in dual-band systems. Such integration is needed for the separation of high and low bands of antennas.

Finally, chapter 8 concludes the thesis with a summary and offers recommendations for future work.

1.6. References

[1-1] R. J. Cameron, C. M. Kudsia, and R. R. Mansour, *Microwave filters for communication systems : fundamentals, design, and applications*. Hoboken, New Jersey: John Wiley & Sons, 2007

[1-2] J. G. Hong and M. J. Lancaster, *Microstrip Filters for Rf/Microwave Applications*, New York: John Wiley & Sons, 2001

[1-3] I. C. Hunter, *Theory and design of microwave filters*. London: Institution of Electrical Engineers, 2001

[1-4] M. Makimoto, S. Yamashita, *Microwave resonators and filters for wireless communication:theory, design and application.* New-York*:* Springer, 2001

[1-5] G.L. Matthaei, L. Young and E.M.T. Jones, *Microwave filters, impedance-matching networks, and coupling structures*, Dedham, MA: Arthec House 1964

[1-6] F. Ellinger, *Radio Frequency Integrated Circuits and Technologies*, Berlin: Springer, 2007

[1-7] Q. Gu, *RF System Design of Transceivers for Wireless Communications*. New-York: Springer, 2005

[1-8] M. N. S. Swamy and K.-L. Du, *Wireless Communication Systems: From RF Subsystems to 4G Enabling Technologies*, New York: Cambridge University Press, 2010

[1-9] G. C. Temes and S. K. Mitra, *Modern filter theory and design*, New York: Wiley-Interscience, 1973

[1-10] D. E. Johnson, *Introduction to filter theory,* New Jersey: Prentice Hall, 1976

[1-11] D. M. Pozar, *Microwave engineering*. 3rd edition, New York: John Wiley & Sons, 2004

[1-12] C. W. Sayre, *Complete wireless design*. New York: McGraw-Hill, 2001.

[1-13] M. E. Van Valkenburg, *Introduction to Modern Network Synthesi,* New York: John Wiley & Sons, 1960

[1-14] G. L. Matthaei, "Comb-line band-pass filters of narrow or moderate bandwidth," *Microwave J.,* vol. 6, pp. 82-91, August 1963

[1-15] H. Oraizi and N. Azadi-Tinat, "A Novel Method for the Design and Optimization of Microstrip Multi-section Bandpass Combline Filters," *36th*

European Microwave Conference, Manchester, UK, September 2006, pp.1217-1220

[1-16] A. D. Vincze, "Practical Design Approach to Microstrip Combline-Type Filters," *IEEE Trans. on Microwave Theory and Tech.,* vol.22, no.12, pp. 1171-1181, December 1974

[1-17] G. L. Matthaei, "Interdigital Band-Pass Filters," *IRE Trans. on Microwave Theory and Tech.*, vol.10, no.6, pp.479-491, November 1962

[1-18] R. Levy, R. V. Snyder, and G. Matthaei, "Design of microwave filters," *IEEE Trans. on Microwave Theory and Tech.,* vol.50, no.3, pp.783-793, March 2002

[1-19] J. W. Bandler, R. M. Biernacki, C. Shao Hua, and H. Ya Fei, "Design optimization of interdigital filters using aggressive space mapping and decomposition," *IEEE Trans. on Microwave Theory and Tech.*, vol.45, no.5, pp.761-769, May 1997

[1-20] C. Saboureau, S. Bila, D. Baillargeat, S. Verdeyme, and P. Guillon, "Accurate computer aided design of interdigital filters applying a coupling identification method," *MTT-S, Int. Microwave Symp. Dig.,* vol.3, pp.2089-2092, 2002

[1-21] S. B. Cohn, "Parallel-Coupled Transmission-Line-Resonator Filters," *IRE Trans. on Microwave Theory and Tech.,* vol. 6, no. 2, pp. 223-231, April 1958

[1-22] H. Oraizi, M. Moradian, and K. Hirasawa, "Optimum design of parallel coupled-line filters," *9th Int. Conf. on Communications Systems*, September 2004, pp.340-344

[1-23] R. A. Dell-Imagine, "A Parallel Coupled Microstrip Filter Design Procedure," *MTT-S, Int. Microwave Symp. Dig.,*vol.70, no.1, pp. 29- 32, May 1970

[1-24] E. G. Cristal and S. Frankel, "Hairpin-Line and Hybrid Hairpin-Line/Half-Wave Parallel-Coupled-Line Filters," *IEEE Trans. on Microwave Theory and Tech.,* vol. 20, no. 11, pp. 719-728, November 1972

[1-25] U. H. Gysel, "New Theory and Design for Hairpin-Line Filters," *IEEE Trans. on Microwave Theory and Tech.,* vol. 22, no. 5, pp. 523-531, May 1974

[1-26] M. Sagawa, K. Takahashi, and M. Makimoto, "Miniaturized hairpin resonator filters and their application to receiver front-end MICs," *IEEE Trans. on Microwave Theory and Tech.s,* vol. 37, no.12, pp.1991-1997, December 1989

[1-27] K. Jen-Tsai, M. Ming-Jyh, and L. Ping-Han, "A microstrip elliptic function filter with compact miniaturized hairpin resonators," *IEEE Microwave and Guided Wave Lett.,* vol.10, no.3, pp.94-95, March 2000

[1-28] D. Yingjie, P. Gardner, P. S. Hall, H. Ghafouri-Shiraz, and Z. Jiafeng, "Multiple-coupled microstrip hairpin-resonator filter," *IEEE Microwave and Wireless Components Lett.,* vol.13, no.12, pp. 532- 534, December 2003

[1-29] J. S. Hong and M. J. Lancaster, "Couplings of microstrip square open-loop resonators for cross-coupled planar microwave filters," *IEEE Trans. on Microwave Theory and Tech.,* vol. 44, no. 11, pp. 2099-2109, November 1996

[1-30] J. S. Hong and M. J. Lancaster, "Theory and experiment of novel microstrip slow-wave open-loop resonator filters," *IEEE Trans. on Microwave Theory and Tech.s,* vol.45, no.12, pp.2358-2365, December 1997

[1-31] J. A. Curtis and S. J. Fiedziuszko, "Miniature dual mode microstrip filters," *MTT-S, Int. Microwave Symp. Dig.*, vol.2, pp.443-446, July 1991

[1-32] H. Yabuki, M. Sagawa, M. Matsuo, and M. Makimoto, "Stripline dual-mode ring resonators and their application to microwave devices," *IEEE Trans. on Microwave Theory and Tech.,* vol.44, no.5, pp.723-729, May 1996

[1-33] W. Shih-Ming, C. Chun-Hsiang, H. Ming-Yu, and C. Chi-Yang, "Miniaturized spurious passband suppression microstrip filter using meandered parallel coupled lines," *IEEE Trans. o Microwave Theory and Tech.,* vol.53, no.2, pp.747-753, February 2005

[1-34] S. Sheng and Z. Lei, "Compact dual-band microstrip bandpass filter without external feeds," *IEEE Microwave and Wireless Comp. Lett.,* vol.15, no.10, pp. 644- 646, October 2005

[1-35] W. Yu-Zhen, W. Chia-An, and L. Kun-Ying, "Miniaturized Paralleled-Coupled Microstrip Bandpass Filters with Spur-Line for Multi-Spurious Suppression," *Asia-Pacific Microwave Conf.,* Bangkok, Thailand, 2007

[1-36] Z. Jiwen and F. Zhenghe, "Microstrip Interdigital Hairpin Resonator With an Optimal Physical Length," *IEEE Microwave and Wireless Comp. Lett.*, vol.16, no.12, pp.672-674, December 2006

[1-37] L. Sheng-Yuan and T. Chih-Ming, "New cross-coupled filter design using improved hairpin resonators," *IEEE Trans. on Microwave Theory and Tech.,* vol.48, no.12, pp.2482-2490, December 2000

[1-38] C. Qing-Xin and C. Fu-Chang, "A Compact Dual-Band Bandpass Filter Using Meandering Stepped Impedance Resonators," *IEEE Microwave and Wireless Comp. Lett.*, vol.18, no.5, pp.320-322, May 2008

[1-39] W. Bian, L. Chang-hong, L. Qi, and Q. Pei-yuan, "Novel Dual-Band Filter Incorporating Defected SIR and Microstrip SIR," *IEEE Microwave and Wireless Comp. Lett.,* vol.18, no.6, pp.392-394, June 2008

2. MICROSTRIP TRANSMISSION LINES AND RESONATORS

2.1. Introduction

Microstrip filters are one the most popular realizations of planar microwave filters. Proposed in 1950's as one of the planar transmission lines [2-1], microstrip become very attractive technology for building passive circuits and microwave integrated circuits (MIC) in 1960's with the advent of 99-percent pure alumina. Nowadays, many novel microstrip and other planar filters with advanced filtering characteristics are developed using novel materials and fabrication technologies such as HTS, liquid crystal polymers (LCP), LTCC, MMIC, and microelectromechanic systems (MEMS) [2-2]. These filters as well as advanced filters built using conventional Alumina or Duroid substrates are designed using novel CAD tools.

Coupled microstrip lines are employed in the design of bandpass filters based on interdigital, parallel coupled and combline structures. Using these lines stronger coupling between resonators can be achieved. This is very important in the design of bandpass filters [2-3], which are in general composed of a number of coupled resonators, tuned at a given center frequency of the passband [2-4]. For the design of bandpass filters with wider bandwidths, stronger coupling between resonators is required. In this chapter background theory for the design of microstrip bandpass filters based on the implementation of coupled lines is presented. Sections 2.2 and 2.3 present brief analysis and main characteristics of microstrip lines and coupled microstrip lines respectively. The structure and physical properties of open-circuited $\lambda_g/2$ and short-circuited $\lambda_g/4$ microstrip resonators, where λ_g is a guided wavelength, are described in section 2.4. These resonators are most frequently used in the design of microstrip bandpass filters. Analysis of coupled resonator circuits is presented in section 2.5.

2.2. Microstrip Lines

Microstrip is the most popular planar transmission structure used in MIC. Planar transmission structure is the one in which the characteristics of the circuit elements, built using this structure, can be determined by the dimensions in a single plane. This is the main requirement for a transmission line to be used in MIC. Microstrip can be fabricated using photolithographic processes. Open configuration makes it easily integrated with other discrete lumped passive and active microwave devices. Microstrip transmission lines consist of a conductor printed on top of thin, grounded dielectric substrate, as it is shown in Figure 2-1 (a). The width of the conductor w, thickness of the substrate h, and relative permittivity ε_r are the main important parameters. Thickness of the top metallic line t is much less important and often can be neglected. This is because the thickness *t* is about 10-20 μm and few electric field lines, shown in Figure 2-1 (b), start on the side planes of the top metallic line. As thickness *t* increases, the field distribution changes as more electric field lines start on the side planes of the top line and this affects the characteristic impedance Z_0 and the effective dielectric constant ε_{eff} of microstrip. From the synthesis formulas for microstrip, which consider the thickness t [2-5], it can be derived that for a microstrip with $t/h \le 0.005$, $2 \le \varepsilon_r \le 10$, and $w/h \ge 0.1$, the effect of thickness *t* on Z_0 and ε_{eff} is approximately about 1% [2-5].

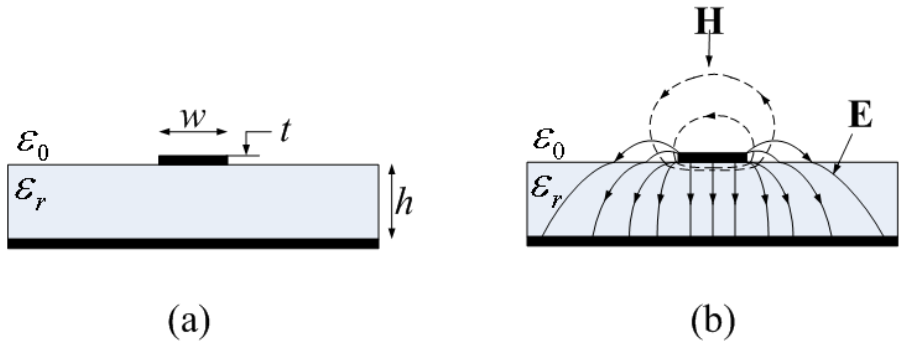

Figure 2-1: Microstrip transmission line: (a) geometry; (b) electric and magnetic field lines.

Due to the abrupt dielectric interface between the air and the substrate, microstrip lines do not support pure transverse electromagnetic (TEM) propagation mode. The

necessity of the longitude component of electric and magnetic fields can be proved using Maxwell's equations. Figure 2-1 (b) illustrates electric and magnetic fields distributions at transverse cross-sectional plane.

The analysis methods used to determine the microstrip characteristic impedance and propagation constant can be divided in two groups, quasi-static analysis methods and full wave analysis methods [2-6]. Full wave analysis methods consider a hybrid mode of propagation and provide more analytically complex and rigorous solutions. These methods show that the characteristic impedance and phase velocity of the microstrip have dispersive nature, i.e. change with frequency.

Quasi-static methods consider microstrip to have pure TEM mode of propagation. Transmission characteristics are found from two electrostatic capacitances: C_a - capacitance per unit length of microstrip line with dielectric replaced by air, and C_0 - capacitance per unit length of microstrip line with dielectric substrate. These methods provide quite accurate results for the frequency up to a few gigahertzes.

The effective dielectric constant defined as

$$\varepsilon_{eff} = \frac{C_0}{C_a} = \frac{c}{v_p} \tag{2.1}$$

where c is a free space velocity of electromagnetic waves and v_p is a phase velocity. Effective dielectric constant has a range of [2-5]

$$\frac{1}{2}(\varepsilon_r + 1) \le \varepsilon_{eff} \le \varepsilon_r \tag{2.2}$$

The effective dielectric constant is introduced in quasi-static analysis. It represents the permittivity of homogeneous medium that replaces dielectric substrate and the air in original microstrip structure. The phase constant β and the characteristic impedance Z_0 of microstrip line can be also written in terms of the distributed capacitances:

$$\beta = \beta_0\left(\frac{C_0}{C_a}\right) = \frac{\omega}{c}\left(\frac{C_0}{C_a}\right) \tag{2.3}$$

$$Z_0 = \frac{1}{\sqrt{(cC_aC_0)}} \tag{2.4}$$

Where ω is an angular frequency and β_0 is a free space phase constant. The approximate synthesis and analysis formulas for microstrip can be found in [2-6]. In modern CAD tools, such as Agilent ADS package, more accurate models presented by Hammerstad and Jensen [2-7] are used.

2.3. Coupled Microstrip Lines

Two microstrip lines placed in close proximity and parallel to each other form coupled microstrip lines. These lines are the basic building elements of directional couplers and filters. There is continuous coupling between electromagnetic fields of the lines. The field distribution of the coupled microstrip lines is shown in Figure 2-2.

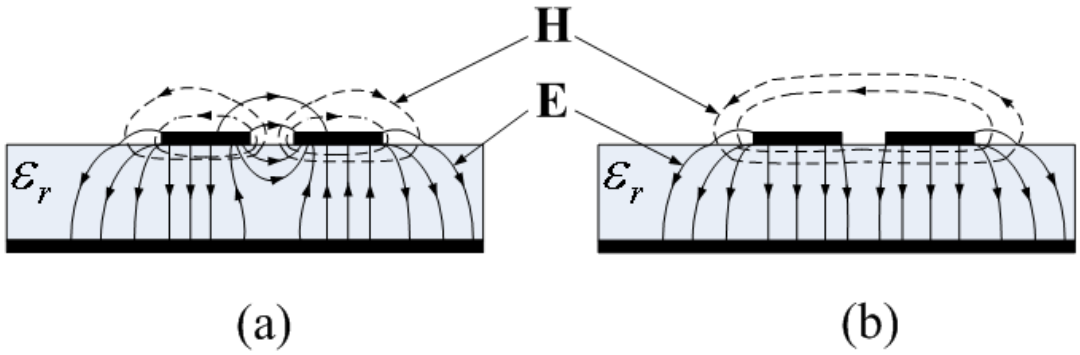

Figure 2-2: Field distribution of coupled microstrip lines: (a) odd mode; (b) even mode.

Coupled lines support two modes of propagations. Even mode exists when charges on both lines are of the same sign, odd mode when the sign is opposite. Each of these modes of propagation has different characteristics of transmission line, namely even and odd mode characteristic impedances Z_{0e} and Z_{0o}, and even and odd mode phase velocities v_{pe} and v_{po}. Even and odd mode characteristic impedances of microstrip coupled lines depends on the dielectric constant ε_r and normalised dimension s/h and w/h, where s is a width of slot of coupled microstrip lines, w is a width of lines and h is a thickness of substrate. The characteristic impedances of coupled lines with different s/h and ε_r can be found using equations presented in [2-8]. Figure 2-3 illustrates even (black solid line) and odd (black dashed line) mode characteristic impedances, which were obtained using ADS Linecalc, of coupled microstrip lines with slot width $s = 0.3$ mm, $h = 0.787$ mm and $\varepsilon_r = 2.2$. It can be seen from this figure that even mode impedance is higher than odd mode and the absolute discrepancy between them increases with the decrease of the width of the lines. Also from impedance curves for coupled lines with different s/h, presented in [2-8] can be seen that with increase

of slot width s even and odd mode impedances are approaching the curve for characteristic impedance of single microstrip line, shown with a grey solid line in Figure 2-3, even mode impedance's curve is moving down and odd mode impedance curve is moving up. It is obvious considering that with the increase of slot width the strength of coupling decreases and two microstrip lines become more and more decoupled.

The approximation $Z_0 \approx \sqrt{Z_{0e} Z_{0o}}$ widely used in the design of coupled-line directional couplers [2-9] is shown in Figure 2-3 with a grey dashed line. This approximation is not good for tight coupling. Another approximation, shown as a black dotted line in Figure 2-3 and that will be used in the analysis presented in next chapter is:

$$Z_1 \approx \frac{1}{2}\left(Z_{0e} + Z_{0o}\right) \tag{2.5}$$

Approximation (2.5) also holds better for more loosed coupling, i.e. for coupled lines with wider slot width s.

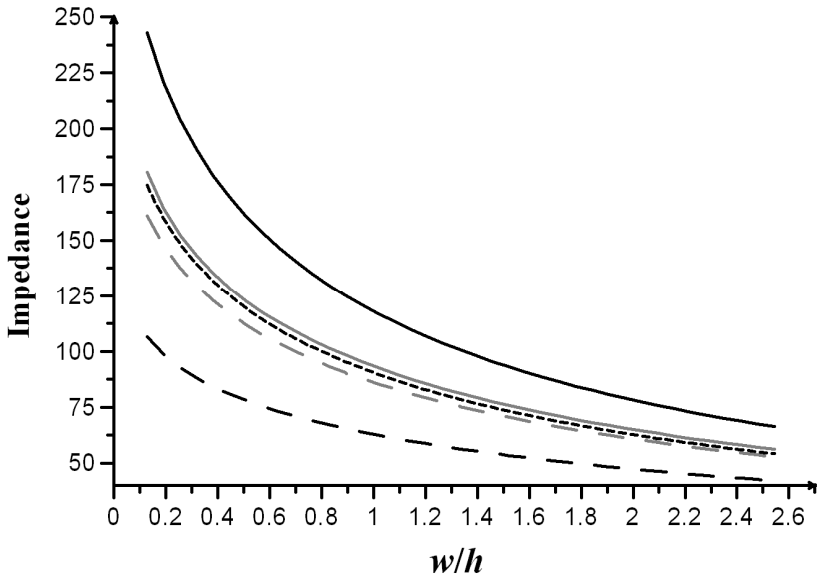

Figure 2-3: Characteristic impedances: even mode (black solid); odd mode (black dashed); single line (grey solid); arithmetic average (black dotted); geometric average(grey dashed).

The effective dielectric constants of coupled microstrip lines are not equal. The even-mode effective dielectric constant is higher than the odd mode's one because for the

odd mode the density of electric field lines in the air is higher than for the even mode, i.e. for odd mode relatively more electric field is concentrated in the air compared to even mode. The curves of modelled even and odd mode frequency dependent effective dielectric constant for RT-Duroid 5870 ($\varepsilon_r = 2.35$ and $h = 0.787$ mm) are given in [2-10]. Even and odd mode electrical lengths of coupled lines calculated using Eq. (2.6) are also different due to different effective dielectric constant ε_{eff} .

$$\theta = \frac{2\pi d f_0}{c}\sqrt{\varepsilon_{eff}} \tag{2.6}$$

However for pure TEM coupled lines, such as for example a stripline, the phase velocity of both modes of propagation is the same and the even and odd mode electrical lengths are equal. Approximation $\theta_e = \theta_o = \theta$ is often used in the analysis of coupled microstrip lines.

The difference in characteristics of modes of propagation can be easily seen in the analysis of coupled lines in terms of distributed capacitances which are shown in the Figure 2-4.The distributed capacitances are equal:

$$C_e = C_p + C_f + C'_f \tag{2.7}$$

$$C_o = C_p + C_f + C_{ga} + C_{gd} \tag{2.8}$$

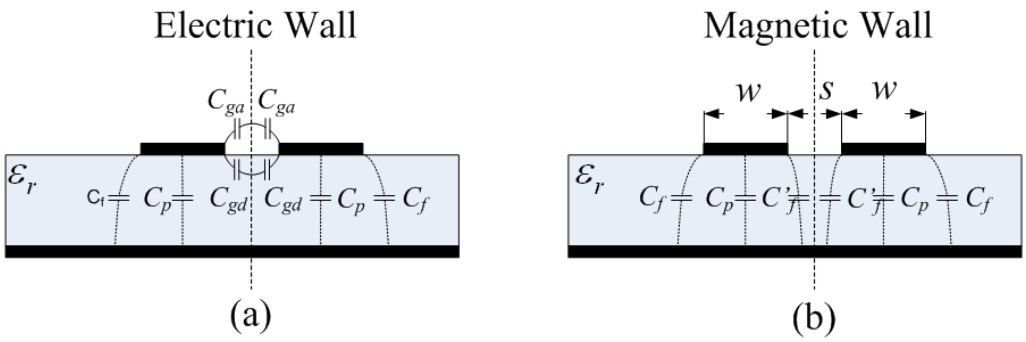

Figure 2-4: Distributed capacitances: (a) odd mode; (b) even mode.

In (2.7) and (2.8) C_p is the parallel plate capacitance between strip and the ground plane, C_f is the fringe capacitance of the outer edge which is equal to the fringe capacitance of single microstrip line, C'_f is the modified fringe capacitance of single

line due to presence of other line, C_{ga} is the capacitance of odd mode for the fringing field across the gap in air region, C_{gd} is equivalent to C_{ga} but in the dielectric region. The analytical and empirical formulas for these capacitances, obtained from dimension s/h and w/h, and ε_r were presented in [2-11]. The characteristic impedance and phase constant of each mode can be found using formulas given for single microstrip line (2.3-2.4), with even and odd mode capacitances of coupled line with dielectric present and with dielectric replaced by air should be used.

To design the coupled microstrip line i.e. to find the dimension for specified even and odd mode impedances the procedure presented in [2-12] can be used. For synthesis and analysis of microstrip coupled lines in this research, we have been suing Agilent ADS Linecalc tool in which formulas by Kirschning and Jansen [2-10] are used.

The equivalent circuit of two coupled transmission lines is shown in Figure 2-5 [2-13]. The C_1, C_2, L_1 and L_2 are self-capacitances and self-inductances of lines and L_m and C_m are mutual inductance and mutual capacitance respectively. If microstrip lines are the same size, then their self-inductances and self-capacitances are equal and their capacitive (electric) and inductive (magnetic) coupling coefficients are:

$$k_C = \frac{C_m}{\sqrt{C_1 C_2}} = \frac{C_m}{C_1} \tag{2.9}$$

$$k_L = \frac{L_m}{\sqrt{L_1 L_2}} = \frac{L_m}{L_1} \tag{2.10}$$

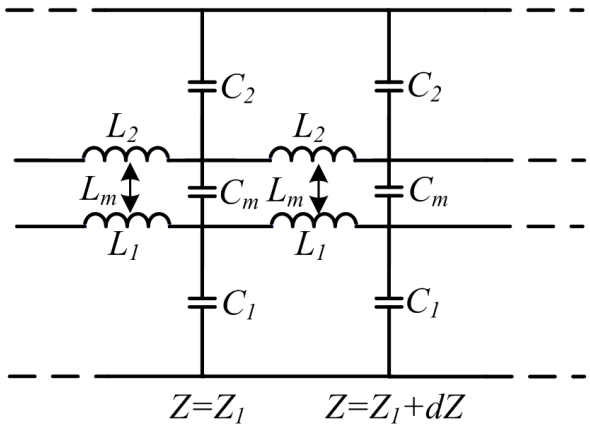

Figure 2-5: Equivalent circuit of coupled transmission lines.

In terms of even and odd mode capacitances inductive and capacitive coupling coefficients can be expressed as [2-14]:

$$k_C = \frac{C_m}{C_1} = \frac{C_o - C_e}{C_o + C_e} \tag{2.11}$$

$$k_L = \frac{L_m}{L_1} = \frac{C_o^a - C_e^a}{C_o^a + C_e^a} \tag{2.12}$$

where C_e and C_o are even and odd mode capacitances which can be found using (2.7-2.8), C_e^a and C_o^a are even and odd mode capacitances for microstrip coupled lines with substrate replaced by air.

Although Eq. (2.11-2.12) give good representation of electric and magnetic coupling coefficients in terms of even and odd mode capacitances, the expressions for these coupling coefficients as functions of physical dimensions of coupled lines are more useful for general understanding of physical properties of microstrip coupled lines. Such empirical expressions were presented in [2-15]:

$$k_C = 0.55 \exp\left[-\left(A_1\, s/h + B_1\, w/h\right)\right] \tag{2.13}$$

$$k_L = 0.55 \exp\left[-\left(A_2\, s/h + B_2\, w/h\right)\right] \tag{2.14}$$

Where A_1 and B_1 are functions of relative permittivity ε_r, A_2 and B_2 are functions of relative permeability μ_r:

$$A_1(\varepsilon_r) = 1 + \frac{1}{4}\ln\left(\frac{\varepsilon_r + 1}{2}\right) \qquad B_1(\varepsilon_r) = \frac{1}{10}\sqrt{\varepsilon_r + 1}$$

$$A_2(\mu_r) = 1 + \frac{1}{4}\ln\left(\frac{\mu_r + 1}{2}\right) \qquad B_2(\mu_r) = \frac{1}{10}\sqrt{\mu_r + 1} \tag{2.15}$$

From Eq. (2.13-2.15) it can be seen that electric coupling is stronger for substrate materials with lower dielectric constant because the electric field is much confined in the substrate closer to microstrip line with higher dielectric constant. It is clear that for microstrip transmission line magnetic coupling is larger than electric coupling due to physical properties of the substrate. Figure 2-6 illustrates electric and magnetic coupling coefficients as a function of width of the slot for fixed width of the lines,

calculated using (2.13-2.15). The electric coupling of coupled microstrip lines for substrate with dielectric constant $\varepsilon_r = 10.2$ is also included in Figure 2-6 to demonstrate the difference in electric coupling coefficients for different substrates.

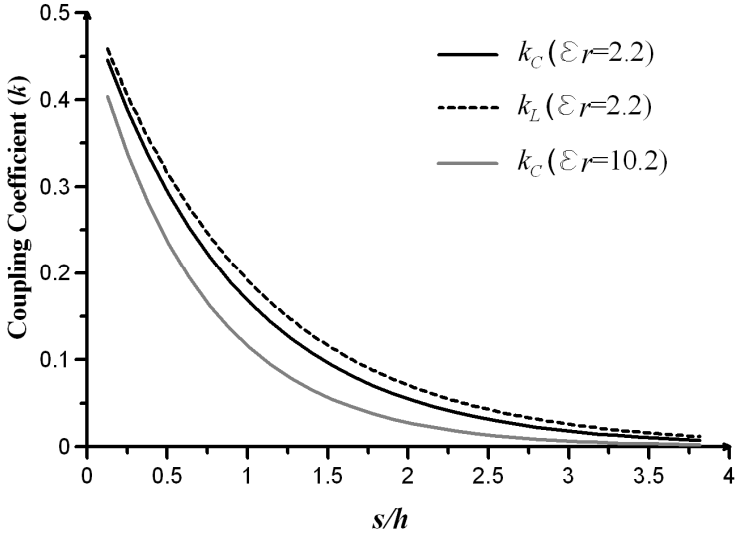

Figure 2-6: Coupling coefficients of coupled microstrip lines.

The exponential increase of the coupling coefficient with a decrease of the slot width is due to the exponential decaying nature of the fringing fields. Electric and magnetic coupling coefficients calculated using Eq. (2.13-2.15) for substrate with $h = 0.8\,\text{mm}$ and fixed slot between coupled lines $s = 0.3$ mm are shown in Figure 2-7.

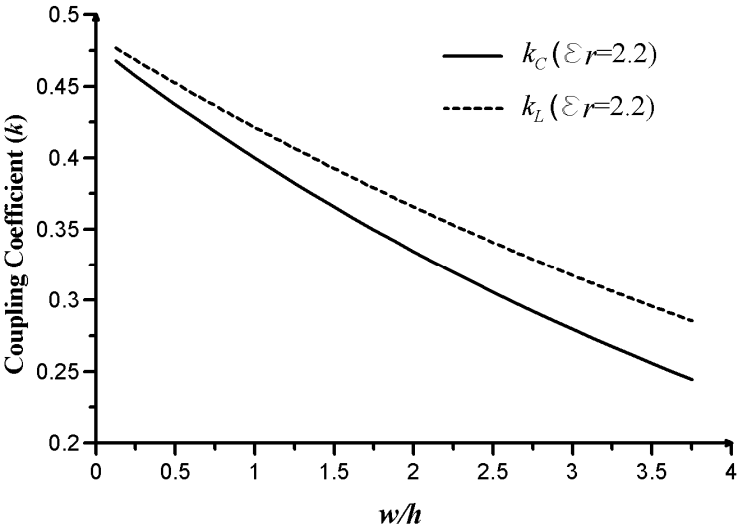

Figure 2-7: Coupling coefficients of coupled microstrip lines with fixed slot width.

the coupling coefficients are decreasing with an increase in the width of microstrip line because the fringing field is stronger for narrow microstrip lines.

2.4. Microstrip Transmission Line Resonators.

Microstrip resonators in the form of terminated transmission line are one of three big groups of distributed microstrip resonators used in the design of filters. Other two groups of distributed resonators are microstrip ring and patch resonators. Microstrip ring resonators are used for the design of dual-mode filters [2-16], [2-17], whereas patch resonators are mostly used in application where high power handling capability is required [2-18], [2-19]. While in general the microstrip resonator can be any structure that can contain at least one oscillating electromagnetic field, a section of microstrip transmission line bounded with two reflective boundaries in the form of open or short circuit becomes microwave resonator at some particular frequencies. Other types of transmission line, such as coaxial line, stripline and hollow waveguide are also used to build microwave resonators.

The input impedance and admittance of lossless open-circuited microstrip line is:

$$Z_{in} = -jZ_0 \cot \beta l = -jZ_0 \cot \theta \tag{2.16}$$

$$Y_{in} = jY_0 \tan \beta l = jY_0 \tan \theta \tag{2.17}$$

Where Z_0, Y_0 and θ are characteristic impedance, admittance, and electrical length of the line. From (2.16) it can be seen that input impedance of open-circuited line is zero when $\theta = (2n-1)\pi/2$, where $n = 1,2,3...$, or at the frequencies at which the physical length of the line l is an odd multiple of quarter wavelength or $l = (2n-1)\lambda_g/4$. Therefore in the vicinity of these frequencies open-circuited line is equivalent to the series resonant circuit, for which the resonant condition is $Z_{in} = 0$. Similarly it can be seen from (2.17) that open-circuited line is equivalent to parallel resonant circuit in the vicinity of frequencies at which the physical length of the line is a multiple of a half wavelength long, i.e. when $\theta = n\pi$, as the resonance condition of parallel resonant circuit is $Y_{in} = 0$. Microstrip $\lambda_g/2$ open-circuited line resonators are basic building blocks of bandpass filters based on the original parallel coupled line bandpass filter [20].

By analogy with the open-circuited line, the behaviour of lossless short-circuited line as a resonator can be seen from formulae for input impedance and admittance.

$$Z_{in} = Z_0 \tan \beta l = Z_0 \tan \theta \tag{2.18}$$

$$Y_{in} = -jY_0 \cot \beta l = -jY_0 \cot \theta \tag{2.19}$$

From (2.18-2.19) the short-circuited line behave as a parallel resonant circuit at frequencies when the length of the line is close to an odd multiple of quarter wavelengths and as series resonator at frequencies when the length of the line is a multiple of half wavelengths. Microstrip $\lambda_g/4$ short-circuited line resonators are used in the design of interdigital bandpass filters [2-21].

Detailed analysis and comparison of these lines with losses and the comparison with resonant circuits is presented in [2-9], [2-22]. The formulae for values of lumped elements of parallel resonator equivalent to $\lambda_g/2$ open-circuited line are:

$$R = \frac{Z_0}{\alpha l} \qquad C = \frac{\pi}{2\omega_0 Z_0} \qquad L = \frac{1}{\omega_0^2 C} \tag{2.20}$$

The values of lumped elements of parallel resonator equivalent to $\lambda_g/4$ short-circuited line are:

$$R = \frac{Z_0}{\alpha l} \qquad C = \frac{\pi}{4\omega_0 Z_0} \qquad L = \frac{1}{\omega_0^2 C} \tag{2.21}$$

In (2.20-2.21) α is the attenuation of microstrip line and ω_0 is the resonant frequency for each of the equivalent resonators.

For distributed transmission line resonators, the distribution of electric and magnetic fields at resonance is very important as it can depict the nature of fields of coupled resonators. The voltage distribution for both resonators at the resonant frequency is shown in Figure 2-8. The *y*-axe on this figure is the exited end of the line, while *l* is the end of the line, open-circuited (a), and short circuited (b). Solid lines show the

distribution at the fundamental resonance frequency of resonators, dashed lines at the first spurious resonance frequency.

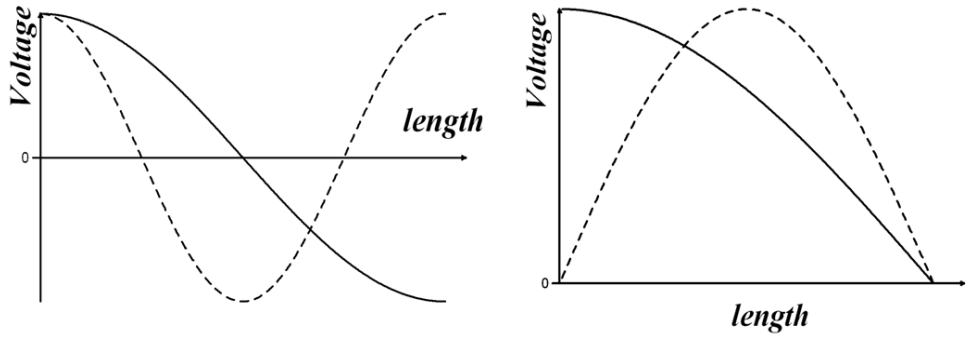

(a) (b)

Figure 2-8: Voltage distribution: (a) $\lambda_g/2$ open-circuited line; (b) $\lambda_g/4$ short-circuited line; n=1 (solid), n=2 (dashed).

Every resonator is characterised by its Q factor, which is used as measure of losses in resonant circuit and is defined as:

$$Q_u = \frac{\omega(\text{average energy stored in the resonant circuit})}{\text{energy loss per second in the rsonant circuit}} \qquad (2.22)$$

As resonant circuit does not exist by itself, it is always coupled to external circuitry, due to which the unloaded Q factor given in (2.22) becomes smaller and is called the loaded Q factor. Loaded Q factor is considered as an average energy stored in resonant circuit over total energy loss per second and can be expressed as:

$$\frac{1}{Q_L} = \frac{1}{Q_e} + \frac{1}{Q_u} \qquad (2.23)$$

Where Q_e is external quality factor, which is the ratio of the average energy stored in resonator to the energy loss per second in the external circuit.

For microstrip transmission line, the unloaded Q factor can be expressed as [2-23]:

$$\frac{1}{Q_u} = \frac{2\alpha}{\beta} = \frac{1}{Q_c} + \frac{1}{Q_d} + \frac{1}{Q_r} \qquad (2.24)$$

Where Q_c, Q_d, and Q_r are Q factors describing conductor, dielectric and radiation losses respectively. The dependence of the total Q factor of microstrip resonators on the characteristic impedance of the line is quite complex and depends also on the other parameters of the microstrip, such as the thickness and dielectric constant of the substrate. In general, the Q factor increases with an increase of characteristic impedance, till it reaches its maximum for the resonators made of the microstrip line with characteristic impedance 80-90 Ohms. With further increase of impedance Q factor's value is falling with about twice the rate as it was increasing before. the curves of the unloaded Q factors as a function of characteristic impedance of resonators made on the different thickness Alumina and Duroid substrates can be found in [2-23] .

The unloaded Q factor can be found using formulae for the transmission type measurements [2-24]:

$$Q_u = \frac{Q_L}{1-10^{S_{21}/20}} \qquad Q_L = \frac{f_0}{f_2 - f_1} \tag{2.25}$$

Where f_2 and f_1 are 3-dB frequencies, f_0 is a resonant frequency and S_{21} is a transmission coefficient in dB. Figure 2-9 illustrates the unloaded Q factor of open-circuited microstrip $\lambda_g/2$ transmission line resonator built using microstrip line with $h = 0.78$ mm and $\varepsilon_r = 2.2$. Q factor is shown in terms of characteristic impedances of microstrip line. It has been extracted using EM simulations and calculated using Eq. (2.25).

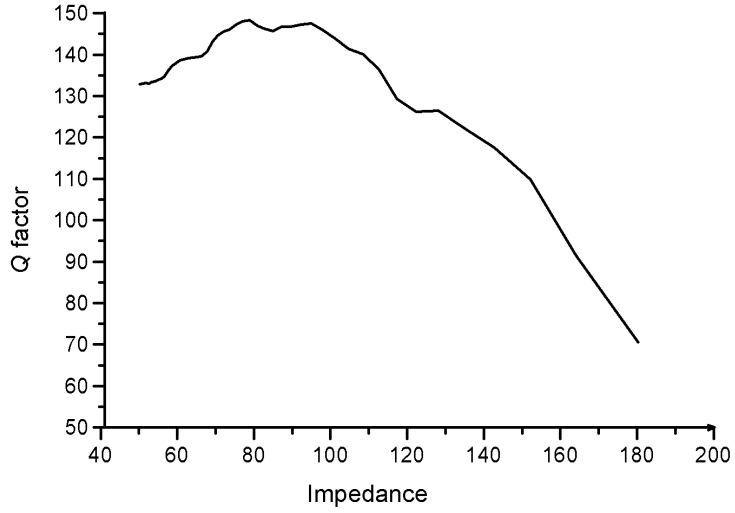

Figure 2-9: Unloaded Q factor of microstrip open-circuited $\lambda_g/2$ resonator

2.5. Coupled Resonators.

Coupling is a transfer of power from one circuit to another. Coupled resonators are very important for filter design. In the development of coupled resonator filters, the same general technique is used despite the physical structure of resonator. Coupling between two coupled resonators, whether synchronously or asynchronously tuned, is characterised by two eigen frequencies that can be indentified by experiment or full wave EM simulation. Extraction of coupling coefficients for electric, magnetic, and mixed coupling of synchronously and asynchronously tuned resonators from critical frequencies was presented in [2-25], [2-26]. The coupling coefficient of coupled microwave resonators can be defined as a ratio of coupled energy to stored energy:

$$k = \frac{\iiint \varepsilon \mathbf{E}_1 \cdot \mathbf{E}_2 dv}{\sqrt{\iiint \varepsilon |\mathbf{E}_1|^2 dv \times \iiint \varepsilon |\mathbf{E}_2|^2 dv}} + \frac{\iiint \mu \mathbf{H}_1 \cdot \mathbf{H}_2 dv}{\sqrt{\iiint \mu |\mathbf{H}_1|^2 dv \times \iiint \mu |\mathbf{H}_2|^2 dv}} \tag{2.26}$$

The $\mathbf{E}$ and $\mathbf{H}$ are vectors of electric and magnetic fields of resonators as it is shown in Figure 2-10. Fields are determined at resonance and volume integrals are over whole effective region with permittivity ε and permeability μ. The resonators 1 and 2 can have different resonance frequencies. The first term is eqn. 1 represents the electric coupling and the second term the magnetic one. The coupling coefficient can have positive or negative sign due to the dot multiplication of fields' space vectors. Negative coupling reduces the storage energy of the uncoupled resonator,

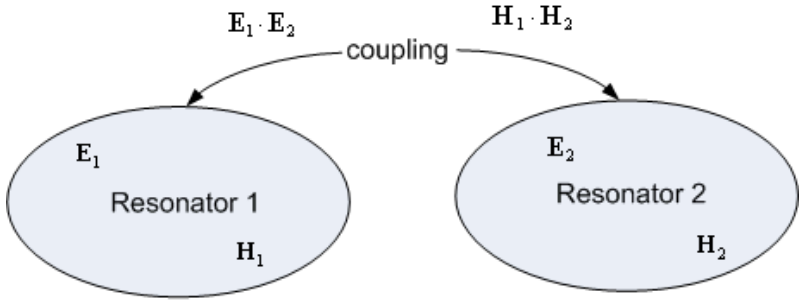

Figure 2-10: General coupled microwave resonators.

The circuits are coupled together if they have a common impedance, which can be a resistance, capacitance, or inductance [2-27]. The common capacitance produces electric coupling, whereas inductance produces magnetic coupling. Mixed coupling is a combination of both. Figure 2-11 illustrates equivalent lumped-element circuit models for magnetic coupling (a) and electric coupling (b).

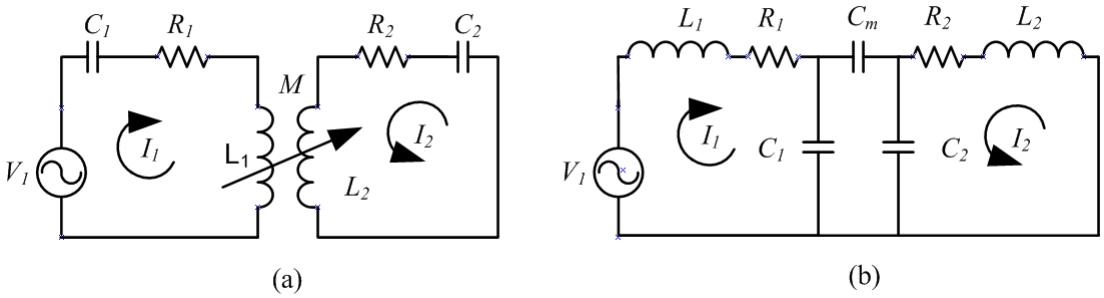

Figure 2-11: Coupled resonators: (a) magnetic coupling; (b) electric coupling.

Where C and L are self-capacitance and self-inductance of resonators, and M and C_m represent mutual inductance and capacitance.

For the circuit on Figure 2-11 (a) we have:

$$\begin{aligned} \mathbf{V}_1 &= \mathbf{I}_1\mathbf{Z}_1 + j\omega M\mathbf{I}_2 \\ 0 &= \mathbf{I}_2\mathbf{Z}_2 + j\omega M\mathbf{I}_1 \end{aligned} \tag{2.27}$$

Where $j\omega M\mathbf{I}_2$ is the voltage induced due to current in the second circuit. In the case of synchronously tuned resonators both circuits are identical and the self-impedance of the circuit is

$$\mathbf{Z}_1 = \mathbf{Z}_2 = R + j(\omega L - 1/\omega C) \tag{2.28}$$

with $R = R_1 = R_2$, $L = L_1 = L_2$, and $C = C_1 = C_2$. We can define coupling coefficient as $k = M/L = M/\sqrt{L_1 L_2}$ and from (2.28) we can get the equations for currents in both circuits:

$$\mathbf{I}_1 = \mathbf{V}_1\mathbf{Z}_2/\left(\mathbf{Z}_1\mathbf{Z}_2 + \omega^2 k^2 L^2\right) \qquad \mathbf{I}_2 = -j\omega kL\,\mathbf{V}_1/\left(\mathbf{Z}_1\mathbf{Z}_2 + \omega^2 k^2 L^2\right) \tag{2.29}$$

At the resonance frequency $\omega_0 = 1/\sqrt{LC}$ currents in the both circuits are:

$$\mathbf{I}_1 = \mathbf{V}_1 R/\left(R^2 + \omega_0{}^2 k^2 L^2\right) \qquad \mathbf{I}_2 = -j\omega k L\,\mathbf{V}_1/\left(R^2 + \omega_0{}^2 k^2 L^2\right) \tag{2.30}$$

As the coupling coefficient becomes smaller the $\mathbf{I}_1$ increases continually, whereas $\mathbf{I}_2$ initially increases and then falls after reaching its maximum value $\mathbf{I}_2 = -\mathbf{V}_1/2R$ when $k = R/(\omega_0 L) = 1/Q$, where $Q = \omega_0 L/R$ is a quality factor of resonator.

At frequency near ω_0 we can introduce new variable $d\omega = \omega - \omega_0$, the reactance of the resonator circuits can be expressed with high accuracy as:

$$(\omega L - 1/\omega C) = \omega_0 L\left(\omega/\omega_0 - \omega_0/\omega\right) \approx 2Ld\omega \tag{2.31}$$

As it assumed in [2-28] and the currents in resonators are:

$$\mathbf{I}_1 = \frac{\mathbf{V}_1\left(R + j2Ld\omega\right)}{\left(R + j2Ld\omega\right)^2 + \omega_0{}^2 k^2 L^2} \qquad \mathbf{I}_2 = \frac{-j\omega_0 k L\mathbf{V}_1}{\left(R + j2Ld\omega\right)^2 + \omega_0{}^2 k^2 L^2} \tag{2.32}$$

The maxima and minima for currents can be found by differentiating and equating to zero the moduli of currents using $d\omega$ as a variable. Three values for the frequencies of the maxima and minima of the current $\mathbf{I}_2$ are:

$$d\omega = 0 \quad \text{and} \qquad d\omega = \pm\frac{\omega}{2Q}\sqrt{\left[(kQ)^2 - 1\right]} \tag{2.33}$$

If in (2.33) $kQ > 1$ there are three real roots and $d\omega = 0$ is a minimum and other two roots are maxima. This is a tight coupling case and resonators are said to be overcoupled. Tight coupling produces two resonances in both circuits and as k increases, resonance peaks move outwards and the trough in the middle deepens.

If $kQ = 1$ then all three roots coincide and $d\omega = 0$ defines the maximum current in the second resonator $|\mathbf{I}_2| = V_1/2R$. This is critical coupling case. If both resonators have the same resonance frequency but different quality factor then critical coupling is $k = 1/\sqrt{Q_1 Q_2}$

If in $kQ < 1$ there is only one real root that defines the maximum. This is loose coupling and in this case circuits are virtually independent and the current in the second resonator is smaller than $|\mathbf{I}_2| = V_1/2R$.

Figure 2-12 illustrates the current $\mathbf{I}_2$ in coupled resonator circuit with $k_0 = 1/Q$ critical coupling. The variations in current of the primary circuit is similar.

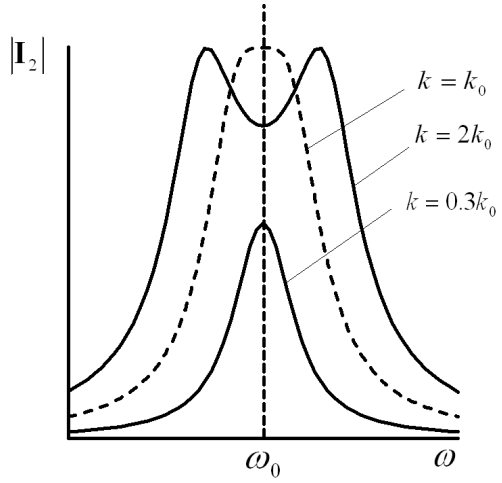

Figure 2-12: Current in the coupled resonator circuit.

The coupling coefficient for the coupled circuit depicted in Figure 2-11 (b) is equal to

$$k = C_m / \sqrt{C_1 C_2} \tag{2.34}$$

Alternative form of two magnetically coupled synchronously tuned resonators with symmetry plane is shown in Figure 2-13 [2-26]. If the symmetry plane T-T' in this figure is replaced by a short-circuit (or an electric wall) the new single resonant circuit will have a resonant frequency

$$f_h = \frac{1}{2\pi\sqrt{(L - L_m)C}} \tag{2.35}$$

where L_m represents mutual inductance. The resonant frequency increases because the coupling reduces the stored flux in the single resonator circuit when short circuit is inserted instead of the symmetry plane.

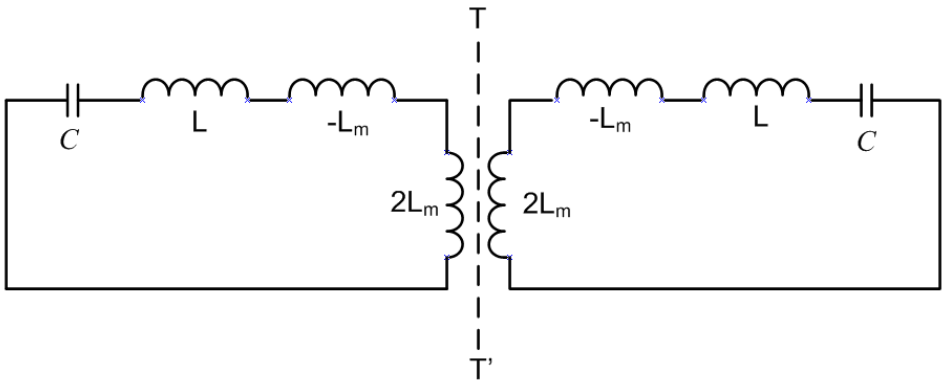

Figure 2-13: Magnetically coupled synchronously tuned resonators

When the symmetry plane is replaced by an open-circuit (or by a magnetic wall) the resonant frequency of single resonator will be:

$$f_l = \frac{1}{2\pi\sqrt{(L+L_m)C}} \tag{2.36}$$

In this case coupling increases the stored flux and the resonant frequency is lower than the resonant frequency of single uncoupled resonator. Using Eq. (2.36) and (2.38) general formula for coupling coefficient in terms of resonant frequencies of two modes can be derived [2-26]:

$$k = \frac{f_h^{\,2} - f_l^{\,2}}{f_h^{\,2} + f_l^{\,2}} \tag{2.37}$$

Eq. (2.37) can be used for synchronously tuned resonators with magnetic, electric and mixed coupling. Eq. (2.37) cannot be used when $f_h = f_l$, i.e. when resonators are critically or loosely coupled, as in this case according to Eq. (2.3) $k = L_m / L = 0$, but as it has been shown above coupled resonators have single resonance mode when $k = 1/Q$ (critical coupling) and when $k < 1/Q$ (loose coupling).

2.6. References

[2-1] H. Howe, "Microwave Integrated Circuits: An Historical Perspective," *IEEE Trans. on Microwave Theory and Tech.,*vol.32, no.9, pp. 997- 1008, September 1984

[2-2] J. G. Hong and M. J. Lancaster, *Microstrip Filters for Rf/Microwave Applications*, New York: John Wiley & Sons, 2001

[2-3] A. Ikuo, "Meaning of resonator's coupling coefficient in bandpass filter design," *Electronics and Communications in Japan (Part II: Electronics)*, vol. 89, no.6 pp. 1-7, 2006

[2-4] M. Dishal, "Alignment and Adjustment of Synchronously Tuned Multiple-Resonant-Circuit Filters," *Proceedings of the IRE*, vol.39, no.11, pp.1448-1455, November 1951

[2-5] T. Edwards, *Foundations for microstrip circuit design*. 2nd edition, Chichester, U.K.: John Wiley & Sons, 1991

[2-6] K.C. Gupta, R. Garg, I.J. Bahl and P. Bhartia *Microstrip Lines and Slotlines*. 2nd edition. Boston: Artech House, 1996.

[2-7] E. Hammerstad and O. Jensen, "Accurate Models for Microstrip Computer-Aided Design," *MTT-S, Int. Microwave Symp. Dig.*, vol.80, no.1, pp. 407- 409, May 1980

[2-8] T. G. Bryant and J. A. Weiss, "Parameters of Microstrip Transmission Lines and of Coupled Pairs of Microstrip Lines," *IEEE Trans. on Microwave Theory and Tech.*, vol.16, no.12, pp. 1021- 1027, December 1968

[2-9] R. E. Collin, *Foundations for microwave engineering*, 2nd edition, New York: McGraw-Hill, 1992.

[2-10] M. Kirschning and R. H. Jansen, "Accurate Wide-Range Design Equations for the Frequency-Dependent Characteristic of Parallel Coupled Microstrip Lines," *IEEE Trans. on Microwave Theory and Tech.,* vol.32, no.1, pp. 83-90, January 1984

[2-11] R. Garg and I. J. Bahl, "Characteristics of Coupled Microstriplines," *IEEE Trans. on Microwave Theory and Tech.,* vol.27, no.7, pp. 700-705, July 1979

[2-12] S. Akhtarzad, T. R. Rowbotham, and P. B. Johns, "The Design of Coupled Microstrip Lines," *IEEE Trans. on Microwave Theory and Tech.,* vol.23, no.6, pp. 486-492, Jun 1975

[2-13] M. K. Krage and G. I. Haddad, "Characteristics of Coupled Microstrip Transmission Lines-I: Coupled-Mode Formulation of Inhomogeneous Lines," *IEEE Trans. on Microwave Theory and Tech.,* vol.18, no.4, pp. 217-222, April 1970

[2-14] M. K. Krage and G. I. Haddad, "Characteristics of Coupled Microstrip Transmission Lines-II: Evaluation of Coupled-Line Parameters," *IEEE Transactions on Microwave Theory and Techniques,* vol.18, no.4, pp. 222-228, Apr 1970

[2-15] S. Kal, D. Bhattacharya, and N. B. Chakraborti, "Empirical Relations for Capacitive and Inductive Coupling Coefficients of Coupled Microstrip Lines," *IEEE Tran. on Microwave Theory and Tech.,* vol.29, no.4, pp. 386- 388, April 1981

[2-16] M. Guglielmi and G. Gatti, "Experimental Investigation of Dual-Mode Microstrip Ring Resonators," *20th European Microwave Conference*, Budapest, Hungary, September 1990, pp.901-906

[2-17] I. Wolff, "Microstrip bandpass filter using degenerate modes of a microstrip ring resonator," *Electronics Letters*, vol.8, no.12, pp.302-303, June 1972

[2-18] H. Jia-Sheng and M. J. Lancaster, "Microstrip triangular patch resonator filters," *MTT-S, Int. Microwave Symp. Dig.,* vol.1, pp.331-334, June 2000

[2-19] R. R. Mansour, B. Jolley, Y. Shen, F. S. Thomson, and V. Dokas, "On the power handling capability of high temperature superconductive filters," *IEEE Trans. on Microwave Theory and Tech.* ,vol.44, no.7, pp.1322-1338, July 1996

[2-20] S. B. Cohn, "Parallel-Coupled Transmission-Line-Resonator Filters," *IRE Trans. on Microwave Theory and Tech.,* vol. 6, no. 2, pp. 223-231, April 1958

[2-21] G. L. Matthaei, "Interdigital Band-Pass Filters," *IRE Trans. on Microwave Theory and Tech.*, vol.10, no.6, pp.479-491, November 1962

[2-22] D. M. Pozar, *Microwave engineering*. 3rd edition, New York: John Wiley & Sons, 2004

[2-23] E. Belohoubek and E. Denlinger, "Loss Considerations for Microstrip Resonators (Short Papers)," *IEEE Trans. on Microwave Theory and Tech.,* vol.23, no.6, pp. 522-526, June 1975

[2-24] D. Kajfez, "*Q factor measurements, analog and digital,"* [Online], Available: http://www.ee.olemiss.edu/darko/rfqmeas2b.pdf.

[2-25] J. S. Hong, "Couplings of asynchronously tuned coupled microwave resonators," *Proc. Inst. Elect. Eng.—Microw., Antennas, Propag.* vol.147, no. 5, pp. 354–358, October 2000

[2-26] J. S. Hong and M. J. Lancaster, "Couplings of microstrip square open-loop resonators for cross-coupled planar microwave filters," *IEEE Trans. on Microwave Theory and Tech.,* vol. 44, no. 11, pp. 2099-2109, November 1996

[2-27] B. I. Bleaney, and Bleaney, B., *Electricity and Magnetism*, vol. 1, 3rd edition, Oxford: Oxford University Press, 1976

[2-28] W. J. Duffin, *Electricity and magnetism*, 3rd edition, London: McGraw-Hill, 1980

3. ANALYSIS OF PSEUDO-INTERDIGITAL LINES AND RESONATORS

3.1. Introduction

Pseudo-interdigital resonators proposed in [3-1] and used in the design of bandpass filter, are modified interdigital resonators with grounding replaced by interconnection of $\lambda_g/4$ resonators in pairs. These resonators can also be treated as intertwined hairpin resonators [3-2], which are folded open-circuited $\lambda_g/2$ resonators. Pseudo-interdigital resonators are used in the design of bandpass filters and they have advantages over both interdigital and hairpin resonators. Compared to interdigital resonators and filters, the pseudo-interdigital filters are cheaper to manufacture as grounding through the holes in substrate is not required. The main advantage over hairpin bandpass filters is that pseudo-interdigital bandpass filters have transmission zeros (TZs) $(S_{21}=0)$ at finite frequencies below and above the passband. This considerably improves the skirt selectivity and can be used in the design of small size and low cost bandpass filters with high selectivity. The main disadvantage of these filters is that due to the complex nature of coupling between the resonators, the simple design procedure for these filters does not exist and the EM simulators and solvers are used for final tuning and optimization of the filters.

In this chapter, the analysis of coupled pseudo-interdigital lines and resonators is presented. In section 3.2, coupled lines and resonators are analyzed in order to derive the approximate TZ conditions and frequencies. These conditions of coupled lines are derived using impedance matrices and method proposed by Swanson for modelling multiple coupled microstrip lines [3-3]. In order to obtain simple equation describing TZ conditions, some assumptions and approximations relevant for coupled thin, i.e. high impedance microstrip lines are used. The dependence of TZ frequencies on physical dimensions of resonators and feeding lines is investigated using EM simulators. Section 3.3 presents the analysis of coupling between pseudo-interdigital resonators, carried out using EM simulators in order to obtain the dependence of coupling coefficient on physical dimensions of coupled pseudo-interdigital resonators.

3.2. Analysis of Transmission Zero Conditions of Coupled Pseudo-Interdigital Lines and Resonators.

A pair of pseudo-interdigital resonators proposed in [3-1] is a key element structure of pseudo-interdigital filter. Figure 3-1 (a) illustrates the pseudo-interdigital resonators which can be considered as a pair of intertwined conventional hairpin resonators, which are shown in Figure 3-1 (b). Conventional hairpin resonators are coupled through proximity coupling by slot s_2. Pseudo-interdigital resonators are coupled through spacing s_1, s_2, and s_3, which is equal to s_1 if resonators have the same length L and height H. Proximity coupling due to slot g is very small and will be neglected in further analysis.

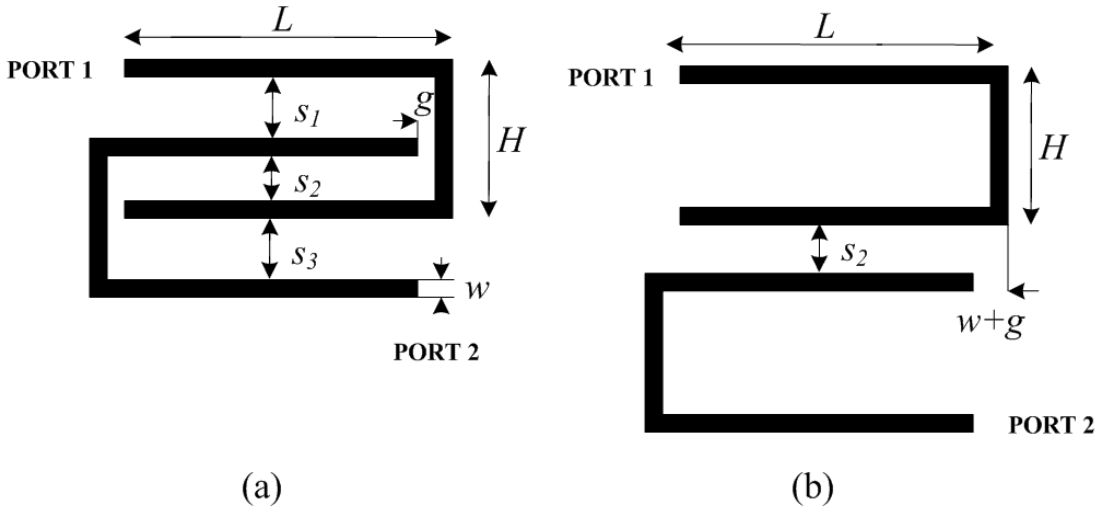

Figure 3-1: Layouts of coupled resonators: (a) pseudo-interdigital resonators; (b) hairpin resonators.

It can be seen from the symmetry of the coupled pseudo-interdigital resonators that the nature of coupling by the slots s_1 is equivalent to the coupling by slot s_3 and both are different from coupling by slot s_2. Coupled microstrip lines can have zero transmission ($S_{21}=0$) at some particular frequencies. These are frequencies at which lines are completely decoupled, i.e. coupling coefficient is equal to zero. These frequencies can be controlled by termination of coupled lines [3-4] and by the length of coupled region [3-5].

Comparative analysis of these two coupled resonators should be started with the analysis of coupled lines, when ports 1 and 2 in Figure 3-1 are connected to 50 Ω lines. As will be shown in next sections, the type of coupling determines the appearance of TZs at finite frequencies, frequencies at which the coupled lines are completely decoupled.

The simulated transmission coefficients for coupled hairpin and pseudo-interdigital lines are shown in Figure 3-2. The dimensions of these resonators are given in Table 3-1.

Slot	(mm)	Line	(mm)
s_1	0.3	w	0.3
s_2	0.3	L	23
s_3	0.3	H	1.5
g	0.3		

Table 3-1: Dimensions of coupled resonators.

Lines are simulated using EM Sonnet [3-6] for RT Duroid 5880 substrate with thickness $h = 0.787$ mm and dielectric constant $\varepsilon_r = 2.2$.

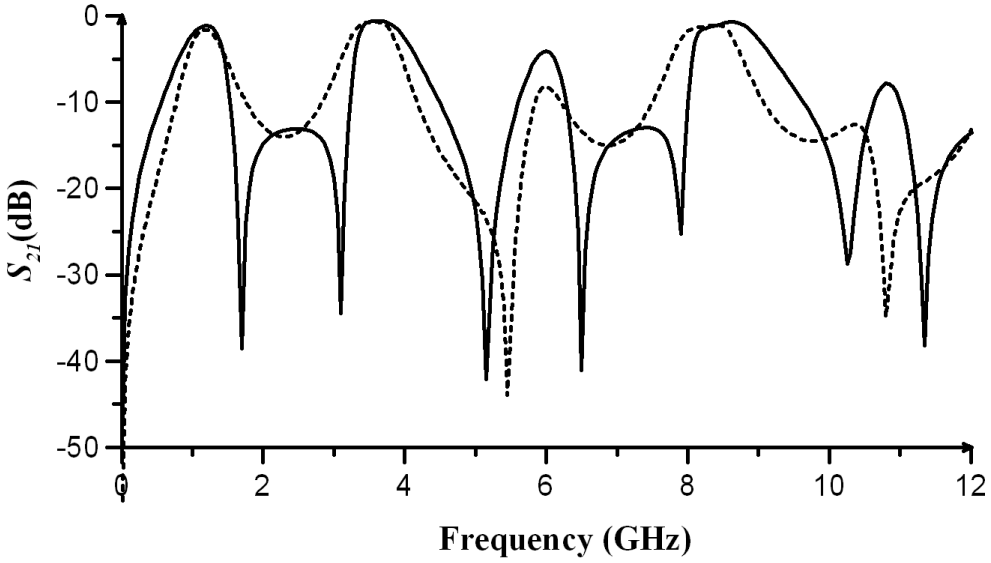

Figure 3-2: Simulated S_{21} for coupled pseudo-interdigital lines (solid) and hairpin lines (dashed).

As it can be seen from Figure 3-2, both structures have TZs around 5 and 11 GHz, 5.45 and 10.8 GHz for coupled hairpin lines and 5.15 and 10.25 GHz for coupled pseudo-interdigital lines. As it will be shown in the next section, TZs appeared at these frequencies are due to coupling through separation s_2. Coupled pseudo-interdigital lines have additional TZs at 1.7 GHz, 3.15 GHz, 6.5 and 7.9 GHz, which can be attributed to coupling through slots s_1 and s_3.

3.2.1. Transmission Zero Conditions of Parallel-Coupled Lines

To obtain the TZ conditions both coupling will be analyzed. For the sake of simplicity the hairpin resonators were unbent and the coupling by slots s_1 and s_2 can be represented using parallel-coupled lines as shown in Figure 3-3.

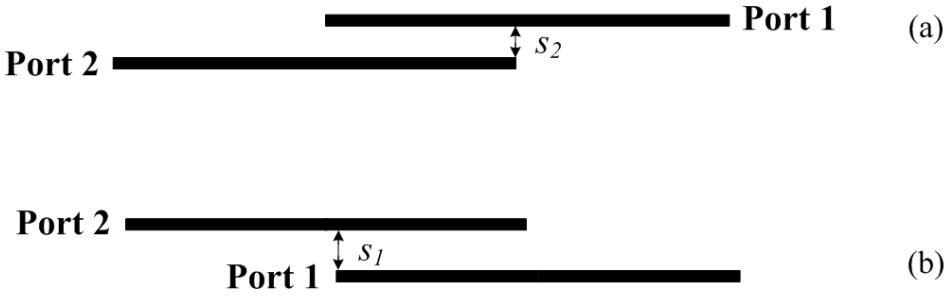

Figure 3-3: Coupling of lines: (a) slot s_2 coupling; (b) slot s_1 coupling.

The structure shown in Figure 3-3 (a) consists of a section of parallel-coupled lines with length *L*, used in the design of parallel-coupled transmission-line-resonator bandpass filters [3-7]. It can be analyzed using the representation of coupled lines as a 4-port network with specified termination conditions $I_2 = I_4 = 0$, as shown in Figure 3-4.

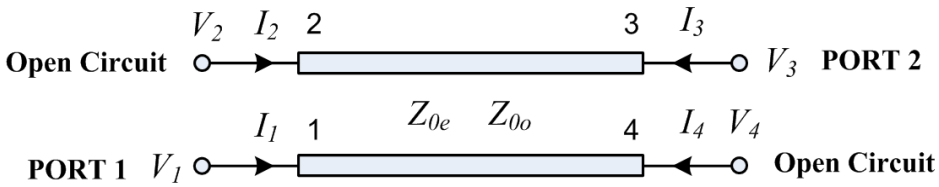

Figure 3-4: Conventional parallel-coupled lines.

The impedance matrix of this 4-port network has been derived in [3-8] and the expressions for its entries in terms of even and odd mode characteristic impedances and electrical lengths Z_{0e}, Z_{0o}, θ_e, and θ_o are:

$$Z_i = Z_{11} = Z_{22} = Z_{33} = Z_{44} = -j\frac{1}{2}\left(Z_{0e}\cot\theta_e + Z_{0o}\cot\theta_o\right) \tag{3.1}$$

$$Z_n = Z_{12} = Z_{21} = Z_{34} = Z_{43} = -j\frac{1}{2}\left(Z_{0e}\cot\theta_e - Z_{0o}\cot\theta_o\right) \tag{3.2}$$

$$Z_f = Z_{13} = Z_{31} = Z_{24} = Z_{42} = -j\frac{1}{2}\left(Z_{0e}\csc\theta_e - Z_{0o}\csc\theta_o\right) \tag{3.3}$$

$$Z_t = Z_{14} = Z_{41} = Z_{23} = Z_{32} = -j\frac{1}{2}\left(Z_{0e}\csc\theta_e + Z_{0o}\csc\theta_o\right) \tag{3.4}$$

Using these expressions and the termination conditions $I_2 = I_4 = 0$, 2×2 impedance matrix $[Z']$ for 2-port network can be derived. Ports 1 and 2 of this network are connected to ports 1 and 3 of 4-port network representing coupled lines.

$$\begin{bmatrix} V_1 \\ V_2 \end{bmatrix} = \begin{bmatrix} Z_{11}^{'} & Z_{12}^{'} \\ Z_{21}^{'} & Z_{22}^{'} \end{bmatrix}\begin{bmatrix} I_1 \\ I_2 \end{bmatrix} = \begin{bmatrix} Z_i & Z_f \\ Z_f & Z_i \end{bmatrix}\begin{bmatrix} I_1 \\ I_2 \end{bmatrix} \tag{3.5}$$

Transmission coefficient S_{21} can be calculated from 2-port impedance matrix using conversion formula [3-9]:

$$S_{21} = \frac{2Z_{21}^{'}Z_0}{(Z_{11}^{'} + Z_0)(Z_{22}^{'} + Z_0) - Z_{12}^{'}Z_{21}^{'}} \tag{3.6}$$

From (3.6) the TZ condition is $Z_{21}^{'} = Z_f = 0$, or

$$Z_{0e}\csc\theta_e = Z_{0o}\csc\theta_o \tag{3.7}$$

The numerical solution of Eq.(3.6) calculated in Matlab for coupled lines with dimension given in Table 3-1, is shown in Figure 3-5. The calculated S_{21} coincides with S_{21} coefficient obtained by simulation of coupled lines using Agilent ADS. From comparison of Figures 3-2 and 3-5 it can be seen that TZs for both coupled hairpin lines and coupled lines analyzed above, appear at the same frequencies.

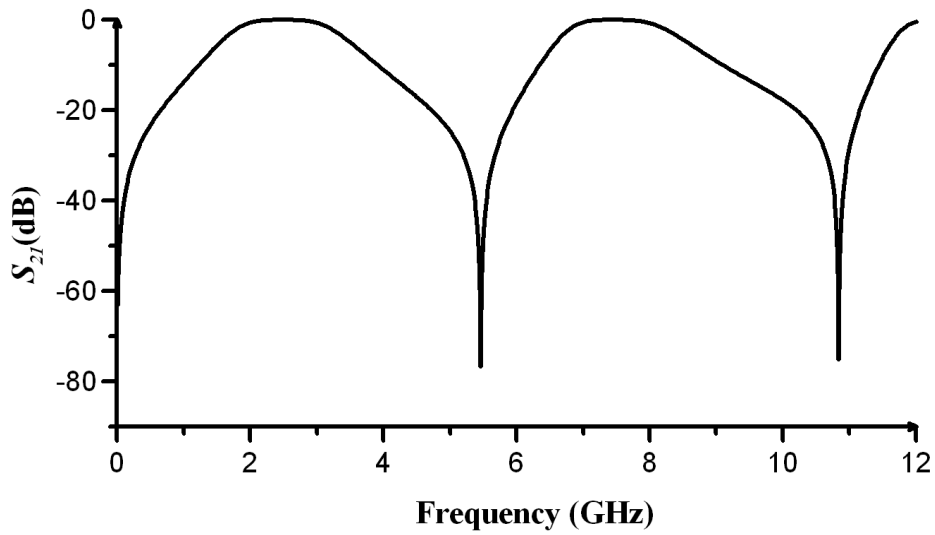

Figure 3-5: Calculated S_{21} for conventional microstrip parallel-coupled lines.

Coupled lines shown in Figure 3-3(b) are analyzed in the similar way and can be treated as asymmetrically terminated coupled lines, as it is shown in Figure 3-6, and can be considered as an analogy to asymmetrically terminated interdigital lines analyzed in [3-10]. Parallel-coupled lines asymmetrically terminated by open-circuited stub are also used in the design of microstrip extracted pole bandpass filters [3-11], [3-12].As it can be seen from this figure, ports 1 and 2 of 2-ports network are connected to ports 1 and 2 of general 4-ports network representing coupled lines, and open-circuited stub is connected to port 4.

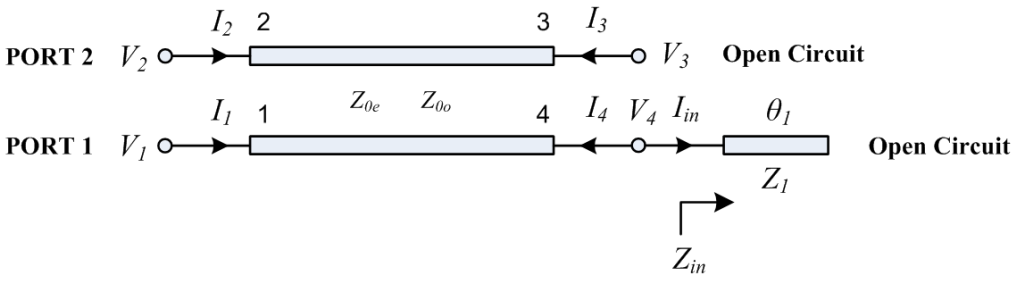

Figure 3-6: Asymmetrically terminated parallel-coupled lines.

The physical length of open-circuited stub is equal to the length of coupled lines. Both these lengths are equal to *L* and equal to quarter-wavelength at 2.5 GHz, which is the fundamental resonant frequency of the considered microstrip line resonator. The microstrip line, with length *L* connected to port 2 of the 4-port network to form the structure shown in Figure 3-3 (b), is removed and is not considered to simplify the

analysis of structure shown in Figure 3-6. This will not affect the occurrence and frequencies of TZs.

The input impedance of the open-circuited stub is equal:

$$Z_{in} = -jZ_1 \cot\theta_1 = -jX_c \tag{3.8}$$

Termination conditions for a 4-ports network are

$$I_3 = 0 \tag{3.9}$$

$$I_4 = -I_{in} = -\frac{V_4}{Z_{in}} \tag{3.10}$$

Using these conditions the system of 4 linear equations with 6 unknowns can be reduced to the system of 2 linear equations with 4 unknowns, in order to obtain impedance matrix for 2-port network:

$$\begin{bmatrix} V_1 \\ V_2 \end{bmatrix} = [\mathbf{Z'}] \begin{bmatrix} I_1 \\ I_2 \end{bmatrix} = \begin{bmatrix} Z_i - \dfrac{Z_t^2}{Z_i + Z_{in}} & Z_n - \dfrac{Z_t Z_f}{Z_i + Z_{in}} \\ Z_n - \dfrac{Z_f Z_t}{Z_i + Z_{in}} & Z_i - \dfrac{Z_f^2}{Z_i + Z_{in}} \end{bmatrix} \begin{bmatrix} I_1 \\ I_2 \end{bmatrix} \tag{3.11}$$

Combining Eq. (3.6) with expressions for entries of 2-port impedance matrix taken from Eq. (3.11) transmission coefficient S_{21} can be calculated:

$$S_{21} = \frac{2Z_0\left(Z_n Z_i + Z_n Z_{in} - Z_f Z_t\right)\left(Z_i + Z_{in}\right)}{\left(\left(Z_{i1} + Z_0\right)\left(Z_i + Z_{in}\right) - Z_t^2\right)\left(\left(Z_{i1} + Z_0\right)\left(Z_i + Z_{in}\right) - Z_f^2\right) - \left(Z_n Z_i + Z_n Z_{in} - Z_t Z_f\right)^2} \tag{3.12}$$

Figure 3-7 depicts S_{21} in dB calculated for structure with dimensions given in Table 3-1. Calculation results coincide with results of simulations which is done using ADS schematic simulation of microstrip transmission lines. Three TZs at 1.2 GHz, 3.6 GHz and 8.46 GHz are observed. Two first TZs are the most important for us as one of

them is below and another is above the fundamental resonant frequency of resonators and both will affect the out-of-band performance of bandpass filter. The TZ condition is:

$$Z_{21}^{'} = Z_n - \frac{Z_f Z_t}{Z_i + Z_{in}} = 0 \tag{3.13}$$

Using formulas for impedance matrix entries of general a 4-port network of coupled lines (3.1)-(3.4) in the Eq. (3.13) TZ condition in terms of even and odd mode characteristic impedances of coupled lines, electric lengths of coupled lines, characteristic impedance of open-circuited stub, and electric length of open-circuited stub can be derived:

$$Z_1 \cot\theta_1 \left(Z_{0e} \cot\theta_e - Z_{0o} \cot\theta_o\right) = \frac{1}{2}\left(Z_{0e}^2 - Z_{0o}^2\right) \tag{3.14}$$

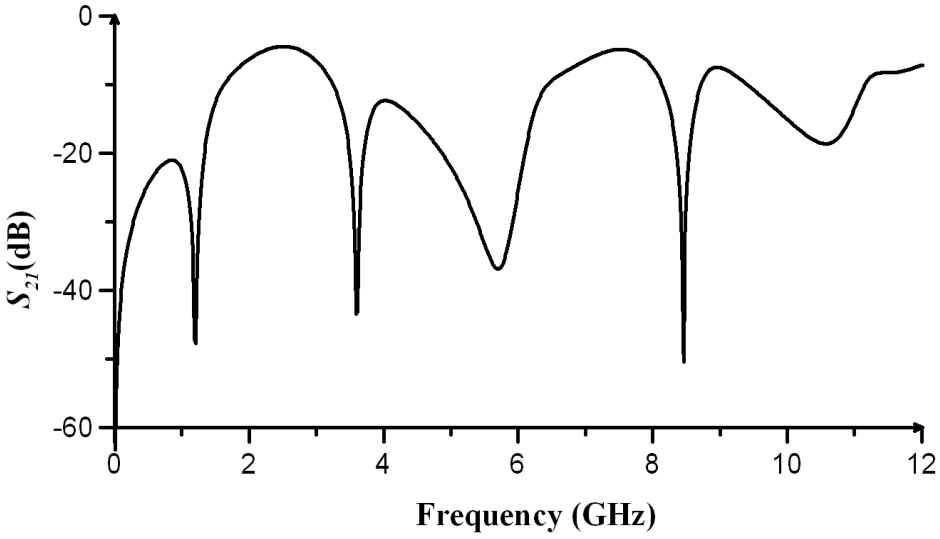

Figure 3-7: Calculated S_{21} for asymmetrically terminated coupled lines.

Eq. (3.14) is complex to analyse; therefore some approximation will be used. The first approximation, which is equivalent to placing a dielectric sheet made from the substrate material on top the conducting strip [3-13], is the equality of propagation constant for even and odd modes $\beta_e = \beta_o = \beta_1$, which means the equality of even and odd mode electrical lengths of coupled lines $\theta_e = \theta_o = \theta_1$. With the application of this approximation TZ condition will be:

$$Z_1 \cot^2 \theta_1 = \frac{1}{2}\left(Z_{0e} + Z_{0o}\right) \tag{3.15}$$

The frequency of two first TZs are shifted from 1.2 GHZ to 1.26GHz and from 3.6 GHz to 3.73 GHz respectively as a result of the usage of this approximation.

From Eq. (3.15), it can be seen that TZ frequencies can be tuned by adjusting the impedance Z_1. The general rule for this tuning obtained from the calculation results is that for low values of Z_1, the first two TZs are located further from each other and with an increase of Z_1 the first two TZs are shifting towards each other. Thus, for $Z_1 = 50$ Ω, TZs occur at 0.84 GHz and 3.99 GHz, for $Z_1 = 100$ Ω they occur at 1.09 GHz and 3.73 GHz, and for $Z_1 = 180$ Ω, the first two TZs occur at 1.31 GHz and 3.5 GHz. Figure 3-7 illustrates the calculated S_{21} for $Z_1 = 135.7\,\Omega$ which is the characteristic impedance of the microstrip line with $w = 0.3$ mm. The width of each of the coupled microstrip lines and the width of the slot between them is also 0.3 mm. For these coupled microstrip lines, another approximation, which has been justified above in the previous chapter, can be used:

$$Z_1 \approx \frac{1}{2}\left(Z_{0e} + Z_{0o}\right) \tag{3.16}$$

Thus, the simplified TZ condition, which is the special case of Eq. (3.15) when Eq. (3.16) holds, can be derived as:

$$\cot^2 \theta_1 \approx 1 \tag{3.17}$$

This TZ condition will be simplified to $\theta_1 = (2n-1)\pi/4$ where $n = 1,2,3\ldots$. This simplification will result in a shift of TZ frequencies from 1.2 to 1.25 GHz and from 3.6 to 3.74 GHz. At 1.25 GHz, the electrical length is $\theta_1 = 45^\circ$ and at 3.74 GHz $\theta_1 = 135^\circ$.Thus, with good approximation the TZs appear at the frequencies at which the electrical length of coupled lines and open-circuited stub is equal to $\theta_1 = (2n-1)\pi/4$.

3.2.2. Transmission Zero Conditions of Coupled Pseudo-Interdigital Lines and Resonators

In this section, analysis of coupled pseudo-interdigital lines and resonators will be presented. It has been carried out in order to derive the TZ conditions and will follow the analysis presented in [3-14], [3-15]. The method for modelling several coupled microstrip lines, proposed by Swanson [3-3], is used. In order to apply this method, the 2-port circuit, representing coupled pseudo-interdigital lines, which is shown in Figure 3-8 (a), should be transformed into 8-port circuit, as it is shown in Figure 3-8 (b).

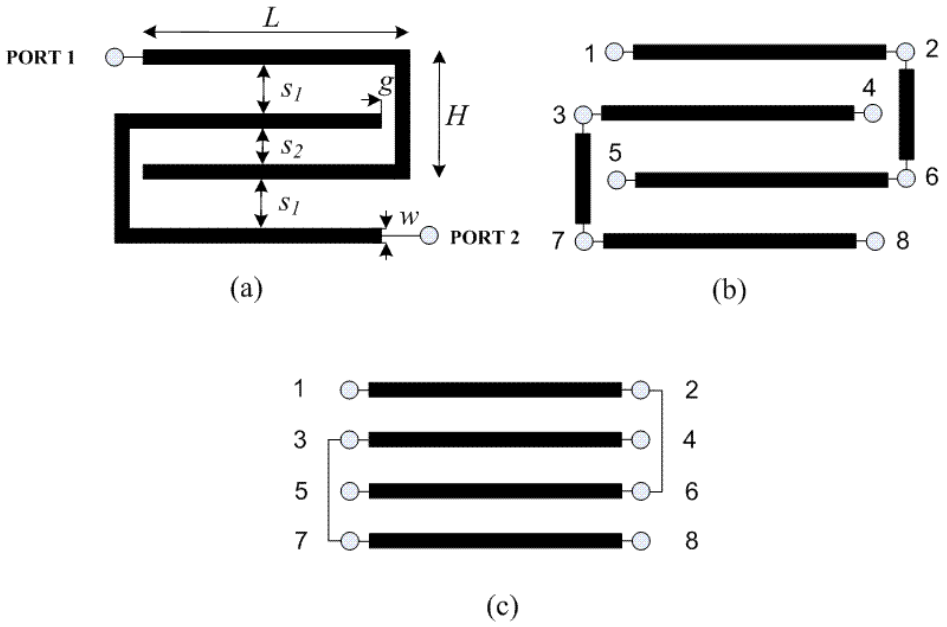

Figure 3-8: Coupled pseudo-interdigital lines: (a) 2-port circuit; (b) 8-port circuit; (c) 8-port model.

The general 8×8 impedance matrix for the structure shown in Figure 3-8 (b), composed as is described in [3-3] and is equal to:

$$\begin{bmatrix} V_1 \\ V_2 \\ V_3 \\ V_4 \\ V_5 \\ V_6 \\ V_7 \\ V_8 \end{bmatrix} = \begin{bmatrix} Z_{s1} & Z_{s2} & Z_n & Z_f & Z_n^{'} & Z_f^{'} & Z_n^{''} & Z_f^{''} \\ Z_{s2} & Z_{s1}+Z_{s1}^{'} & Z_f & Z_n & Z_f^{'} & Z_{s2}^{'}+Z_n^{'} & Z_f^{''} & Z_n^{''} \\ Z_n & Z_f & Z_{s1}+Z_{s1}^{'} & Z_{s2} & Z_n & Z_f & Z_{s2}^{'}+Z_n^{'} & Z_f^{'} \\ Z_f & Z_n & Z_{s2} & Z_{s1} & Z_f & Z_n & Z_f^{'} & Z_n^{'} \\ Z_n^{'} & Z_f^{'} & Z_{s2} & Z_f & Z_{s1} & Z_{s2} & Z_n & Z_f \\ Z_f^{'} & Z_{s2}^{'}+Z_n^{'} & Z_f & Z_n & Z_{s2} & Z_{s1}+Z_{s1}^{'} & Z_f & Z_n \\ Z_n^{''} & Z_f^{''} & Z_{s2}^{'}+Z_n^{'} & Z_f^{'} & Z_n & Z_f & Z_{s1}+Z_{s1}^{'} & Z_{s2} \\ Z_f^{''} & Z_n^{''} & Z_f^{'} & Z_n^{'} & Z_f & Z_n & Z_{s2} & Z_{s1} \end{bmatrix} \cdot \begin{bmatrix} I_1 \\ I_2 \\ I_3 \\ I_4 \\ I_5 \\ I_6 \\ I_7 \\ I_8 \end{bmatrix} \quad (3.18)$$

In Eq. (3.18) two impedance matrix's entries of single unit element, i.e. of single lossless microstrip line with length θ will be calculated for long lines and short lines:

$$Z_{s1} = -jZ_0 \cot\theta \quad (3.19)$$

$$Z_{s2} = -jZ_0 \csc\theta \quad (3.20)$$

In Eq. (3.18) the terms Z_{s1}, Z_{s2}, $Z_{s1}^{'}$ and $Z_{s2}^{'}$ are calculated using (3.19) and (3.20) for long and short lines respectively, Z_n, Z_f, $Z_n^{'}$, $Z_f^{'}, Z_n^{''}$ and $Z_f^{''}$ are calculated using (3.2) and (3.3). Z_n and Z_f are entries of the impedance matrix of two adjacent coupled lines. Impedances $Z_n^{'}$ and $Z_f^{'}$ are impedance matrix entries for nonadjacent coupled lines, such as line connecting ports 1 and 2 coupled to the line connecting ports 5 and 6 of the circuit shown in Figure 3-8 (b). Impedances $Z_n^{''}$ and $Z_f^{''}$ are used for line connecting ports 1 and 2 coupled to line connecting ports 7 and 8. The only termination condition of this model is:

$$I_4 = I_5 = 0 \quad (3.21)$$

Using this terminal condition and (3.18) we will have system of 8 linear equations and 14 unknowns. Thus it is not possible to derive the impedance matrix for 2-port circuit, shown in Figure 3-8 (a), as it has been done in previous sections. Therefore, some assumptions will be made to get the approximate solution. First the length of short lines connecting port 2 to 6 and port 3 to 7 is assumed to be negligible and pseudo-interdigital lines can be presented as it is shown in Figure 3-8 (c). This results in

additional termination conditions: $V_2 = V_6$, $V_3 = V_7$, $I_2 = -I_6$ and $I_3 = -I_7$. Thus, now there will be 10 unknown and 8×8 impedance matrix can be transformed to 2×2 impedance matrix of 2-port network. Another assumption, which has already been made, is that the width of lines *w* and width of slots *s* are equal for all pairs of coupled lines, which means that pairs of adjacent coupled lines have the same even and odd mode impedances and effective dielectric constants. We also assume that the coupling for nonadjacent line can be neglected. Thus, all entries in matrix (3.18) which describe coupling between nonadjacent lines will be equal to 0 and new simplified version of Eq. (3.18) will be:

$$\begin{bmatrix} V_1 \\ V_6 \\ V_7 \\ V_4 \\ V_5 \\ V_6 \\ V_7 \\ V_8 \end{bmatrix} = \begin{bmatrix} Z_i & Z_t & Z_n & Z_f & 0 & 0 & 0 & 0 \\ Z_t & Z_i & Z_f & Z_n & 0 & 0 & 0 & 0 \\ Z_n & Z_f & Z_i & Z_t & Z_n & Z_f & 0 & 0 \\ Z_f & Z_n & Z_t & Z_i & Z_f & Z_n & 0 & 0 \\ 0 & 0 & Z_n & Z_f & Z_i & Z_t & Z_n & Z_f \\ 0 & 0 & Z_f & Z_n & Z_t & Z_i & Z_f & Z_n \\ 0 & 0 & 0 & 0 & Z_n & Z_f & Z_i & Z_t \\ 0 & 0 & 0 & 0 & Z_f & Z_n & Z_t & Z_i \end{bmatrix} \cdot \begin{bmatrix} I_1 \\ -I_6 \\ -I_7 \\ 0 \\ 0 \\ I_6 \\ I_7 \\ I_8 \end{bmatrix} \tag{3.22}$$

Solving Eq. (3.22) for voltages and currents at ports 1 and 8 the entries of impedance matrix of 2-port network shown in Figure 3-8 (a) will be:

$$Z_{11}^{'} = Z_{22}^{'} = Z_i + \frac{2Z_tZ_nZ_f - 2Z_iZ_n^2 - 2Z_iZ_t^2}{4Z_i^2 - Z_f^2} \tag{3.23}$$

$$Z_{12}^{'} = Z_{21}^{'} = \frac{4Z_iZ_tZ_n - Z_fZ_t^2 - Z_fZ_n^2}{4Z_i^2 - Z_f^2} \tag{3.24}$$

The comparison of simulated S_{21} with the one calculated using Eq. (3.23-3.24) and (3.6) of the structure with dimensions given in Table 3-1 is shown in Figure 3-9. The even and odd impedances and effective dielectric constant of lines with these dimensions were obtained using ADS Linecalc: $Z_{0e} = 179.23\,\Omega$, $Z_{0o} = 84.298\ \Omega$, $\varepsilon_{effe} = 1.776$ and $\varepsilon_{effo} = 1.547$.

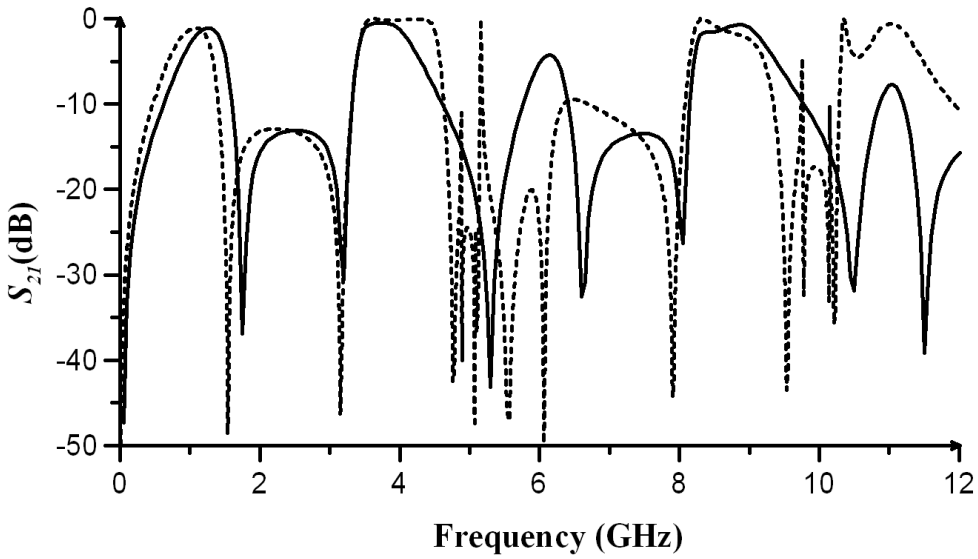

Figure 3-9: Simulated (solid) and calculated (dashed) S_{21} of coupled pseudo-interdigital lines.

As it can be seen from Figure 3-9, usage of formulas (3.23-3.24) provides good approximation, at least till 4.5 GHz. According to the calculations, two first TZs appear at 1.54 and 3.16 GHz, which is very close to 1.7 and 3.15 GHz, obtained by simulation. The TZ condition is $Z_{12}^{'} = Z_{21}^{'} = 0$ and after using (3.1-3.4) in (3.24) becomes too complex to analyse. Therefore, further simplification is required. First the equality of even and odd modes electrical lengths $\theta_e = \theta_o = \theta$ is assumed. With this assumption the TZ condition reduces to:

$$(Z_{0e} + Z_{0o})^2 \cot^2\theta = \frac{1}{4}(Z_{0e} + Z_{0o})^2 \csc^2\theta + \frac{1}{4}(Z_{0e} - Z_{0o})^2 \cot^2\theta \qquad (3.25)$$

From Eq. (3.25) the TZ frequency can be manipulated by adjusting the even and odd mode characteristic impedances. These impedances depend on the physical dimensions of the coupled microstrip lines. Thus, tuning of TZ frequencies can be done by adjusting the dimensions of coupled microstrip line. The easiest approach to such tuning is to change the width of the slot between lines of fixed width or by changing the width of the coupled lines with the fixed width of slot. Table 3-2 contains calculated TZ frequencies for coupled microstrip lines with different dimensions. It can be seen from this table that both TZ frequencies are shifting to lower values with increase of the slot's width between lines when the width of lines is fixed. When the width of slot is

fixed TZ frequencies are shifting to lower frequencies with an increase of the width of the lines. Thus, it can be seen that TZ frequencies can be controlled by the difference between even and odd mode impedances. This also can be assumed from Eq. (3.25). With the increase of the difference between the even and odd mode impedances, the TZ frequencies are shifting to the higher values.

s (mm)	w (mm)	Z_{0e} (Ω)	Z_{0o} (Ω)	f_{T1} (GHz)	f_{T2} (GHz)
0.1	0.3	196	59.17	1.59	3.3
0.5	0.3	168.3	97.7	1.57	3.2
1	0.3	153	114.62	1.51	3.12
0.3	0.1	242.94	106.55	1.6	3.29
0.3	0.5	146.74	73	1.57	3.2
0.3	1	103.53	57.42	1.52	3.12

Table 3-2: TZ frequencies for coupled microstrip lines with different size

Looking at the values of even and odd modes characteristic impedances in Table 3-2 for thin microstrip lines with thin slot between them, it can be said that:

$$(Z_{0e} + Z_{0o})^2 >> (Z_{0e} - Z_{0o})^2 \tag{3.26}$$

Using this simplification the TZ condition can be reduced to:

$$\cos^2 \theta \approx \frac{1}{4} \tag{3.27}$$

Eq. (3.27) can be considered as a special case for Eq. (3.25) that can be applied when condition in Eq. (3.26) is true. Figure 3-10 illustrates the comparison of calculated coefficient $A = \cos^2 \theta - 1/4$ in dB with simulated transmission coefficient S_{21}.

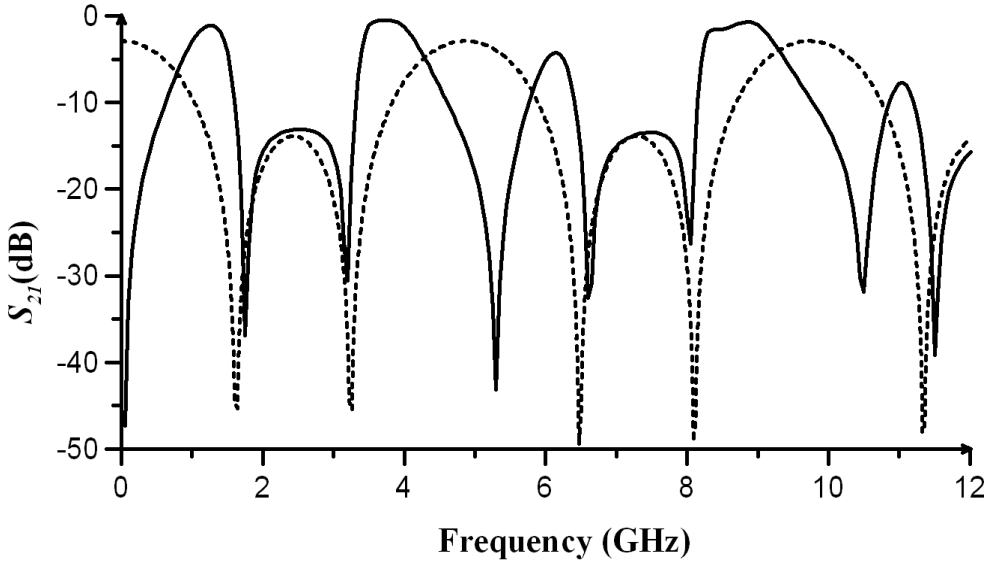

Figure 3-10: Simulated (solid) S_{21} of coupled pseudo-interdigital lines and calculated (dashed) coefficient describing TZ condition.

As it can be seen from this figure, Eq.(3.27) provides good approximation for TZs, caused by the coupling due to slot separations s_1 and s_3 of the resonators shown in Figure 3-1 (a). Therefore, it will be correct to assume that the combination of coupling by slot s_1 with the coupling by slot s_3, changes the approximate frequencies of TZs from ones described by (3.17) to the ones described by (3.27). The TZ frequencies of simulated S_{21} are at 1.7 GHz, 3.15 GHz, 5.66 GHz and 8.1 GHz, whereas these frequencies calculated using (3.27) are 1.62 GHz, 3.24 GHz, 6.48 GHz and 8.1 GHz. These are frequencies at which the electrical lengths of single microstrip lines are equal to 60º, 120º, 240º and 300º respectively, which are all solutions of Eq. (3.27). The TZs of simulated lines at 5.3 GHz and 10.5 GHz, are not given by Eq. (3.27). They can be found with good approximation using Eq. (3.7), because, as it has been noted before, they appear due to coupling by slot s_2 or by coupling depicted on Figure 3.3 (a).

As a result of analysis carried out in these sections, the TZ frequencies of coupled pseudo-interdigital lines can be approximately obtained using Eq. (3.7) and Eq. (3.17). These approximate conditions depend solely on the physical length of coupled lines, but as it has been shown in the analysis of coupled lines, the maximum degree of coupling between two parallel-coupled lines occurs when the coupling length is $\lambda_g / 4$

i.e. when $\theta = \pi/2$ [3-16]. Therefore, in order to achieve maximum coupling, the length of coupled lines should be fixed and dependence of TZ frequencies in the other physical dimensions of coupled pseudo-interdigital lines should be investigated using electromagnetic (EM) simulators.

In order to compare the effects of the couplings through slots s_1 and s_2 on the frequency of TZs, the structure shown in Figure 3-8 (a) was simulated with the condition that $s_1 + s_2 = 2$ mm. The total length of hairpin line corresponds to the length of resonators with fundamental resonance at 2.5 GHz. The simulated frequencies of the first and the second TZs (f_{T1} and f_{T2}) changing with respect to coupling space s_1 are shown in Figure 3-11.

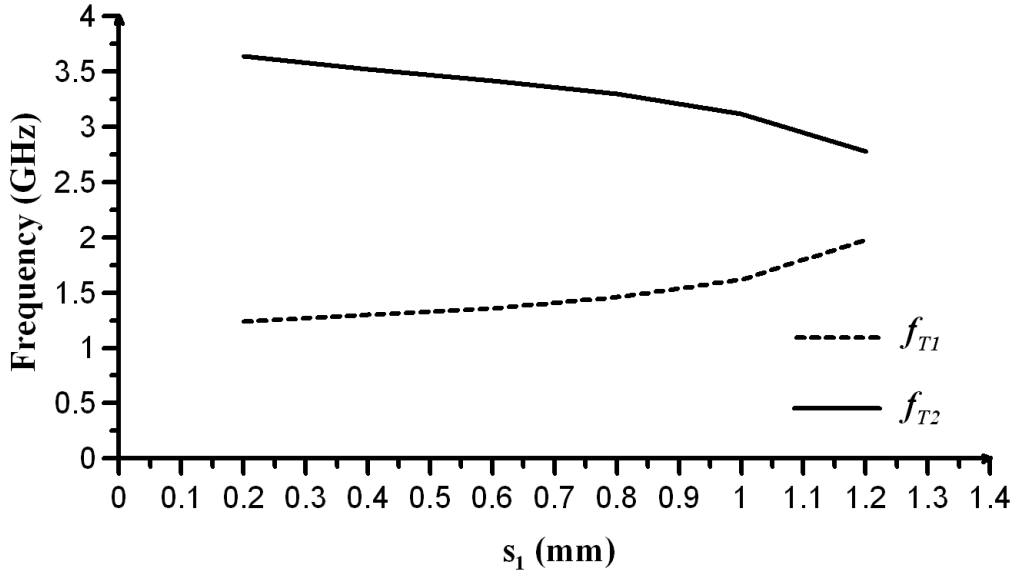

Figure 3-11: Simulated TZ frequencies.

As it can be seen from Figure 3-11, both TZs occur symmetrically, with good approximation, with respect to the resonant frequency of resonators. This also can be derived from (3.27). TZs occur at frequencies shifting towards the fundamental resonance frequency with increasing s_1, i.e. with decreasing coupling through spacing s_1 and increasing coupling through spacing s_2. When $s_1 > 1.2$ mm, TZs do not occur, as coupling becomes equivalent to coupling of hairpin lines used in the design of conventional hairpin bandpass filter.

It should be noted that Eq. (3.27) and Figure 3-11 provide the information about TZs for coupled pseudo-interdigital lines, which can be modelled as 8-port network consisting of coupled lines as it is shown in Figure 3-8 (b). As it was discussed in the previous chapter, transmission line resonators consist of a section of transmission line bounded from both ends either by open-circuited or short-circuited termination. Therefore, in the design of bandpass filters, pseudo-interdigital resonators coupled to the feeding lines are used. The two most popular feeding approaches are the feeding through parallel-coupled lines and tapped-lines feeding [3-17]. As one of the aims of this work is to design compact filters, feeding through parallel-coupled lines will be used.

It has been observed during simulations that the replacement of 50 Ω feeding line at ports 1 and 8 of structure shown in Figure 3-8 (b) by feeding through additional parallel-coupled lines causes the change of TZ frequencies. This result is obvious, as now resonators with feeding lines should be modelled as 12 ports network consisting of 6 coupled lines, and using the same procedure as above 12×12 impedance matrix should be used. In this case simple expression for TZ conditions, analogous to Eq. (3-27) has not been obtained. Therefore, EM simulations are used to determine the dependence of TZ frequencies on the physical dimensions of coupled resonators and feeding line.

First of all, similarly to Eq. (3.27) the electrical length of coupled lines, assuming that all lines are of equal length, is the main parameter that affects TZ frequencies. This parameter will not be changed as the length of resonators controls the resonance frequency, i.e. center frequency of filter. The second parameter that affects the location of TZs is the type of feeding of coupled resonators. It has been observed that the stronger the feeding the bigger the gap between the first and the second TZ frequencies f_{T1} and f_{T2} respectively. Thus, the gap between resonance frequency and the frequency of TZ above and below resonance frequency, is increasing as well. The biggest gap is given by (3.27) for the strongest feeding through simple straight connection of 50 Ω line to pseudo-interdigital resonators, as it shown in Figure 3-8 (a). Table 3-3 contains TZ frequencies for coupled pseudo-interdigital resonators with fundamental resonance frequency 2.5 GHz. Feeding by parallel-coupled line with three

different slots' width s_f is included to demonstrate the rate of change of TZ frequencies. All values in table are in GHz.

Type of feeding	f_{T1}	f_{T2}	$f_0 - f_{T1}$	$f_{T2} - f_{T1}$
Strait connection of 50 Ω line	1.69	3.105	0.81	0.605
Coupled line feeding ($s_f = 0.1\,\text{mm}$)	1.875	2.94	0.625	0.44
Coupled line feeding ($s_f = 0.3\,\text{mm}$)	1.93	2.88	0.57	0.38
Coupled line feeding ($s_f = 0.6\,\text{mm}$)	1.995	2.82	0.505	0.32
Gap feeding ($s_f = 0.3\,\text{mm}$)	2.2	2.74	0.3	0.24

Table 3-3: TZ frequencies for different feeding of coupled pseudo-interdigital resonators.

For the weakest feeding through the serial gap, the TZs are very close to low and high resonance peaks of coupled resonators, which occur at 2.225 and 2.69 GHz. The feeding of coupled resonators plays crucial role in the design of bandpass filter and the width of slot s_f is adjusted very carefully in order to obtain required filters' performance. Therefore, the possibility to tune the frequency of TZs by adjusting the width of feeding slots is very limited.

The third parameter affecting frequency and occurrence of TZs is the width of slots s_1 and s_2 between different arms of coupled pseudo-interdigital resonators. As it has been reported before, TZs below and above resonant frequency occur due to coupling by slot s_1 and in situation when $s_1 + s_2$ is fixed, the TZs do not occur for small s_2, i.e. when coupling of conventional hairpin resonators prevails. As it shown in Figure 3-11, for $s_1 > 1.2$ mm, i.e. for $s_2 < 0.8$ mm TZs do not occur. Figure 3-12 illustrates the extracted TZ frequencies for $s_1 + s_2 = 1\,\text{mm}$ and for $s_1 + s_2 = 2$ mm for coupled resonators with feeding through parallel-coupled line with $s_f = 0.3$ mm. These both curves are similar to the one shown in Figure 3-11. They can be used in the design of bandpass filters to predict the frequencies of TZs below and above the passband.

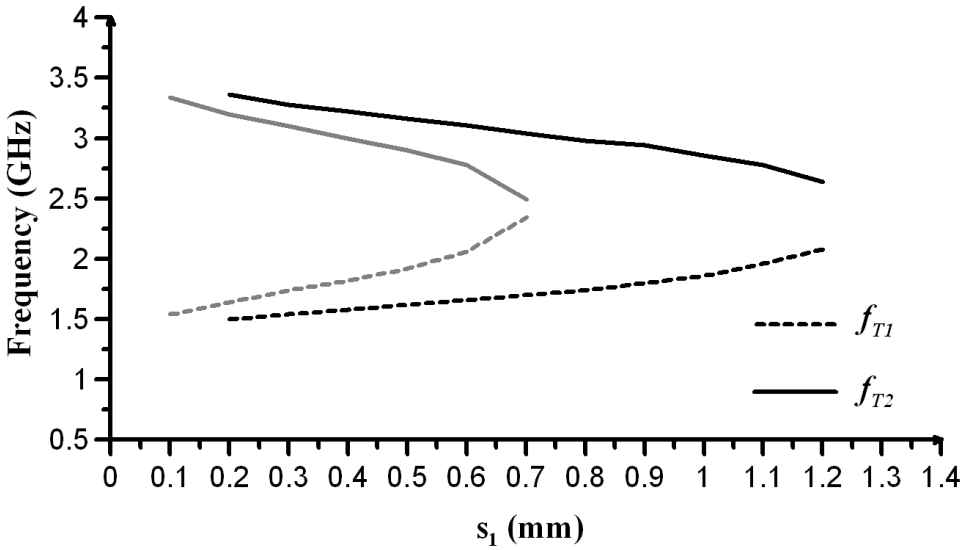

Figure 3-12: Simulated TZ frequencies: $s_1 + s_2 = 2$ mm (black); $s_1 + s_2 = 1$ mm (grey).

From Figure 3-12 it can be seen that TZs do not occur when $s_1 > 0.7$ mm for the case when $s_1 + s_2 = 1$ mm, and when $s_1 > 1.2$ mm for the case when $s_1 + s_2 = 2$ mm. The dependence of TZ frequencies on s_1 and s_2 is very important because these dimensions will be used to control coupling coefficient between resonators and, as a consequence, to control the bandwidth of bandpass filters.

3.3. Coupling of Pseudo-Interdigital Resonators

The comparative investigation of coupling of pseudo-interdigital resonators and hairpin resonators was presented in [3-18]. As it was mentioned above, the coupling of pseudo-interdigital and hairpin resonators is a proximity coupling through the fringe fields. Coupling of pseudo-interdigital resonators with very good approximation can be considered as a combination of proximity couplings due to slots s_1, s_2, and s_3, as it is shown in Figure 3-13 (a). If resonators have the same dimensions *L* and *H* then the widths of slots s_1 and s_3 are equal. In order to determine the contribution of couplings due to each of these slots, structures shown in Figure 3-13 have been investigated using the EM simulator.

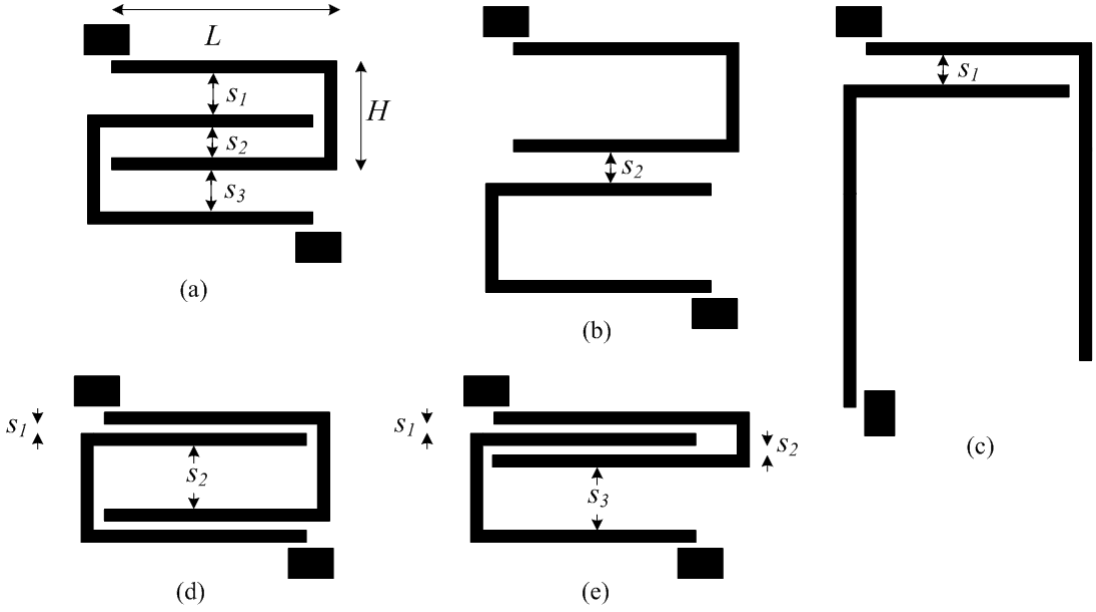

Figure 3-13: Coupled $\lambda_g/2$ resonators: (a) Pseudo-interdigital; (b) Hairpin; (c) Coupled through slot s_1; (d) Coupled through slots s_1 and s_3; (e) Coupled through slots s_1 and s_2.

All microstrip resonators used in this investigation are $\lambda_g/2$ open-circuited resonators with fundamental resonance at 2.5 GHz and width equal 0.3 mm. All coupling slots, except s_3 in Figure 3-13 (d) and s_3 in Figure 3-13 (e) were chosen to be 0.3 mm. The feeding of resonators is arranged through short parallel-coupling with 50 Ω feeding

lines. The dielectric constant of the substrate used in the simulation is $\varepsilon_r = 2.2$ and the thickness is $h = 0.787$ mm. The width of the slot s_2 of coupled resonators shown in Figure 3-13 (d) was chosen to be 2.4 mm. This is the minimum width of slot s_2 at which coupled hairpin resonators, shown in Figure 3-13 (b), are critically coupled, i.e. simulated S_{21} of coupled resonators have only one peak at resonant frequency, and the contribution to total coupling by separation spacing s_2 can be neglected. This value has been found by simulating coupled resonators shown in Figure 3-13 (b). Similarly, by simulating the coupled resonators shown in Figure 3-13 (c), it has been found that when the width of slot reaches $s_1 = 2.8$ mm resonators become critically coupled. Therefore, the width of slot s_3 of the structure shown in Figure 3-13 (e) was chosen to be 2.8 mm and contribution to total coupling by separation spacing s_3 can be neglected. The physical length of coupled lines is 22.4 mm for resonators shown in Figure 3-12 (a-c), 21 mm for resonators shown in Figure 3-12 (d), and 20.8 mm for resonators shown in Figure 3-13 (e). This difference occurred due to the condition that all resonators should have the same electrical length and the length of coupled lines is chosen to be as long as possible, approaching 90º.

Simulated S_{21} of all resonators shown in Figure 3-13 are shown in Figure 3-14.

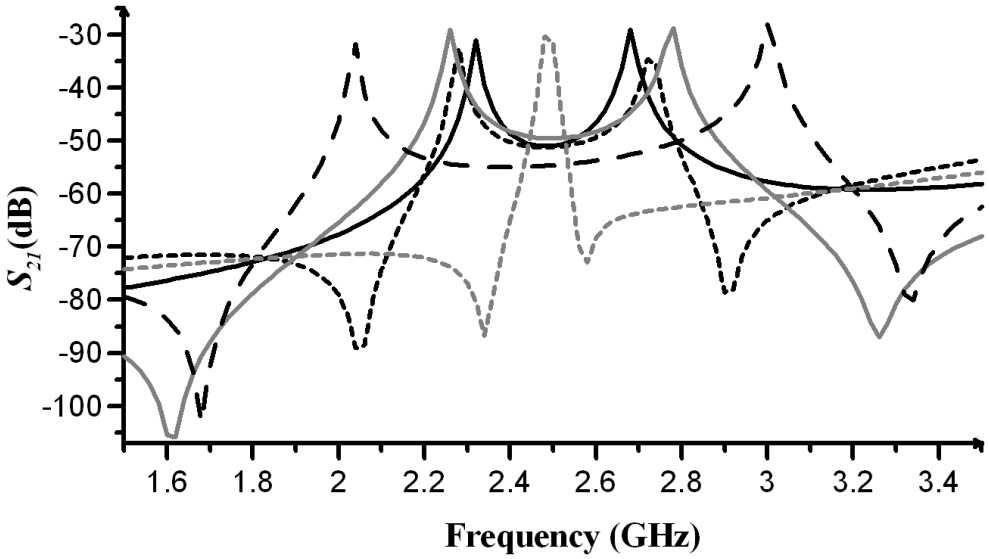

Figure 3-14: Simulated S_{21} of resonators: Pseudo-interdigital (black dotted); Hairpin (black solid); Coupled through Slot s_1 (grey solid); Coupled through slots s_1 and s_3 (black dashed); Coupled through slots s_1 and s_2 (grey dotted).

At first, it can be seen that all coupled resonators which contribute to total coupling by the separation spacing s_1 or s_3 i.e. all coupled resonators except conventional coupled hairpin resonators, have TZs at finite frequencies higher and lower resonant peaks. The TZ conditions of lines coupled as it is shown in Figure 3-13 (a) and (c) have been approximately derived in sections 3.2.2 and 3.2.1 respectively.

It also can be seen that the coupling coefficients, which can be found using formula derived in [19], are different for all structures. The coupling coefficient can be calculated using following Eq. (2.37) to obtain the coupling coefficient from the frequencies of high and low resonant peaks f_h and f_l. Eq. (3.27) can be used only in case when $f_h > f_l$, i.e. simulated coupled resonator have two resonance modes.

Eq. (2.37) is used to obtain the coupling coefficient of synchronously tuned resonators, i.e. resonators with equal resonant frequencies. Stronger coupling occurs when resonant peaks occur further from each other and therefore the strongest coupling is between resonators coupled through slots s_1 and s_3 for the coupled resonators shown in Figure 3-13 (d).

The simulated and calculated coupling coefficients of structures shown in Figure 3-13, as a function of the length of coupled lines, are shown in Figure 3-15.

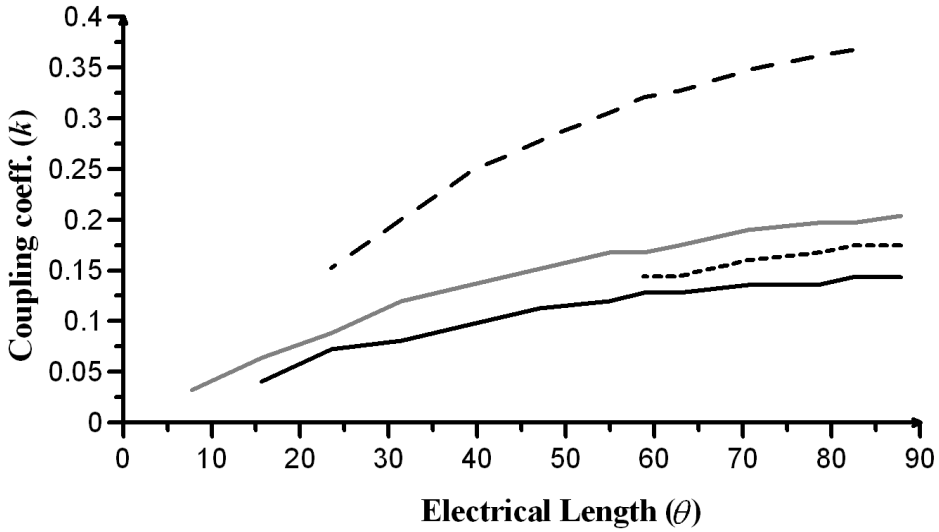

Figure 3-15: Simulated and calculated coupling coefficient as a function of θ: Pseudo-interdigital (black dotted); Hairpin (black solid); Coupled through slot s_1 (grey solid); Coupled through slots s_1 and s_3 (black dashed).

The coupling coefficient of resonators coupled in the way shown in Figure 3-13 (e) for all lengths θ is equal to $k_e \approx 1/Q$, i.e. $k_e \approx 0.009$ as the Q factor of these resonators is equal to 117 and resonators are critically coupled. The following approximate assumptions can be made from Figure 3-15.

First, the coupling coefficient k_d of resonators coupled through slots s_1 and s_3, as it is shown in Figure 3-13 (d), is approximately twice the coupling coefficient k_c of resonators coupled by separation spacing s_1 only, which is shown in Figure 3-13 (c), i.e. $k_d \approx 2k_c$. This assumption is based on the identical physical nature of coupling through slots s_1 and s_3, and a combination of couplings by slots s_1 and s_3 can be considered as a sum of coupling caused by each of these slots separately.

The second assumption is that couplings due to slots s_1 and s_2 are opposite in sign and cancel each other and the combination of both couplings has a very small value, as it has been observed for resonators shown in Figure 3-13 (e) which are critically or even loosely coupled, i.e. $k_e \approx k_1 - k_2 \approx 0.009$. The coupling coefficient k_a of pseudo-interdigital resonators, shown in Figure 3.13(a), can be approximately considered as:

$$k_a = k_1 + k_3 - k_2 \tag{3.28}$$

where the subscript of the coupling coefficient corresponds to the subscript of the separation slots. It should be noted that these assumptions are approximate because although all resonators shown in Figure 3.13 are equal in length, the length of the coupled line region is different for each pair of coupled resonators. Thus, coupling coefficient k_d, is about 0.02 to 0.03 smaller than $2k_c$ and the difference between coupling of pseudo-interdigital resonators k_a and coupling due to slots s_1 and s_3 minus coupling due to slot s_2, i.e. $k_d - k_b$ is about 0.04 to 0.05.

3.4. Summary

In this chapter analysis of coupled pseudo-interdigital lines and resonators is presented.

In section 3.2 the lines and resonators are analyzed in order to find out the dependence of TZ frequencies on physical dimensions of the resonators and lines. Using impedance matrices and some approximations for coupled microstrip lines, it has been found that, with an approximation of about 7%, the frequencies at which pseudo-interdigital lines and resonators are completely decoupled, depend mainly on the length of coupled lines. The EM simulations have been used to investigate the effect of other parameters, such as the width of coupling slots between resonators, and between resonators and feeding lines, on TZ frequencies.

In section 3.3 the coupling between pseudo-interdigital resonators is analyzed. EM simulators and Eq. (3.28) have been used to investigate the coupling nature and to find the effect of width of slots between resonators' arms on coupling coefficient. Other dimensions do not have much influence on coupling between resonators. It has been found that coupling due to the separation of slots s_1 and s_3 is opposite in sign to the coupling due to separation slot s_2. Using this fact, wide range in couplings can be achieved by manipulating the width of these slots.

3.5. References

[3-1] J. S. Hong and M. J. Lancaster, "Development of new microstrip pseudo-interdigital bandpass filters," *IEEE Microwave and Guided Wave Lett.,* vol. 5, no. 8, pp. 261-263, August 1995

[3-2] E. G. Cristal and S. Frankel, "Hairpin-Line and Hybrid Hairpin-Line/Half-Wave Parallel-Coupled-Line Filters," *IEEE Trans. on Microwave Theory and Tech.,* vol. 20, no. 11, pp. 719-728, November 1972

[3-3] D. G. Swanson, Jr., "A novel method for modeling coupling between several microstrip lines in MIC's and MMIC's," *IEEE Trans. on Microwave Theory and Tech.,* vol. 39, no. 6, pp. 917-923, June 1991

[3-4] T. Chih-Ming, L. Sheng-Yuan, and L. Hong-Ming, "Transmission-line filters with capacitively loaded coupled lines," *IEEE Trans. on Microwave Theory and Tech.,* vol. 51, no. 5, pp. 1517-1524, May 2003

[3-5] D. Gao Le, Z. Xiu Yin, C. Chi Hou, X. Quan, and X. Ming Yao, "An Investigation of Open- and Short-Ended Resonators and Their Applications to Bandpass Filters," *IEEE Trans. on Microwave Theory and Tech.,* vol. 57, no.9 pp. 2203-2210, September 2009

[3-6] *Sonnet EM Suite,* Sonnet Software Inc., Liverpool, NY.

[3-7] S. B. Cohn, "Parallel-Coupled Transmission-Line-Resonator Filters," *IRE Trans. on Microwave Theory and Tech.,* vol. 6, no. 2, pp. 223-231, April 1958

[3-8] G. I. Zysman and A. K. Johnson, "Coupled Transmission Line Networks in an Inhomogeneous Dielectric Medium," *IEEE Tran. on Microwave Theory and Tech.,* vol.69, no.1, pp. 329- 337, May 1969

[3-9] D. M. Pozar, *Microwave engineering*. 3rd edition, New York: John Wiley & Sons, 2004

[3-10] S. Sheng and Z. Lei, "Wideband microstrip bandpass filters with asymmetrically-loaded interdigital coupled lines," *Int. Conf. on Microwave and Millimeter Wave Tech.*, Nanjing, China, April 2008, pp.10-13

[3-11] S. J. Hedges and R. G. Humphreys, "An Extracted Pole Microstrip Elliptic Function Filter using High Temperature Superconductors," *24th European Microwave Conference*, Cannes, France, September 1994 pp. 517-521

[3-12] J. G. Hong and M. J. Lancaster, *Microstrip Filters for Rf/Microwave Applications*, New York: John Wiley & Sons, 2001

[3-13] M. Horno and F. Medina, "Multilayer Planar Structures for High-Directivity Directional Coupler Design," *IEEE Trans. on Microwave Theory and Tech.,* vol.86, no.1, pp. 283- 286, June 1986

[3-14] W. Wen, J. S. Fu, L. Yilong, and X. Yong Zhong, "A compact bandpass filter using folded lambda/4 coupled-line resonators," *Int. Conf. on Microwave and Millimeter Wave Tech.*, Nagoya, Japan, October 2004.

[3-15] T. Chih-Ming, L. Sheng-Yuan, C. Chia-Cheng, and T. Chin-Chuan, "A folded coupled-line structure and its application to filter and diplexer design," *IEEE MTT-S, Int. Microwave Symp. Dig.,* vol.3, pp.1927-1930, June 2002

[3-16] T. Edwards, *Foundations for microstrip circuit design*. 2nd edition, Chichester, U.K.: John Wiley & Sons, 1991

[3-17] J. S. Wong, "Microstrip Tapped-Line Filter Design," *IEEE Trans. on Microwave Theory and Tech.,* vol.27, no.1, pp. 44- 50, January 1979

[3-18] J. S. Hong and M. J. Lancaster, "Investigation of microstrip pseudo-interdigital bandpass filters using a full-wave electromagnetic simulator," *Int. J. Microwave and Millimeter-Wave Computer-Aided Engineering,* vol. 7, pp.231-240, May 1997

[3-19] J. S. Hong and M. J. Lancaster, "Couplings of microstrip square open-loop resonators for cross-coupled planar microwave filters," *IEEE Trans. on Microwave Theory and Tech.,* vol.44, no.11, pp.2099-2109, November 1996

4. COMPACT PSEUDO-INTERDIGITAL BANDPASS FILTERS

4.1. Introduction

A pair of pseudo-interdigital resonators, investigated in the previous chapter, has two transmission zeros, appearing below and above fundamental resonance frequency due to the nature of coupling. This, together with very compact size, makes these resonators very attractive for the design of compact bandpass filters with improved skirt selectivity. One of the designs consists of three pairs of pseudo-interdigital resonators, together with the concept of development of these resonators from interdigital resonators, was proposed in [4-1]. The main challenge in design of pseudo-interdigital filters is determine the dimensions of the resonators from the required bandwidth and central passband frequency. This can be done by cut-and-try method using modern EM simulators. A more constructive approach, which will be described further in this chapter, is based on the image parameter method (IPM) applied to distributed structures [4-2]. This approach proposes application of IPM directly to distributed microwave structure without consideration of the lumped prototype. This is a more flexible design procedure in which technological constraints can be easily incorporated. As this method solely relies on the accuracy of modelling of distributed structures, EM simulators are used for modelling, as well as for the final tuning and optimization of filters obtained using IPM.

In this chapter, the development of compact microstrip bandpass filter that consists of one pair of pseudo-interdigital resonators is presented. This design approach is based on the image parameter design of parallel-coupled transmission-line-resonator bandpass filters. Bandpass characteristics of image impedance of parallel-coupled microstrip lines are described in the section 4.2. Section 4.3 presents the image parameter design of second order parallel-coupled transmission-line-resonator bandpass filter using procedures described in [4-3], [4-4]. This is technology-driven procedure, and therefore the width of microstrip resonators has been chosen to be equal to 0.2 mm, which is the smallest width of the line realizable with available manufacturing

facilities. In section 4.4 design of hairpin bandpass filter, which is a modification of filter designed in previous section is presented. In this filter the parallel-coupled resonators are bent to form U-shaped hairpin resonators. This is an intermediate step in the design of pseudo-interdigital bandpass filter, in which two intertwined hairpin resonators are used. Section 4.5 presents the design of compact pseudo-interdigital bandpass filter. The results from investigations the dependence of coupling coefficient and transmission-zero frequencies of coupled pseudo-interdigital resonators on the physical dimensions, discussed in previous chapter, were used to design the bandpass filter of required bandwidth with good skirt selectivity, improved by transmission zeros occurred at finite frequencies below and above the passband of the filter.

4.2. Image Impedance of Coupled Microstrip Lines

The impedance matrix of two coupled microstrip lines with ports 2 and 4 open-circuited, as shown in Figure 4-1 (a) has been used in the previous chapter to derive the condition of transmission zeros that occur due to the physical nature of coupling.

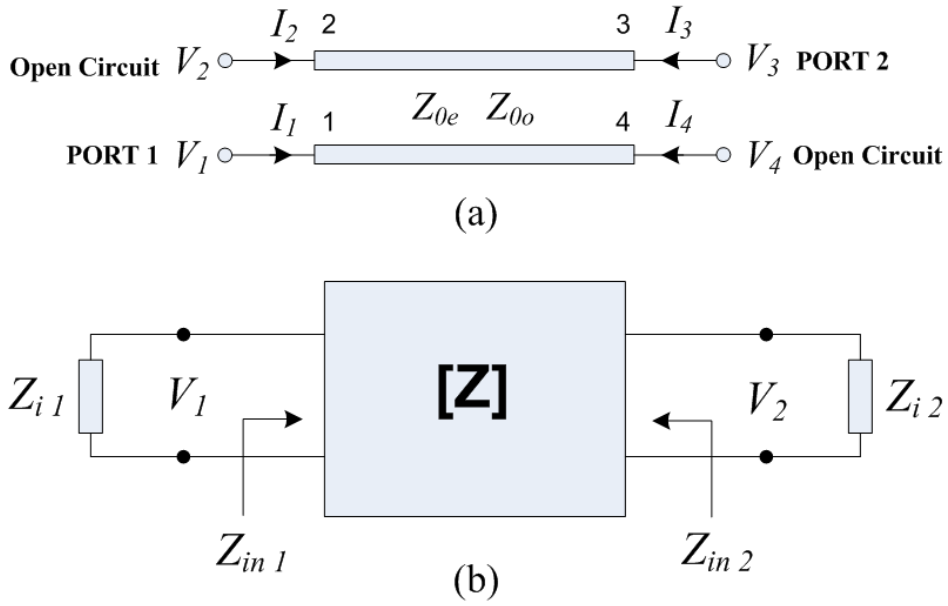

Figure 4-1: (a) Coupled microstrip lines; (b) two port network terminated in its image impedance.

With approximation $\theta_e = \theta_o = \theta$, and using Eq. (3-1)-(3-4), the impedance matrix of coupled lines presented as 2-port network, as is shown in Figure 4-1 (b), is equal to:

$$[Z] = -j\frac{1}{2}\begin{bmatrix} (Z_{0e}+Z_{0o})\cot\theta & (Z_{0e}-Z_{0o})\csc\theta \\ (Z_{0e}-Z_{0o})\csc\theta & (Z_{0e}+Z_{0o})\cot\theta \end{bmatrix} \tag{4-1}$$

The electrical length θ in (4-1) can be replaced by arithmetic or geometric mean of even and odd mode lengths in order to find the electrical length of microstrip coupled lines.

The bandpass performance of coupled lines can be derived using the concept of image impedances. Image impedance Z_{i1}, shown in Figure 4-1 (b), is an input impedance at

port 1 when port 2 is terminated with Z_{i2} and visa–versa. If both ports of 2-port network are terminated with their image impedances, they are matched.

The image impedance of coupled microstrip lines can be found using formulas (4-2) to obtain image impedances of general two-port network from its impedance matrix [4-4]. It is clear that for symmetrical network image impedances are equal.

$$Z_{i1} = \sqrt{\frac{Z_{11}}{Z_{22}}\det[\mathbf{Z}]} \qquad Z_{i2} = \sqrt{\frac{Z_{22}}{Z_{11}}\det[\mathbf{Z}]} \tag{4-2}$$

By applying Eq. (4-1) and (4-2) the image impedance of a section of coupled microstrip line is:

$$Z_{i1} = Z_{i2} = \sqrt{\det[\mathbf{Z}]} = \sqrt{\left(\frac{Z_{0e}+Z_{0o}}{2}\right)^2 - \frac{Z_{0e}Z_{0o}}{\sin^2(\theta)}} \tag{4-3}$$

Figure 4-2 illustrates the real and imaginary parts of the image impedance of coupled lines, given by (4-3). It is calculated for even mode impedance $Z_{0e} = 186.67\ \Omega$ and odd mode impedance $Z_{0o} = 112.3\ \Omega$. The electrical length of coupled lines is calculated using the arithmetic mean of even-odd mode effective dielectric constant, from 60º to 120º. Image impedance is normalized to $(Z_{0e} - Z_{0o})/2$, which is the value of image impedance at $\theta = \pi/2$

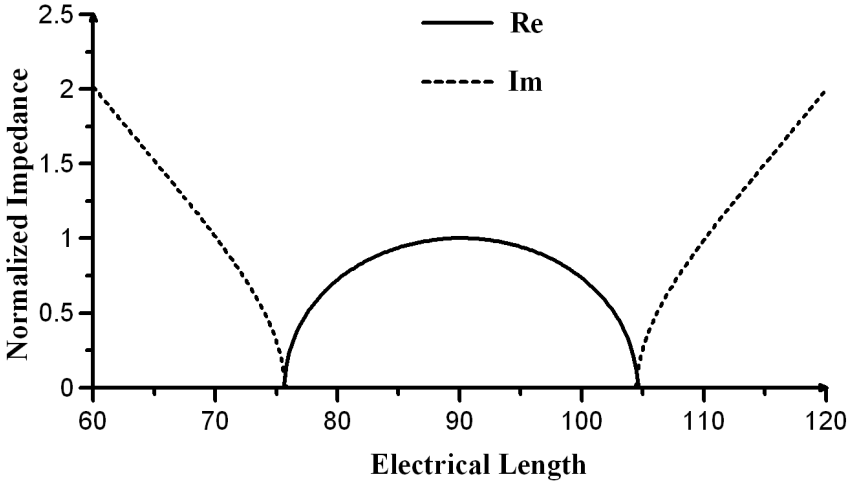

Figure 4-2: Normalized image impedance of coupled lines.

The coupled-line section has an image passband when the image impedance is real and from Eq. (4-3) this condition can be derived as:

$$\sin^2(\theta) \geq 4\frac{Z_{0e}}{Z_{0o}}\left(\frac{Z_{0e}}{Z_{0o}}+1\right)^{-2} \tag{4-4}$$

As sine is a periodic function, there is infinite number of sets of solutions of (4-4). Each of them is symmetrical with respect to $\theta = (2n-1)\pi/2$, which corresponds to the length of the coupled lines equal to odd multiples of quarter wavelength. For the fundamental passband two boundary values of θ are:

$$\theta_1 = \sin^{-1}\left[2\sqrt{\frac{Z_{0e}}{Z_{0o}}}\left(\frac{Z_{0e}}{Z_{0o}}+1\right)^{-1}\right], \qquad \theta_1 < \frac{\pi}{2} \tag{4-5}$$

$$\theta_2 = \pi - \theta_1 \tag{4-6}$$

For the image impedance shown in Figure 4-2 $\theta_1 \approx 75.6^\circ$ and $\theta_2 \approx 104.4^\circ$, and the relative image passband width is:

$$w_I = \frac{\theta_2 - \theta_1}{\pi/2} = 2 - \frac{4}{\pi}\sin^{-1}\left[2\sqrt{\frac{Z_{0e}}{Z_{0o}}}\left(\frac{Z_{0e}}{Z_{0o}}+1\right)^{-1}\right] \tag{4-7}$$

As it can be seen from Eq. (4-7), the relative image passband width depends only on the ratio of even to odd mode impedances. Therefore any relative passband width can be achieved by properly defining even and odd mode impedances of coupled lines, and only practical realization of these lines limits the passband width to some maximally achieved value, which varies for different substrates of microstrip.

4.3. Design of Parallel-Coupled Microstrip Bandpass Filter Using Image Parameter

The parallel-coupled transmission-line-resonator filter proposed in [4-5] is still one of the most popular microstrip transmission line filters used for the design of narrow and moderate bandwidth filters. The implementation of this filter is very cheap as it does not require such assembly operations as via holes or bond wire connections. The design procedure for this filter is well known and formulas, used to determine the even and odd impedances of coupled lines from the bandwidth of the filter and values of elements of used prototype, give good results for fractional bandwidth (FBW) up to about 30%. For wider bandwidth, the synthesis formulas give less accuracy and the coupling between the two lines of the first and last sections of coupled lines is so tight that it becomes unpractical for realization. One of the methods proposed to improve the bandwidth is to replace the end-coupled line sections by quarter-wavelength transformers [4-6].

The design of microstrip parallel-coupled transmission-line-resonator filters using the image parameter proposed in [4-3] can be used for the development of moderate and wideband bandpass filters avoiding the fabrication problems of the conventional design approach. The image parameter method can be applied directly to coupled microstrip lines without any consideration of lumped prototype. The design procedure proposed in [4-3], [4-4] is applied further to design a second order parallel-coupled transmission-line-resonator bandpass filter with FBW 25% and the central frequency 3.8 GHz. The development of this filter is the first step in the design of very compact pseudo-interdigital bandpass filter. The order of the designed filter is two because the proposed pseudo-interdigital filter consists of a pair of pseudo-interdigital resonators and the selectivity of second order parallel coupled bandpass filter will be improved by the introduction of transmission zeros, as will be shown in section 4.5.

The image parameter method can be considered as technology driven and can be used to design bandpass filters with wide passbands that can be realized with manufacturing limits in fabrication of narrow lines and tight gaps. In order to design the super compact pseudo-interdigital bandpass filter, the width of coupled line has been chosen to be

0.2 mm, which for a substrate with dielectric constant $\varepsilon_r = 2.2$ and thickness $h = 0.78$ mm will have characteristic impedance of $152.15\,\Omega$. Therefore, the filter specifications $f_0 = 3.8$ GHz, FBW equal to 25%, $N = 2$ will have additional starting parameter - width of the coupled lines $w = 0.2$ mm and the substrate with parameters given above.

From Eq. (4-7) the ratio of even to odd mode impedances from known relative image passband width w_I can be found as:

$$\frac{Z_{0e}}{Z_{0o}} = \left[\frac{1 + \sin\left(\frac{\pi w_I}{4}\right)}{\cos\left(\frac{\pi w_I}{4}\right)} \right]^2 \tag{4-8}$$

As at θ_1 and θ_2 the image impedance is zero, then FBW of the filter should be always smaller than the relative image passband and can be expressed as:

$$FBW = w_I / \delta \tag{4-9}$$

where δ is a margin factor, which is bigger than one. Using (4-8) and taking the relative image passband to be 30% , and a margin factor of 1.2, the even to odd mode impedance ratio will $Z_{0e}/Z_{0o} \approx 1.6$. ADS Linecalc was used to find the width of the slot between two coupled 0.2 mm wide microstrip lines, such that even to odd mode impedance ratio will be equal to 1.6. After a few iteration it has been found that coupled microstrip lines with slot width equal to 0.6 mm, have even mode impedance $Z_{0e} = 186.3\ \Omega$ and odd mode impedance $Z_{0o} = 113.8\,\Omega$ and even to odd mode impedance ratio is equal to 1.63.

The next step is to find the length of coupled line section, which should correspond to electrical length of 90º at the center frequency f_0 or, in other words, to be equal to a quarter of wavelength at this frequency. As the formula for wavelength for microstrip lines includes effective dielectric constant, and microstrip coupled lines have two modes of propagation with different dielectric constants, the arithmetic or geometric

mean of these two constants should be used to find the approximate wavelength. For our coupled line arithmetic and geometric means are almost equal and the arithmetic mean will be used in further calculations.

$$l = \frac{\lambda_g}{4} - \Delta l_o = \frac{c}{4 f_0 \sqrt{(\varepsilon_{effe} + \varepsilon_{effo})/2}} - \Delta l_o \tag{4-10}$$

where Δl_o denotes the equivalent length of microstrip open end and can be found using an approximate expression of extension length of single microstrip line [4-7]:

$$\Delta l_o = 0.412h\left(\frac{\varepsilon_{eff} + 0.3}{\varepsilon_{eff} - 0.258}\right)\left(\frac{w/h + 0.262}{w/h + 0.813}\right) \tag{4.11}$$

Using Eq. (4-10)-(4-11) the length will be $l \approx 15$ mm. This length has been tuned and it was found that 14.8 mm long parallel-coupled lines can be used to design a filter with passband centered at about 3.84 GHz.

The last step is to add the impedance transformers to the end-coupled sections. The impedance of transformer is found using formula:

$$Z_T = \sqrt{Z_0 Z_{\mathrm{Im}}} \tag{4-12}$$

where Z_0 is 50 Ω and Z_{Im} is maximum image impedance at the mid-band frequency equal to:

$$Z_{\mathrm{Im}} = (Z_{0e} - Z_{0o})/2 \tag{4-13}$$

The length of impedance transformer is found using Eq.(4-10)-(4-11) with effective dielectric constant of transformer's. The impedance of transformer is 44.16 Ω, with corresponding width of the line equal to 2.86 mm and the length to 13.4 mm.

The layout of designed second order parallel-coupled microstrip bandpass filter with impedance transformers is shown in Figure 4-3.

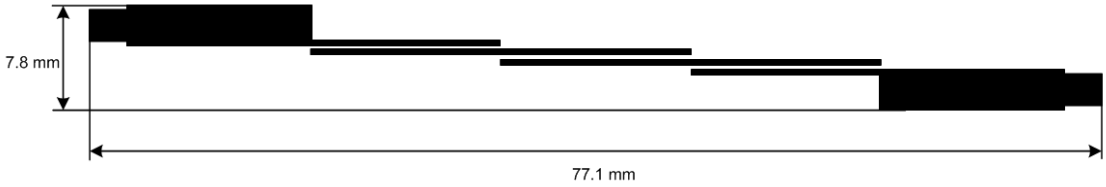

Figure 4-3: Layout of parallel-coupled bandpass filter with impedance transformers.

The simulated S-parameters of designed filter simulated using ADS Momentum are shown in Figure 4-3 (a). Filter has 0.7 dB insertion loss and 15 dB return loss. Figure 4-4 (b) shows the simulated S-parameters of filter without impedance transformer.

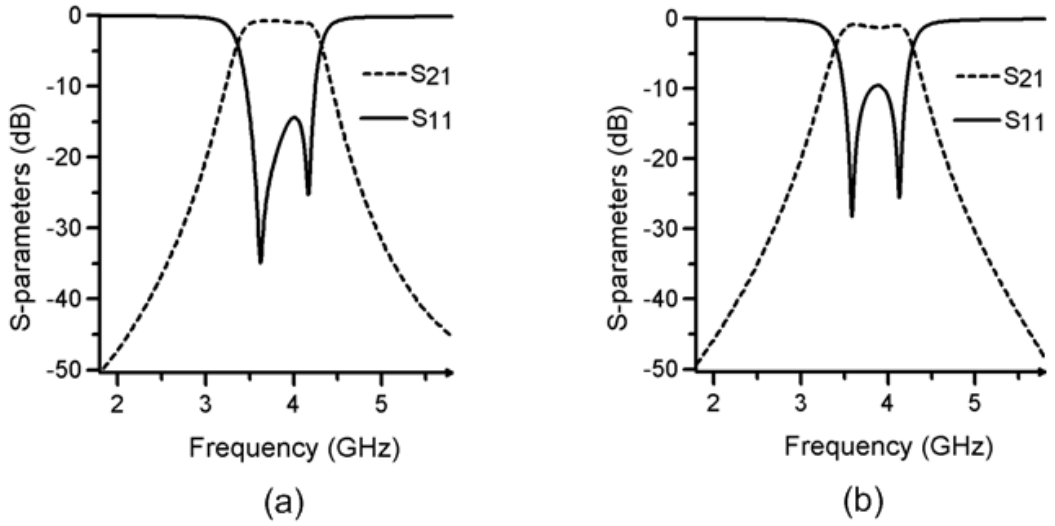

Figure 4-4: Simulated S-parameters of edge-coupled filter: (a) with impedance transformer; (b) without impedance transformer.

It can be seen from Figure 4-4 (b) that filter without impedance transformer is not optimized and has larger insertion loss and smaller return loss. The FBW of the filter without transformer is about 22.8% and in order to achieve 25% bandwidth, the gap between all coupled lines should be decreased from 0.6 mm to 0.5 mm. By doing this, a bigger even to odd mode impedance ratio will be achieved. Therefore, the simple rule, for the image parameter design of coupled-lines filter, which also can be obtained from Eq. (4-7), is to increase the even to odd mode impedance ratio in order to increase the bandwidth of the filter. This is achieved only by decreasing the gap between the coupled lines or, in the other words, by increasing the coupling between the resonators.

4.4. Design of Hairpin Microstrip Bandpass Filter

The hairpin bandpass filter introduced in [4-8] is a modification of the conventional parallel-coupled bandpass filter with resonators bent to form U-shaped resonators that look like a hairpin. Analysis and design of these filters are based on the sparse induction matrix assumption, as in the original paper, or the sparse capacitance matrix, as it was presented in [4-9]. Both these approaches provide satisfactory approximation for the design of hairpin filters with open circuited feeding line with FBW up to 20-25%. The conventional design approaches of hairpin filters have inherited the limit in the realization of a wide bandwidth filter due to a very small width of slot between the feeding lines and the edge resonators.

In this section, the hairpin bandpass filter will be designed as a modification of filter presented in previous section in order to design compact technology-driven filter. As second order bandpass filter has poor out-of-band insertion loss the design presented here will be used as an intermediary step in the design of pseudo-interdigital bandpass filter in which out-of-band rejection will be improved by the appearance of the transmission zeros at finite frequencies above and below the passband.

The first step is the extraction of the coupling coefficient of resonators of parallel-coupled bandpass filter designed above. As this filter consists of two identical coupled $\lambda_g/2$ resonators with feeding through coupled lines and has no finite frequency attenuation poles, the synthesized network of this filter can always be described by three constants: center frequency f_0, coupling coefficients $K_{r(r+1)}$ between resonators r and $(r+1)$, and the decrement of resonator r or Q factor $Q_r = 1/d_r$ [4-10]. The unloaded Q factors of hairpin and simple $\lambda_g/2$ resonators can be found using simulations and equation (2.25). The Q factor of straight line resonators used in the design of edge-coupled filters is 117, whereas the Q factor of hairpin resonators, that will be used later, is 113. This small decrease in the unloaded Q factor is caused by additional radiation losses due to additional discontinuities.

The coupling coefficient of coupled resonators of parallel-coupled filter is found using Eq. (2.37) and simulating the structure shown in Figure 4-3 with impedance transformer and feeding through coupled line replaced by end-coupled feeding. Using low and high resonance frequencies and Eq. (2.37) the coupling coefficient is found to be equal to 0.137.

The layout of hairpin bandpass filter is shown in Figure 4-5. The length of the resonator is $\lambda_g/2$ or $L \approx \lambda_g/4$, the width of the slot *s* is found from the design curve in order to obtain the coupling coefficient equal to the coupling of resonator in the parallel-coupled filter. The length of connecting line L_c also called arm separation in most practical realizations is about five dielectric thicknesses [4-11]. From one side, the arm separation should be increased in order to minimise self-coupling of both arms of the resonators, which is happening because voltages at opposite ends of the hairpin resonator are in antiphase. But the arm separation cannot be made as big as possible because in this case the length of coupled lines will be short and in order to achieve the same coupling the slot, *s* should be very small. Thus, a good compromise should be found.

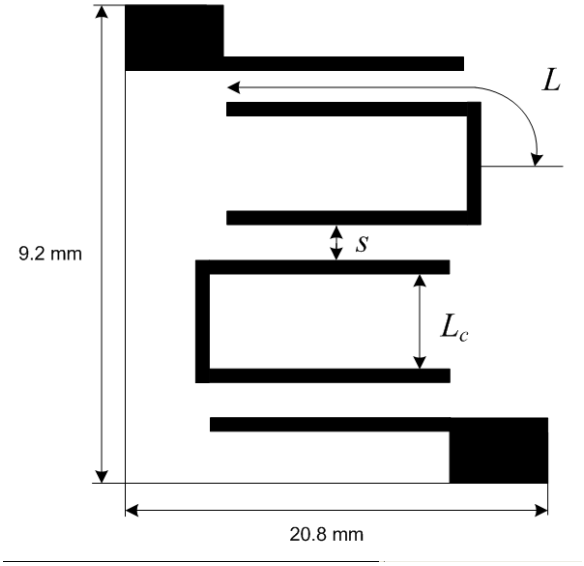

Figure 4-5: Layout of hairpin bandpass filter.

The length of the connecting line has been chosen to be 1.2 mm, or six times the width of resonators' line as it will keep the length of coupled lines almost equal to the length in the edge coupled filter. Using the design curve, shown in Figure 4-6, we can get the

width of slot s between the resonators. This design curve was obtained by the full wave EM simulation of a pair of coupled hairpin resonators to extract the coupling coefficient against the width s of the gap between coupled lines. From this curve it is found that when the slot width is 0.4 mm the coupling between hairpin resonators is equal to 0.133. This slot width can be used as a starting value for our design in order to obtain coupling between hairpin resonators equal to coupling between parallel-coupled resonators used in the design of filter described in section 4.3. The same slot width has been chosen as a starting value for the slot between feeding lines and resonators.

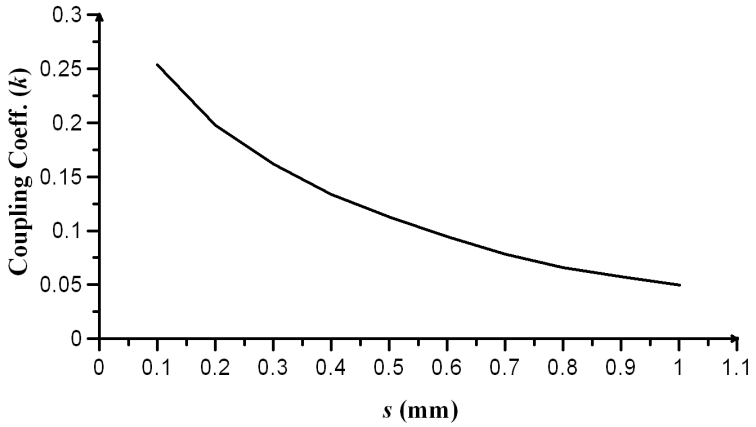

Figure 4-6: Coupling coefficients of hairpin resonators.

Hairpin filter with $L = 14.8$ mm, $L_c = 1.2$ mm, and $s = 0.4$ was simulated using ADS Momentum. The simulated S-parameters are shown in Figure 4-7. The filter has central frequency 3.81 GHz, FBW 25 %, insertion loss 1.1 dB and return loss 13.3 dB.

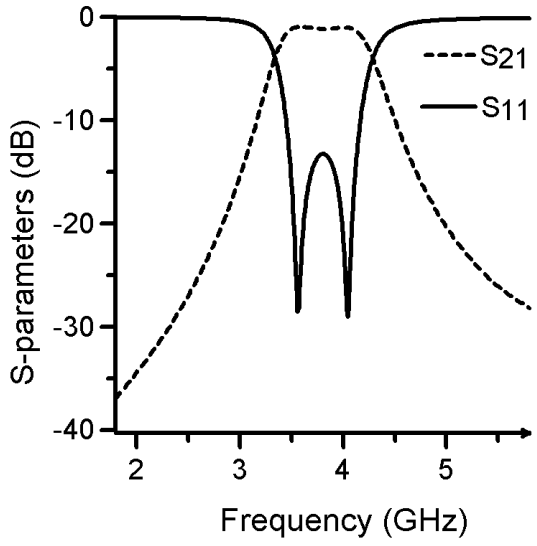

Figure 4-7: Simulated S-parameters of hairpin filter.

4.5. Design of Compact Pseudo-Interdigital Microstrip Bandpass Filter

the design of compact pseudo-interdigital bandpass filter is based on the use of two intertwined hairpin resonators in the way they have coupling due to three parallel-coupled sections. The resonators proposed in [4-1] and analysed in [4-12] were called pseudo-interdigital resonators, as they are similar to interdigital resonators with grounding replaced by interconnections of $\lambda_g/4$ resonators. The currents distribution of these resonators at resonance is similar to the current distribution of interdigital resonators.

The layout of compact bandpass filter designed using a pair of pseudo-interdigital resonators is shown in Figure 4-8. The main design parameters are the length *L*, width of the line *w*, and widths of slots s_1, s_2, and s_f . As it was discussed in the previous chapter, coupling due to separation s_2 is equivalent to coupling or resonators in hairpin bandpass filter and opposite in sign to the coupling due to separations s_1. Slot width s_f controls the coupling to feeding lines. In design of conventional parallel-coupled and hairpin bandpass filters small s_f is the main problem in the development of moderate and wideband filters. The length is $L \approx \lambda_g/4$, the same as in the hairpin filter, the width $w = 0.2\,\text{mm}$ also has been chosen to be the same.

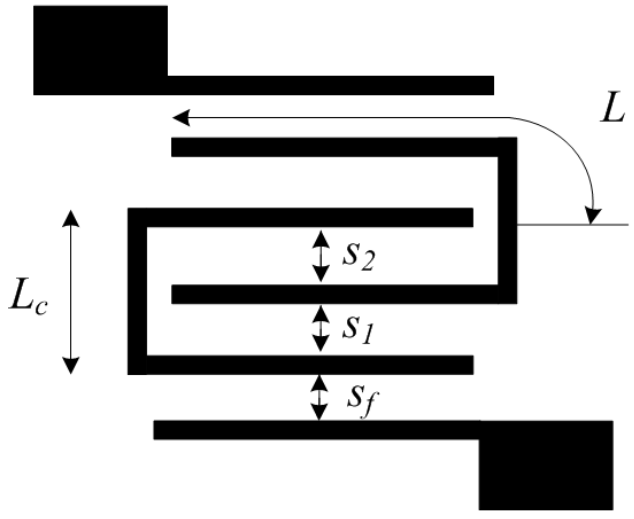

Figure 4-8: Layout of pseudo-interdigital bandpass filter.

To design the bandpass filter with FBW=25%, all three slots' widths described above should be determined. First the slot width s_1 and s_2 which control the coupling between resonators should be found. The simplest option is to set $s_1 = s_2$ and to extract using EM simulation the coupling coefficient in terms of the slot width and to build design curve. Figure 4-9 illustrates the design curve for resonators with width of the line 0.2 mm and total length 31 mm. The total length of resonators is constant and the length of coupled lines section decreases due to the increase of length L_c of interconnecting line, caused by the increase of slots' width.

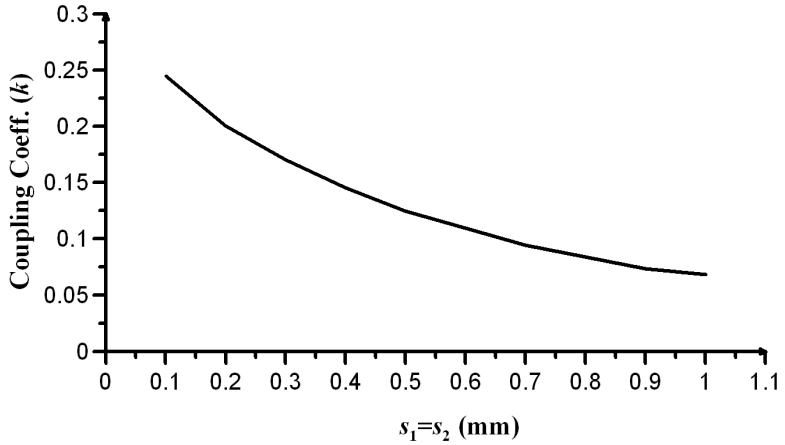

Figure 4-9: Coupling coefficient of pseudo-interdigital resonators.

From Figure 4-9 the width of slots can be found, with which the closest to 0.137 coupling coefficient can be achieved. Due to manufacturing limitations multiples of 0.1mm will be chosen first as initial values for slot widths. The closest is 0.4 mm with which coupling coefficient 0.145 can be achieved. By analogy with parallel-coupled and hairpin bandpass filters, feeding coupling slot s_f has been chosen to be the same as s_1 and s_2. The simulated pseudo-interdigital filter has 21.3 % FBW, 1 dB insertion loss and 11.8 dB return loss in the passband. As the only way to increase bandwidth is to have stronger coupling between resonators, new bandpass filter has been designed with a gap between coupled lines of resonators equal to 0.3 mm. With the same gap between feeding lines bandpass filter has 24.7 % FBW, 0.68 dB insertion loss and 17 dB return loss in the passband. Further modifications in the original design have been made in order to decrease the total filter size and to suppress spurious harmonic at $2f_0$,

that is done by reducing the length of the feeding coupled line. The layout of the developed filter is shown in Figure 4-10.

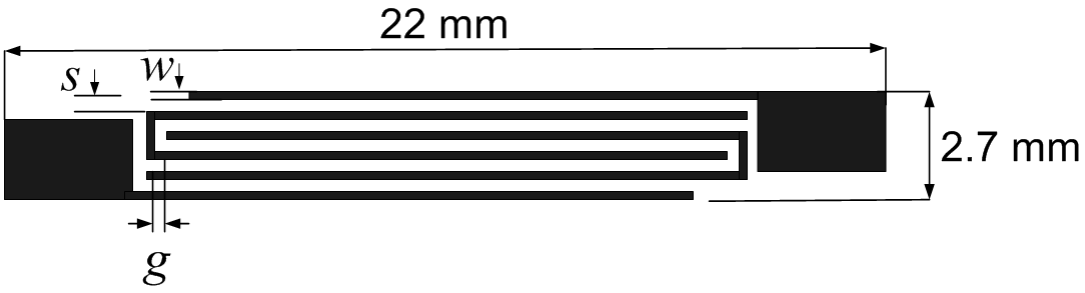

Figure 4-10: Layout of compact microstrip bandpass filter ($w = 0.2$ mm, $s = 0.3$ mm, $g = 0.3$ mm).

The S-parameters of presented filter simulated using ADS Momentum are shown in Figure 4-11 by the dashed lines.

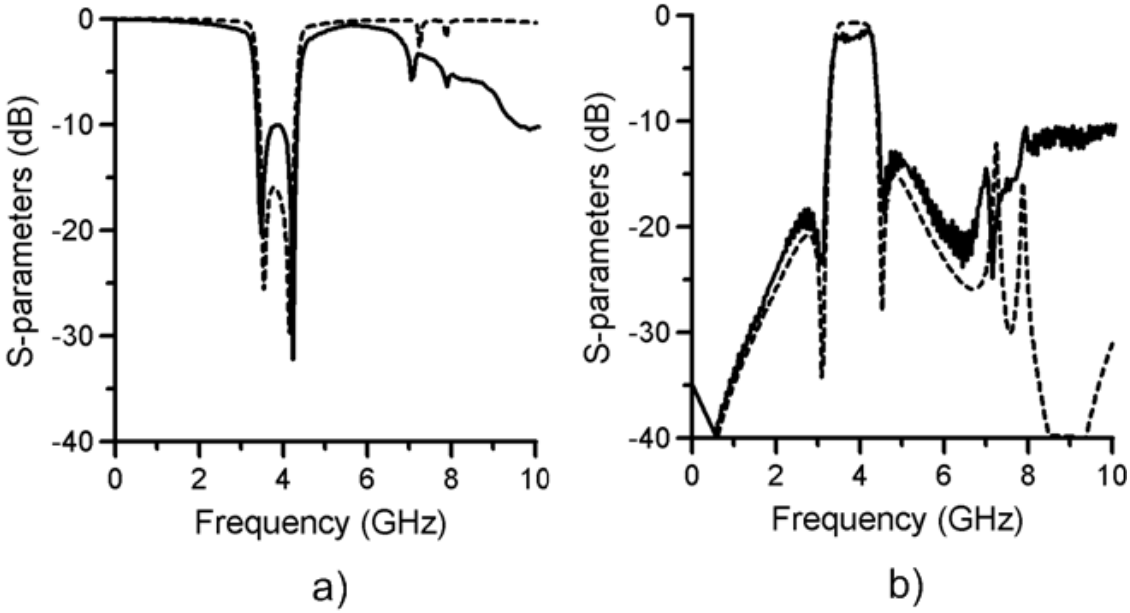

Figure 4-11: Simulated (dashed) and measured (solid) S-parameters of pseudo-interdigital bandpass filter: (a) S_{11} coefficients; (b) S_{21} coefficients

The microstrip bandpass filter was fabricated on 0.762 mm thick Rogers RT/Duroid 5880 ($\varepsilon_r = 2.2$), and measured with Agilent PNA (E8361A) network analyzer [4-13]. A photograph of the fabricated filter is shown in Figure 4-12 and the measured S-parameters of filter are shown in Figure 4-11 by the solid lines.

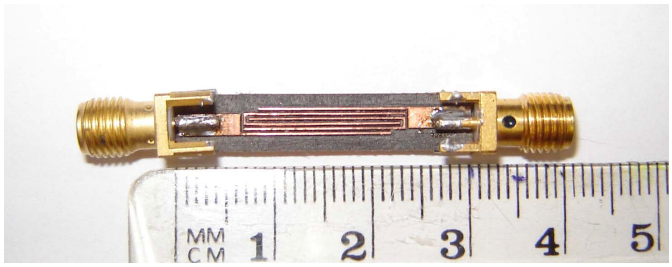

Figure 4-12: Photograph of fabricated bandpass filter.

From Figure 4-11, it can be seen that the frequency shift between simulated and measured S-parameters is minimal. An increase of insertion loss to 2.4 dB and a decrease of return loss to 10 dB at the center frequency is observed and is attributable to imperfect manufacturing and additional losses caused by this. The decrease of measured S_{11} and S_{21} at frequencies above 7 GHz is due to increased radiation losses which at high frequencies are also attributable to manufacturing tolerances. The developed microstrip bandpass filter has size of 22.00 x 2.70 mm at a center frequency of 3.80 GHz, which is approximately $0.25\lambda_g \times 0.04\lambda_g$. The appearance of transmission zeros at 3.13 and 4.5 GHz improve the skirt selectivity of the filter. Thus, the out-of-band insertion loss attributable to the high order bandpass filters is achieved with just two resonators. This feature of the proposed filter, along with its size, which is very close to the width of 50 Ohms line, makes it very attractive for applications in the design of diplexers/multiplexer and antenna filters. The first spurious response of the filter is at $3f_0$, the same as the conventional interdigital bandpass filter. Thus this filter can be used for the design of bandpass filter with improved stopband performance.

Although, due to the complex nature of coupling of resonators, full analysis of this structure is difficult, this filter is easy to develop and the results are easily reproducible. The steps described above, the approximate dimensions of the filter can be found and the final layout can be obtained using EM simulators. As the initial design of the edge-coupled filter is technology-driven, it can be very quickly determined whether the required performance of the filter can be achieved with the existing manufacturing limits on width of microstrip lines and slots. For example, it has been found that using

the same substrate and with the smallest width of line 0.2 mm and gap 0.1 mm compact pseudo-interdigital bandpass filter with FBW up to 40-45 % can be developed.

4.6. Summary

In this chapter design of compact microstrip pseudo-interdigital bandpass filter is presented.

Section 4.2 describes the image impedance of parallel-coupled microstrip lines and image passband limits. As it is derived in this section, the bandwidth of image passband depends solely on the ratio of even to odd mode impedances of the coupled microstrip lines.

Section 4.3 presents the design of second-order parallel-coupled bandpass filters using IPM. In order to implement the limits of manufacturing facilities and to achieve compactness in the final design the width of the microstrip resonators is chosen to be 0.2 mm and the required even to odd mode impedances ratios is achieved by adjusting the width of the slot.

In section 4.4 compact microstrip hairpin bandpass filter is presented. This filter is designed using the bandpass filter presented in section 4.3 with parallel-coupled transmission-line resonators bent to form U-shaped hairpin resonators.

Section 4.5 presents design of compact pseudo-interdigital bandpass filter which consists of a pair of coupled pseudo-interdigital resonators. This filter has very compact size and skirt selectivity improved by the appearance of transmission zeros at finite frequencies below and above the passband.

4.7. References

[4-1] J. S. Hong and M. J. Lancaster, "Development of new microstrip pseudo-interdigital bandpass filters," *IEEE Microwave and Guided Wave Lett.,* vol. 5, no. 8, pp. 261-263, August 1995

[4-2] M. Salerno, R. Sorrentino, and F. Giannini, "Image Parameter Design of Noncommensurate Distributed Structures: An Application to Microstrip Low-Pass Filters," *IEEE Trans. on Microwave Theory and Tech.,* vol.34, no.1, pp. 58- 65, January 1986

[4-3] G. Bianchi, R. Sorrentino, M. Salerno, and F. Alessandri, "Image Parameter Design of Parallel Coupled Microstrip Filters," *18th European Microwave Conference,* Stockholm, Sweden, September 1988, pp.979-984.

[4-4] G. Bianchi, R. Sorrentino, Electronic Filter Simulation & Design. New York: Mc Graw-Hill, 2007

[4-5] S. B. Cohn, "Parallel-Coupled Transmission-Line-Resonator Filters," *IRE Trans. on Microwave Theory and Tech.,* vol. 6, no. 2, pp. 223-231, April 1958

[4-6] P. A. Kirton and K. K. Pang, "Extending the Realizable Bandwidth of Edge-Coupled Stripline Filters," *IEEE Tran. on Microwave Theory and Tech.,* vol. 25, no. 8, pp. 672-676, August 1977

[4-7] T. Edwards, *Foundations for microstrip circuit design*. 2nd edition, Chichester, U.K.: John Wiley & Sons, 1991

[4-8] E. G. Cristal and S. Frankel, "Hairpin-Line and Hybrid Hairpin-Line/Half-Wave Parallel-Coupled-Line Filters," *IEEE Trans. on Microwave Theory and Tech.,* vol. 20, no. 11, pp. 719-728, November 1972

[4-9] U. H. Gysel, "New Theory and Design for Hairpin-Line Filters," *IEEE Trans. on Microwave Theory and Tech.,* vol. 22, no. 5, pp. 523-531, May 1974

[4-10] M. Dishal, "Alignment and Adjustment of Synchronously Tuned Multiple-Resonant-Circuit Filters," *Proceedings of the IRE*, vol.39, no.11, pp.1448-1455, November 1951

[4-11] T. H. Lee, *Planar microwave engineering : a practical guide to theory, measurement, and circuits*. Cambridge, U.K.: Cambridge Univ. Press, 2004

[4-12] J. S. Hong and M. J. Lancaster, "Investigation of microstrip pseudo-interdigital bandpass filters using a full-wave electromagnetic simulator," *Int. J. Microwave*

and Millimeter-Wave Computer-Aided Engineering, vol. 7, pp.231-240, May 1997

[4-13] D. Zayniyev, D. Budimir, and G. Zouganelis, "Super Compact Microstrip Pseudo Interdigital Bandpass Filters," *11th Int. Symp. on Microwave and Optical Tech.,* Monte Porzio Catone, Italy, 17-21 Dec 2007

5. PSEUDO-INTERDIGITAL STEPPED IMPEDANCE BANDPASS FILTERS

5.1. Introduction

Stepped impedance resonators (SIR) are widely used in the design of modern microstrip bandpass filters. The first reported application of SIR was in design of coaxial bandpass filters [5-1], in which SIR were employed to achieve compact size without degradation of the Q factor. Nowadays SIR are used where control over the frequency of the first spurious response is required. The distinguishing feature of SIR is the possibility to shift spurious resonance frequencies by adjusting the impedance ratio R_Z. Thus, on the one hand, SIR are used to tune the second harmonic of bandpass filters to generate two passbands in the design of dual-band bandpass filters [5-2], [5-3]. On the other hand, SIR are employed to push the first spurious passband to higher frequencies to achieve wide stopband of bandpass filters [5-4], [5-5]. The improvement of the stopband performance of bandpass filters can also be achieved by the implementation of elements with bandstop performance. These can be the elements realized on top of the microstrip, such as spur-line, and elements realized in the ground plane, such as the defected ground structures (DGS). These elements are employed to generate stopbands which are tuned to the harmonic frequency of the bandpass filters.

This chapter presents designs of advanced pseudo-interdigital bandpass filters. The key modification in bandpass filter presented in the previous chapter is the implementation of SIR. The description of the fundamental characteristics of SIR is given in section 5.2. Section 5.3 presents the design of compact dual-band SIR pseudo-interdigital bandpass filters. In this filter, SIR are used to shift the spurious passband from $3f_0$ to $2.27f_0$. The designs of single-band bandpass filters with improved stopband are presented in section 5.4. In all bandpass filters, discussed in this section, SIR are employed to shift the first spurious harmonic from $3f_0$ to $3.6f_0$. Section 5.4 is divided into two parts. In the first one, the bandstop performance of spur-line and the open-circuited stub are discussed and the design of the pseudo-interdigital SIR bandpass filter with stopband improved by the inclusion of these two elements is presented. In the second part, DGS structures are analysed and the designs of bandpass filters with stopband improved using DGS spirals are presented.

5.2. Description of Stepped Impedance Resonators

Stepped impedance resonator is a TEM or quasi-TEM mode transmission line resonator that consists of two or more than two lines with a different characteristic impedance [5-6]. The two most popular SIR are short-circuited $\lambda_g/4$ and open-circuited $\lambda_g/2$ resonators that are shown in Figure 5-1. As it can be seen from this figure, the quarter-wavelength SIR consists of the short-ended line with characteristic impedance Z_1 and electrical length θ_1 connected to open-ended line with characteristic impedance Z_2 and electrical length θ_2. This structure can be considered as a fundamental element of SIR and half-wavelength resonators consist of two such elements connected to each other by short-circuited ends with the grounding replaced by this connection.

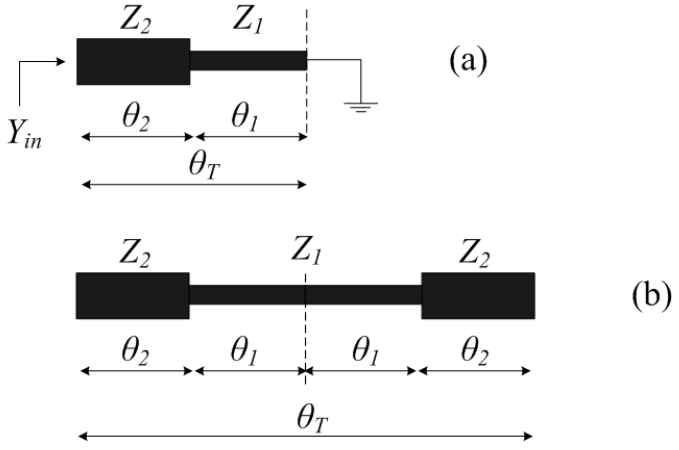

Figure 5-1: Stepped impedance resonators: (a) quarter-wavelength type; (b) half-wavelength type.

The input admittance of $\lambda_g/4$ SIR, shown in Figure 5-1 (a) is equal to:

$$Y_{in} = jY_2 \frac{Y_2 \tan\theta_1 \cdot \tan\theta_2 - Y_1}{Y_2 \tan\theta_1 + Y_1 \tan\theta_2} \tag{5.1}$$

As it was discussed in chapter 2, short-circuited $\lambda_g/4$ resonator behaves like a parallel resonant circuit. The parallel resonance condition $Y_{in} = 0$ of quarter-wavelength SIR will be:

$$\tan\theta_1 \cdot \tan\theta_2 = Y_1/Y_2 = Z_2/Z_1 = R_z \tag{5.2}$$

Eq. (5.2) shows that the resonant condition of SIR is determined by θ_1 , θ_2, and impedance ratio R_Z. Compared to conventional uniform impedance resonators (UIR), analysed in chapter 2, the resonance condition of which is solely determined by the electrical length, SIR have one more extra degree of freedom that can be used in future designs.

The total electrical length of resonator, given in Figure 5-1 (a) as θ_T, for resonant condition (5.2) is equal to:

$$\theta_T = \theta_1 + \theta_2 = \theta_1 + \tan^{-1}\left(R_Z/\tan\theta_1\right) \tag{5.3}$$

Figure 5-2 illustrates the total electrical length of SIR in terms of θ_1 for different impedance ratios R_Z.

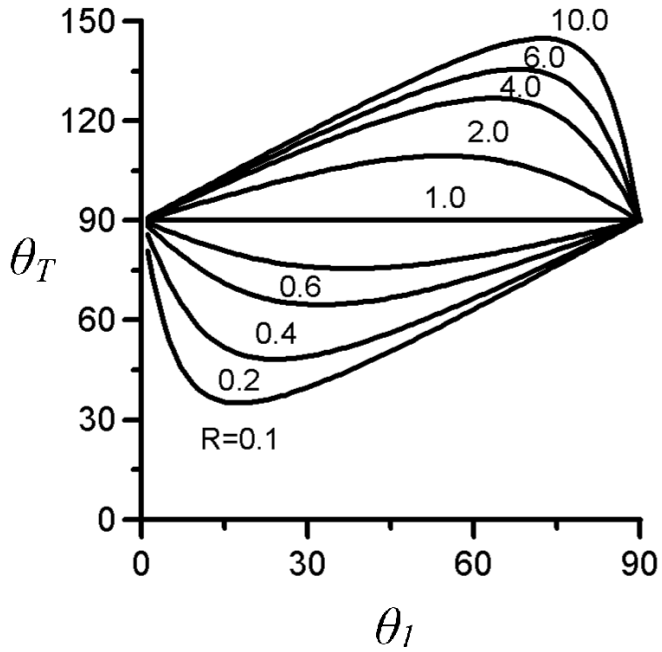

Figure 5-2: Relationship between total electrical length and θ_1 for resonant condition given for different impedance ratios.

As it can be seen, the total electrical length of resonator has maximum value when $R_Z \geq 1$ and minimum value when $R_Z \leq 1$. The condition for these maximum and minimum values has been derived as [5-1]:

$$\theta_1 = \theta_2 = \tan^{-1}\sqrt{R_Z} \tag{5-4}$$

The condition $\theta_1 = \theta_2$ is a special condition which gives the maximum and minimum length of SIR which can be expressed as [5-7]:

$$\theta_{T\min} = \theta_{T\max} = \tan^{-1}\left(\frac{2\sqrt{R_Z}}{1-R_Z}\right) \tag{5-5}$$

Eq. (5-5) provides minimum value for θ_T when $0 < R_Z < 1$ and $0 < \theta_T < \pi/2$, and maximum value for θ_T when $R_Z > 1$ and $\pi/2 < \theta_T < \pi$.

The distinct feature of SIR comparing with UIR is that the resonators' length can be controlled using the impedance ratio R_Z. This can be used to design SIR which are shorter than their UIR counterparts resonating at the same fundamental resonance frequency. In bandpass filter design, SIRs are employed to control the first spurious passband of filters. This is used to design bandpass filters with extended stopband [5-8], as well as to design dual-band bandpass filters [5-9]. The ratio of the first spurious resonance frequency to the fundamental resonance frequency of SIR is given by:

$$\frac{f_S}{f_0} = \frac{\pi}{\tan^{-1}\sqrt{R_Z}} - 1 \tag{5-6}$$

$$\frac{f_S}{f_0} = \frac{\pi}{2\tan^{-1}\sqrt{R_Z}} \tag{5-7}$$

where Eq. (5-6) is the ratio of the quarter-wavelength SIR, for which $f_S/f_0 = 3$ when $R_Z = 1$, and Eq. (5-7) is the ratio of the half-wavelength SIR, for which $f_S/f_0 = 2$

when $R_Z = 1$. Figure 5-3 illustrates normalised spurious resonance frequencies for both types of resonators.

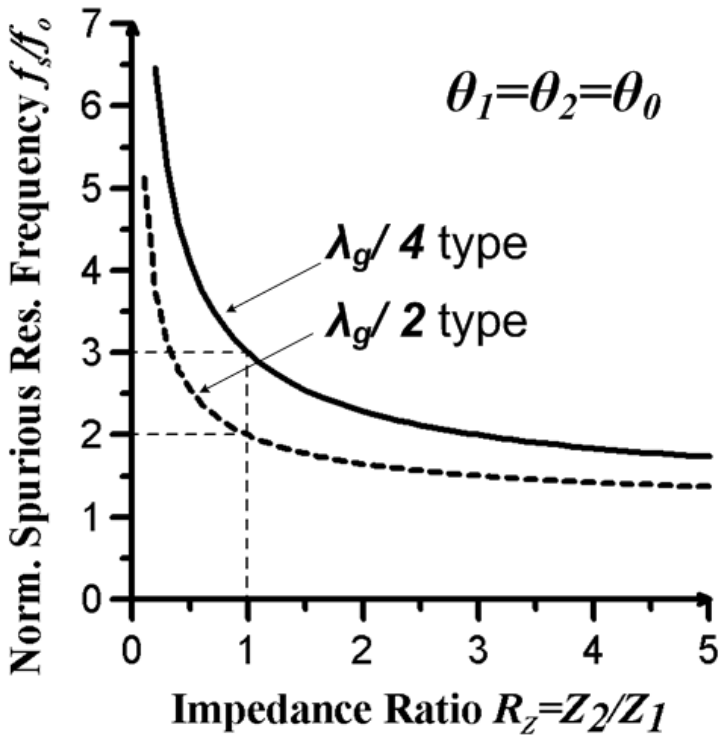

Figure 5-3: Relationship between normalized spurious resonance frequency and impedance ratio.

5.3. Design of Compact Microstrip Dual-Band Pseudo-Interdigital Stepped Impedance Bandpass Filters

The pseudo-interdigital bandpass filter presented in the previous chapter has the first spurious response at $3f_0$. The spurious response at $2f_0$ has been suppressed to about -15 dB for the resonant peaks. As pseudo-interdigital resonators were developed from interdigital resonators with grounding replaced by interconnection of two $\lambda_g/4$ resonators [5-10] with good approximation, the two arms of pseudo-interdigital resonators can be treated as two $\lambda_g/4$ resonators with interconnected ends replaced by groundings. This approximation is also based on the field pattern of resonators around the resonant frequency. The field patterns obtained from simulated current distributions of resonators at resonant frequency are shown in Figure 5-4. The current distributions of both the pseudo-interdigital and hairpin resonators were simulated using EM Sonnet. As it can be seen from this figure, these resonators have different field patterns. It is also clear that field patterns of pseudo-interdigital resonators look similar to the field patterns of conventional interdigital resonators with maximum current at the short-circuited ends and maximum electric field at the open-circuited ends of resonators. Thus, both arms of pseudo-interdigital resonators can be treated as $\lambda_g/4$ short-circuited resonators and Eq. (5-6) can be used in order to find the approximate spurious resonance frequency from the impedance ratio R_Z.

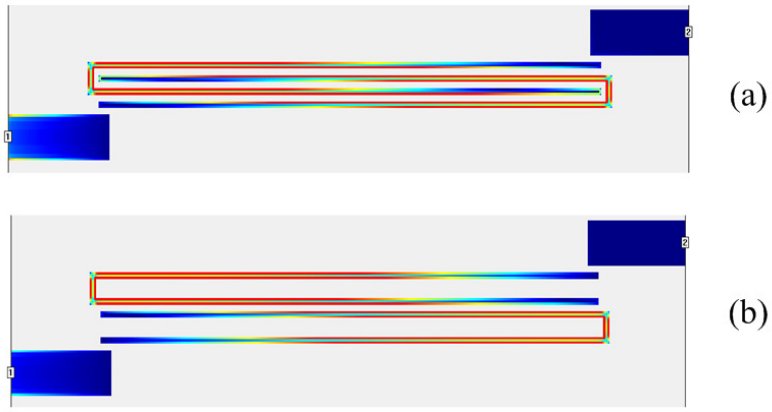

Figure 5-4: Simulated current distributions: (a) pseudo-interdigital resonators; (b) hairpin resonators.

In the most microstrip dual-band filters with SIR $\lambda_g/2$ type of SIR are used and the impedance ratio is adjusted to control the second passband using Eq. (5-7) [5-2], [5-11]. However, microstrip dual-band filters with $\lambda_g/4$ type SIR have also been reported [5-12], [5-13].

The layout of the proposed dual-band bandpass filter is shown in Figure 5-5. The width of high impedance lines is 0.4 mm and 2.8 mm is the width of the low impedance lines. The bandpass filter has been simulated for Rogers RO4003 substrate with thickness 1.524 mm and dielectric constant 3.55. Thus, the characteristic impedances of SIR are $Z_2 = 127.46\Omega$, and $Z_1 = 56.03\Omega$, and impedance ratio $R_Z = 2.27$. Using this data and Eq. (5-6), the calculated ratio of the first spurious resonance frequency to the fundamental resonance frequency is $f_S / f_0 = 2.19$.

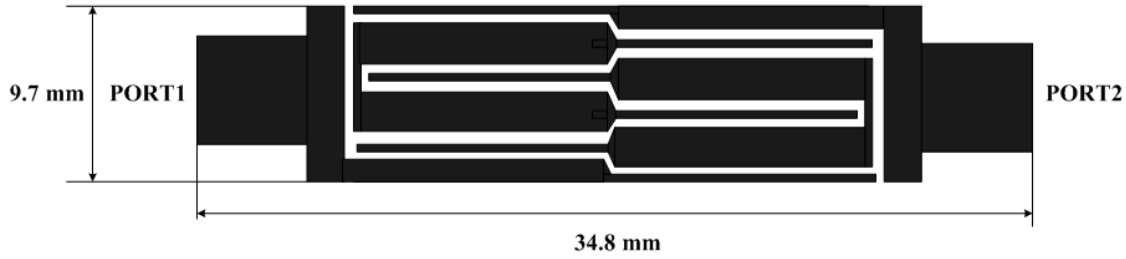

Figure 5-5: Layout of compact microstrip pseudo-interdigital SIR bandpass filter.

The width of slots between coupled lines is 0.3 mm and width of SIR lines has been chosen to satisfy the requirements of design and to meet manufacturing limits. The size of the filer is 34.8×9.7 mm or $0.3\lambda_g \times 0.1\lambda_g$, where λ_g is a wavelength at 2.03 GHz. Taper lines have been used to minimise losses due to step impedance discontinuities. Feeding lines also have been adjusted to achieve maximum degree of coupling by keeping constant the width of the coupling slot, and to improve the second passband of the filter. The filter was simulated using ADS Momentum. The simulated S-parameters are shown in Figure 5-6 by dashed lines.

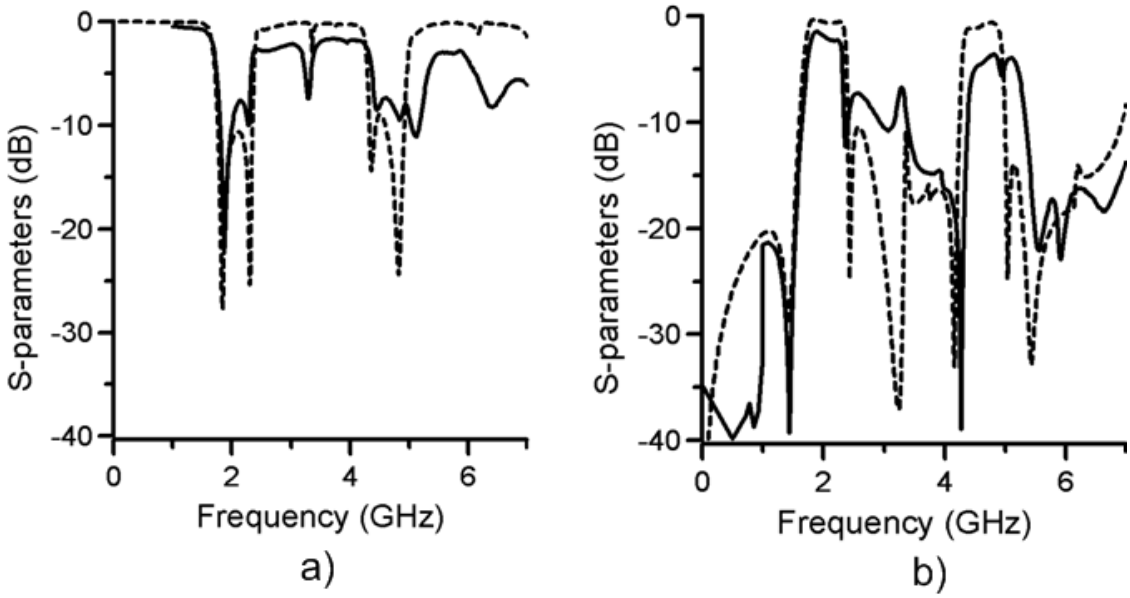

Figure 5-6: Simulated (dashed) and measured (solid) S-parameters of pseudo-interdigital SIR dual-band bandpass filter: (a) S_{11} coefficients; (b) S_{21} coefficients

As it can be seen from simulation results, the center frequencies of the first and the second passbands are 2.03 and 4.623 GHz respectively. The FBW of the first passband is 33.3%. For the second passband, the bandwidth is 14%. Skirt selectivity of both passbands is improved by TZs at finite frequencies, above and below the passband. The ratio of spurious resonance frequency to fundamental resonance frequency extracted from simulation is equal to 2.27. This is bigger than the calculated ratio of 2.19. One of the reasons of this discrepancy can be that SIR used in the design are just approximations of short-circuited $\lambda_g/4$ type SIR. However, calculated f_S/f_0 is a good approximation and can be used as a starting value for the filter designs with subsequent tuning and optimisation.

The microstrip bandpass filter was fabricated on 1.524 mm thick Rogers RO4003 substrate ($\varepsilon_r = 3.55$) [5-14]. Figure 5-6 shows the measured S-parameters by the solid lines. The response of the fabricated filter was measured with Agilent PNA (E8361A) network analyzer.

The measured center frequency is 2 GHz for the first passband and 4.8 GHz for the second passband. The measured bandwidths of the first and the second passbands are 30.3% and 17.3% respectively. It can be seen from Figure 5-6 that there is slight

frequency shift between the simulated and measured results. An increase of the insertion losses and a decrease of the return losses at both passband frequencies are observed and are attributable to poor manufacturing and additional losses caused by this. The parasitic resonance peak measured at 3.3GHz can be due to increased parasitic coupling caused by inexact manufactured slots between the microstrip lines. This also can be a reason of increased losses and deteriorated bandwidth of the second passband.

A photograph of the fabricated filter is shown in Figure 5-7.

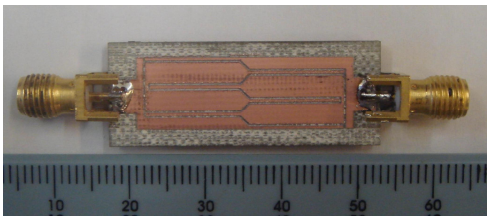

Figure 5-7: Photograph of the fabricated bandpass filter.

5.4. Design of SIR Bandpass Filters with Improved Stopband Performance

5.4.1. Bandpass Filters with Extended Stopband

The implementation of SIR in the design of bandpass filters is also used for the improvement of stopband performance of single-band filters. In this scenario, an impedance ratio $0 < R_Z < 1$ is chosen and from Eq. (5-6, 5-7) and the graph in Figure 5-3 the first spurious resonance frequency becomes higher than $2f_0$ for $\lambda_g/2$ type resonators, and higher than $3f_0$ for $\lambda_g/4$ type resonators respectively. Usually a minimum value of R_Z is determined taking into account the manufacturing limits and degradation of insertion loss of filters due to the additional losses caused by step discontinuities.

To demonstrate the ability to extend the stopband of pseudo-interdigital bandpass filter using SIR, a bandpass filter with SIR and impedance ratio $R_Z = 0.596$ has been developed. This filter will be used in the design of bandpass filters with stopband performance improved by the implementation of spur-line and DGS, which are presented in next sections. From Eq. (5-6) the first spurious response of SIR should be at approximately $3.78f_0$. An impedance ratio was realized using microstrip line with 0.4 mm and 1.1 mm width on the 0.867 mm thick substrate with $\varepsilon_r = 2.2$. The layout of the designed filter, with total size 26×4 mm, is shown in Figure 5-8.

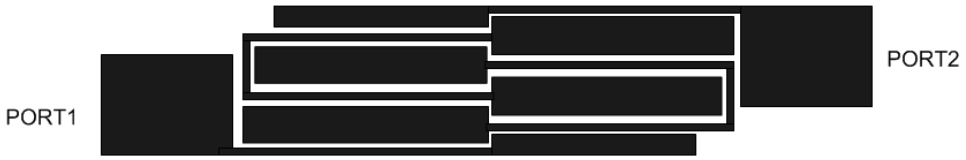

Figure 5-8: Layout of compact microstrip pseudo-interdigital SIR bandpass filter with extended stopband.

The S-parameters of filters simulated using ADS Momentum are shown in Figure 5-9. The center frequency of the simulated filter is 2.5 GHz, bandwidth 0.75 GHz and 3dB

FBW is 30%. The center frequency of the first spurious harmonic is 9.35 GHz or $3.75f_0$. This value is very close to $3.78f_0$, calculated using Eq. (5-6). Spurious resonance at $2f_0$ has been suppressed till 20-25 dB. The appearance of TX zeros at 1.97 a 3.14 GHz provides good skirt selectivity of the first passband. Although extension of the stopband to $3.75f_0$ is not a considerable improvement of stopband performance, this filter will be used as the initial building block for the bandpass filters discussed in next sections.

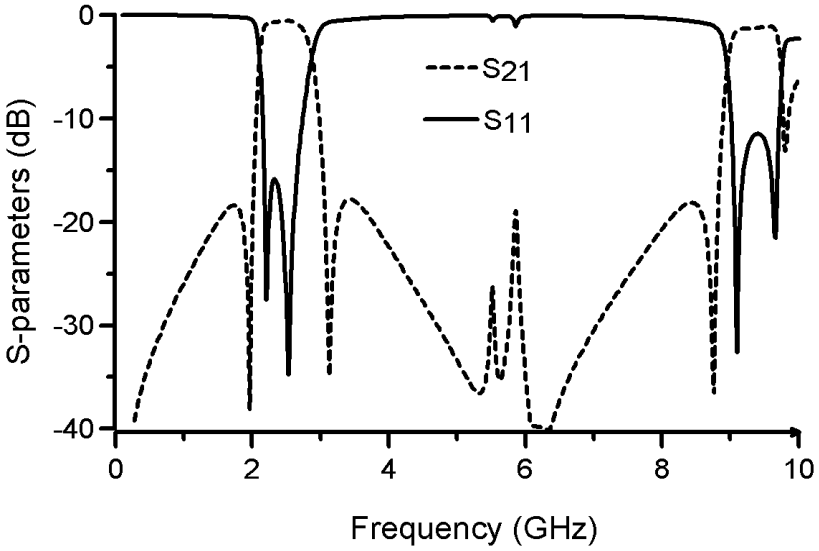

Figure 5-9: Simulated S-parameters of compact microstrip pseudo-interdigital SIR bandpass filter with extended stopband.

5.4.2. Analysis of Spur-line and Open-Circuited Stubs

One of the ways to suppress the spurious passband in the design of bandpass filter is an implementation of spur-line, which can be embedded into resonators [5-15], into the feeding line [5-16], and into both, resonators and feeding lines [5-17]. The spur-line section, introduced in the design of bandstop filters in homogeneous propagation medium [5-18], is shown in Figure 5-10 (a). The spur-line section consists of a pair of coupled microstrip lines of length *L*, which is approximately a equal to quarter wavelength at stopband center frequency f_0.

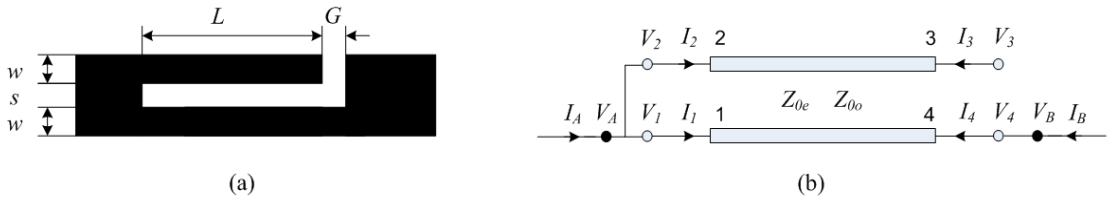

Figure 5-10: Spur-line section: (a) Layout; (b) Terminal conditions.

Spur-line section can be modelled as 4-port parallel-coupled transmission line network with terminal conditions, as it is shown in Figure 5-10 (b). The elements of the impedance matrix of this 4-port network are given in Eq. (3-1)–(3-4), and terminal conditions of spur-line section are:

$$\begin{aligned} V_A &= V_1 = V_2 \qquad V_B = V_4 \\ I_A &= I_1 + I_2 \qquad I_B = -I_4 \\ I_3 &= 0 \end{aligned} \tag{5-8}$$

where V_A, V_B, I_A, and I_B are voltages and currents of 2-ports network that can be obtained from the original 4-port network after applying terminal conditions. Similarly with analysis presented in Chapter 3, 2-port network's impedance matrix can be derived from the terminal conditions. This matrix is not very useful for our analysis; therefore transmission matrix of two-port network has been derived.

Transmission, or ABCD matrix, is a 2×2 matrix used in analysis of microwave circuits, which consist of a cascade connection of two or more than two 2-port networks. ABCD matrix is defined in terms of voltages and currents of 2-port network:

$$\begin{bmatrix} V_1 \\ I_1 \end{bmatrix} = \begin{bmatrix} A & B \\ C & D \end{bmatrix} \begin{bmatrix} V_2 \\ I_2 \end{bmatrix} \tag{5-9}$$

where V_1 and I_1 are voltage and current at port 1 of network, and V_2 and I_2 are voltage and current at port 2 respectively. The main feature of ABCD matrix, used for the analysis of microwave circuits, is that the ABCD matrix of cascade connection of two or more two-port networks is equal to multiplication of ABCD matrices of individual networks [5-19] .

Transmission matrix of spur-line section has been derived as [5-20]:

$$\begin{bmatrix} V_A \\ I_A \end{bmatrix} = \begin{bmatrix} \cos\theta_e & \frac{1}{2} j\left(Z_{0e}\sin\theta_e + Z_{0o}\tan\theta_o\cos\theta_e\right) \\ j2Y_{0e}\sin\theta_e & \cos\theta_e - \frac{Z_{0o}}{Z_{0e}}\sin\theta_e\tan\theta_o \end{bmatrix} \begin{bmatrix} V_B \\ I_B \end{bmatrix} \tag{5-10}$$

One of the decomposition of matrix (5-10) is:

$$\begin{bmatrix} V_A \\ I_A \end{bmatrix} = \begin{bmatrix} \cos\theta_e & \frac{1}{2} jZ_{0e}\sin\theta_e \\ j2Y_{0e}\sin\theta_e & \cos\theta_e \end{bmatrix} \begin{bmatrix} 1 & \frac{1}{2} jZ_{0o}\tan\theta_o \\ 0 & 1 \end{bmatrix} \begin{bmatrix} V_B \\ I_B \end{bmatrix} \tag{5-11}$$

This decomposition corresponds to equivalent circuit that consist of transmission line with characteristic impedance $Z_{0e}/2$ and electrical length θ_e connected in series with short-circuited stub with characteristic impedance $Z_{0o}/2$ and electrical length θ_o, as shown in Figure 5-11. As the short-circuited stub is connected in series, the sum of impedances of both lines should be used to find the total input impedance. From Eq. (2-18) it can be seen that the impedance of short-circuited line becomes infinite when the electrical length of this line is $\pi/2$. Therefore, condition of bandstop caused by the

infinite impedance of short-circuited line is $\theta_0 = \pi/2$. Thus, the length of spur-line is equal to:

$$L = \frac{v_{po}}{4f_0} - \Delta L \tag{5-12}$$

where ΔL is an effective length due to the gap *G*, which can be found from odd mode fringing capacitance using the following formula:

$$\Delta L = \frac{v_{po}}{2\pi f_0} \tan^{-1}\left(4\pi f_0 C_{fo} Z_{0o}\right) \tag{5-13}$$

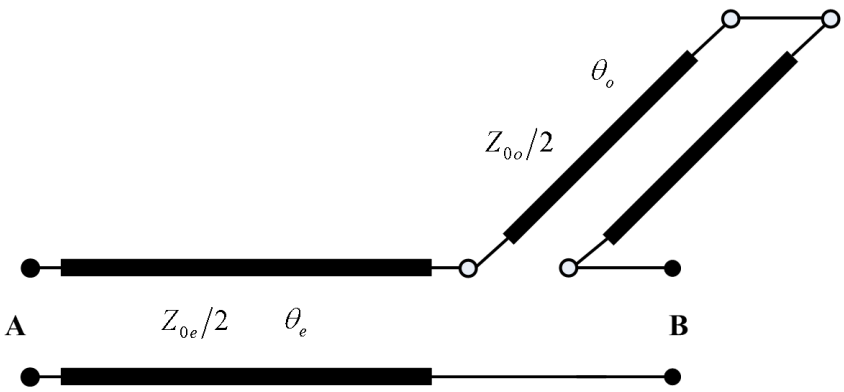

Figure 5-11: Equivalent circuit of spur-line.

The even and odd mode characteristic impedances have a significant effect on the skirt selectivity of spur-line bandstop filters [5-21] . In our scenario, when the total width of spur-line section is equal to the width of the 50 Ω line, the general rule is to make the slot's width *s* as small as possible in order to achieve the best skirt selectivity, or in other words, the smallest 3dB bandwidth of the bandstop. In this case the insertion loss introduced by the spur-line section at the passband frequency of the bandpass filter is the smallest. The width of slot $s = 0.3$ mm has been chosen, as it is small and easy to fabricate. From the simulation results, it has been found that the spur-line with a slot width 0.3 mm introduces 0.2-0.3 dB insertion loss at frequencies from 2 GHz to 3 GHz.

The bandstop filters with open-circuited stubs are one of the most popular bandstop filters. The exact design of these filters for homogeneous medium is described in [18]. This design is based on the bandstop characteristics of the open-circuited stubs. Nowadays these properties are also used to improve the stopband performance of bandpass filters [5-22].

The microstrip open-circuited stub is shown in Figure 5-12 (a). Its equivalent circuit is a shunt connected open-circuited stub, which is shown in Figure 5-12 (b). The shunt connected line has a stopband at frequencies when its admittance is infinite. From Eq.(2-17) the input admittance of the open-circuited line is infinite when the electrical length of the line is equal to $(2n-1)\pi/2$ for n=1,2,3… and the first stopband frequency corresponds to $\theta = \pi/2$, i.e. when stub is a quarter wavelength long.

Figure 5-12: Microstrip open-circuited stub: (a) layout. (b) equivalent circuit.

The characteristic impedance of the open-circuited stub has effect on the skirt selectivity of bandstop response, which affects the insertion loss in the out-of-band region. Using EM simulations it has been found that high impedance open-circuited stubs have better bandstop skirt selectivity and smaller out-of-band insertion loss than low impedance stubs.

5.4.3. Bandpass Filters with Improved Stopband

A bandpass filter with improved stopband pseudo-interdigital SIR bandpass filter, as discussed in section 5.3.1, has been designed with an impedance ratio $R_Z = 0.66$ and the first spurious response at $3.6 f_0$. This impedance ratio has been chosen to obtain a smaller insertion loss at the fundamental passband of filter. In the case when the impedance ratio is $R_Z < 1$, a small impedance ratio R_Z can be obtained only by the increase of the difference between the impedances of the lines resonators. Big difference between these impedances introduces more losses due to additional losses due to radiation on the impedance step. Thus the insertion loss of filter increases as well.The center frequency of bandpass filter is 2.75 GHz with first spurious harmonic from 9.5 to 12 GHz. To suppress this passband, a spur-line section has been embedded into feeding line and open-stub has been connected as shown in Figure 5-13.

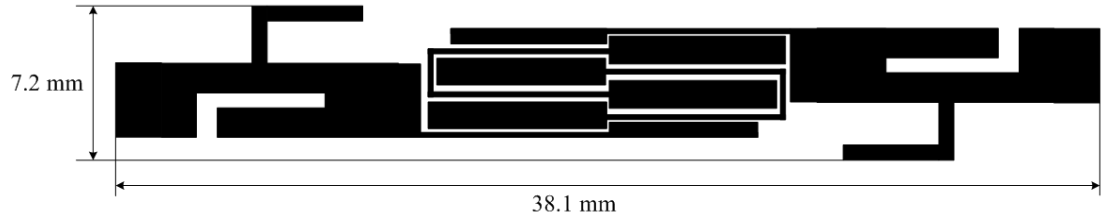

Figure 5-13: Layout of bandpass filter with spur-line and open-circuited stubs.

The spur-line sections and open-circuited stubs have been designed to have bandstop peaks at frequencies from 9.5 to 12 GHz with approximately 1 GHz between each other. The simulated S-parameters of spur-line section with open-circuited stub are shown in Figure 5-14. The bandstop frequencies of open-circuited stub and spur-line section simulated separately are 11.2 and 12 GHz. After the connection of the stub to spur-line, the bandstop frequencies shifted to 11.25 and 12.5 GHz respectively. As it can be seen from Figure 5-15, the open-circuited stub integrated with spur-line section have a performance of not optimised bandstop filter with TZs at 11.25 and 12.5 GHz.

After integration of spur-line section and open-circuited stub with bandpass filter two additional TZ zeros occurred in the stopband of the filter at 11.6 and 12.3 GHz [5-23]. The simulated S-parameters of pseudo-interdigital bandpass filter with improved

stopband are shown in Figure 5-15. As a result of the integration with spur-line section embedded into feeding line and open-circuited stub, the stopband of bandpass filter has been extended to about $5.5f_0$.

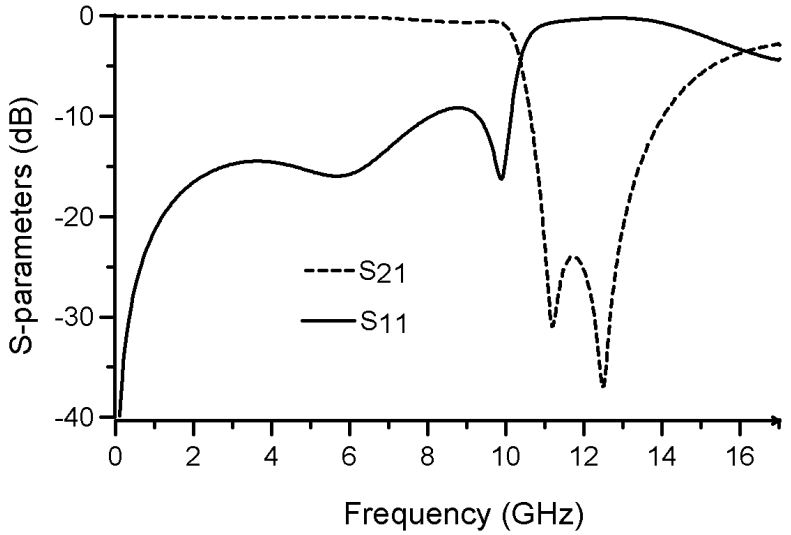

Figure 5-14: Simulated S-parameters of spur-line section and open-circuited stub.

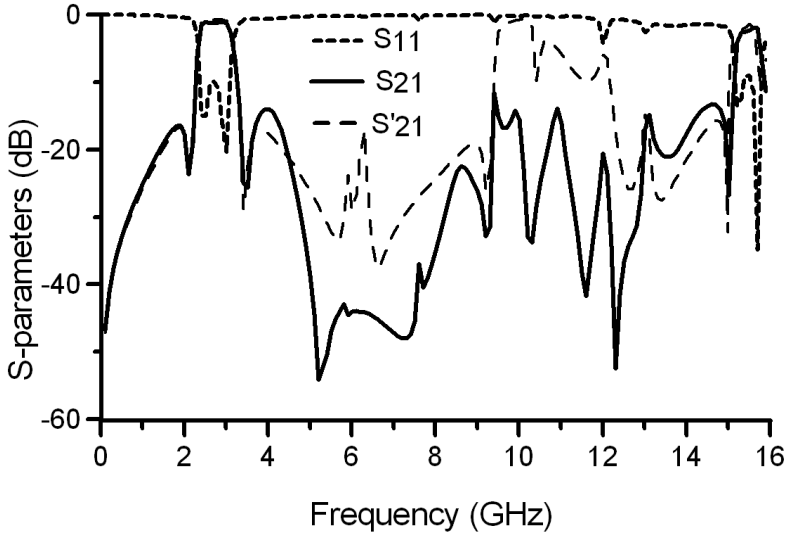

Figure 5-15: Simulated S-parameters of compact microstrip pseudo-interdigital SIR bandpass filter with improved stopband.

The simulated transmission coefficient of bandpass filter without spur-line and open-circuited stub is included in Figure 5-15 and noted as S'_{21}. The comparison of the transmission performance of these two filters clearly shows the effect of inclusion of spur-line section and open circuited stub on the stopband performance of bandpass filter.

5.4.4. Analysis of Defected Ground Structures

The defected ground structures (DGS) is a common name of slots etched in the ground plane of microstrip and coplanar waveguide transmission lines. DGS can be treated as electromagnetic bandgap (EBG) structures as they forbid or allow the wave propagation at certain frequency bands. EBG effects occur at some frequency because any periodic slots or structures etched on the ground plane can disturb the field distribution of guided electromagnetic waves. Although this feature of DGS has been used for suppression of harmonics in the design of power dividers [5-24], to improve efficiency of power amplifiers [5-25], and in the design of other RF front-end applications, the most frequently DGS structures are used in the design of lowpass filters [5-26].

One of the most frequently employed and the simplest for analysis DGS structures is a dumbbell-shaped slot (DSS), which is shown in Figure 5-16 (a). The simplest model of DSS, that excludes radiation, dielectric and conductor losses, is a parallel LC resonator [5-27]. The square slots of DSS etched on the ground plane are equivalent to inductance, and the narrow slot that connects two square slots is equivalent to capacitance. The square slots of DGS are equivalent to inductance because due to the presence of the narrow slot, the direct path for current propagation under metallic line of microstrip is broken. Thus, current is flowing along the edge of square slots and increased current density can be observed from the EM simulations. Two square slots with current flowing along their edge become equivalent to loops with current. This current produces a magnetic field and generates magnetic flux which is characterized by the inductance used to model DGS. The values of elements of equivalent circuit can be extracted from the simulation results, which is for one DSS is equivalent to a one pole Butterworth type lowpass filter. The series inductance can be calculated from the prototype elements of Butterworth prototype, and the value of capacitance can be extracted from the bandstop frequency. The bandstop performance of DSS will be used for the suppression of harmonics in the design of bandpass filter with improved stopband.

The spiral shaped slots (SSS), shown in Figure 5-16 (b), is a DGS structure which also has been used in the design of lowpass and bandpass filters. SSS is a modification of DSS with square slots replaced by spiral shaped slots. For the same occupied areas, the attenuation poles of SSS occur at the lower frequencies, compared to DSS. This can be used to reduce the size of the whole structure. The simplest proposed model of SSS consists of an inductor and a short-circuited stub, which represents the periodic frequency response [5-28]. The characteristic impedance Z_S and inductance L_S also can be extracted from elements values of first order Butterworth prototype. For scenarios when the fundamental and spurious stopbands of SSS are used equivalent circuit in which shorted stub with stepped impedances should be used to predict spurious frequencies more accurately [5-29].

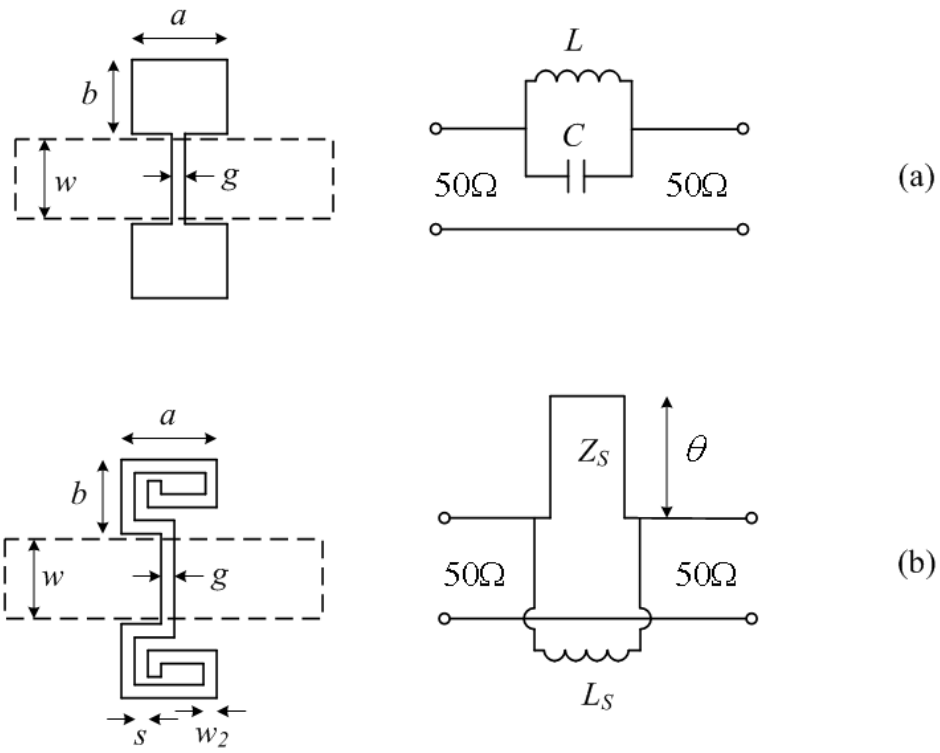

Figure 5-16: Structure and equivalent circuit of DGS: (a) dumbbell-shaped slot; (b) spiral shaped slot.

To compare the bandstop performance of DSS and SSS, there have been simulated using HFSS for substrate with $\varepsilon_r = 2.2$ and thickness 0.867 mm. The total sizes of DSS and SSS are chosen to be equal with dimensions $a = 1.8\,\text{mm}$, $b = 1.6\,\text{mm}$, $g = s = w_2 = 0.2\,\text{mm}$, and width of 50 Ω line $w = 2.6\,\text{mm}$. The simulated S-parameters

are shown in Figure 5-17. The bandstop frequencies of SSS and DSS are 8.91 GHz and 13.2 GHz respectively. It is clear that in order to achieve the same bandstop frequency using DSS the size of square slots should be increased. This is one of the reasons why SSS have been chosen for the suppression of spurious harmonics of bandpass filters. Another reason is that due to large total area of slots etched in the ground plane for DSS, the skirt selectivity of DSS is worse than the skirt selectivity of SSS. Thus, the insertion loss at the out-of-band frequencies caused by the implementation of DSS type, the DGS is large than the insertion loss caused by SSS type DGS.

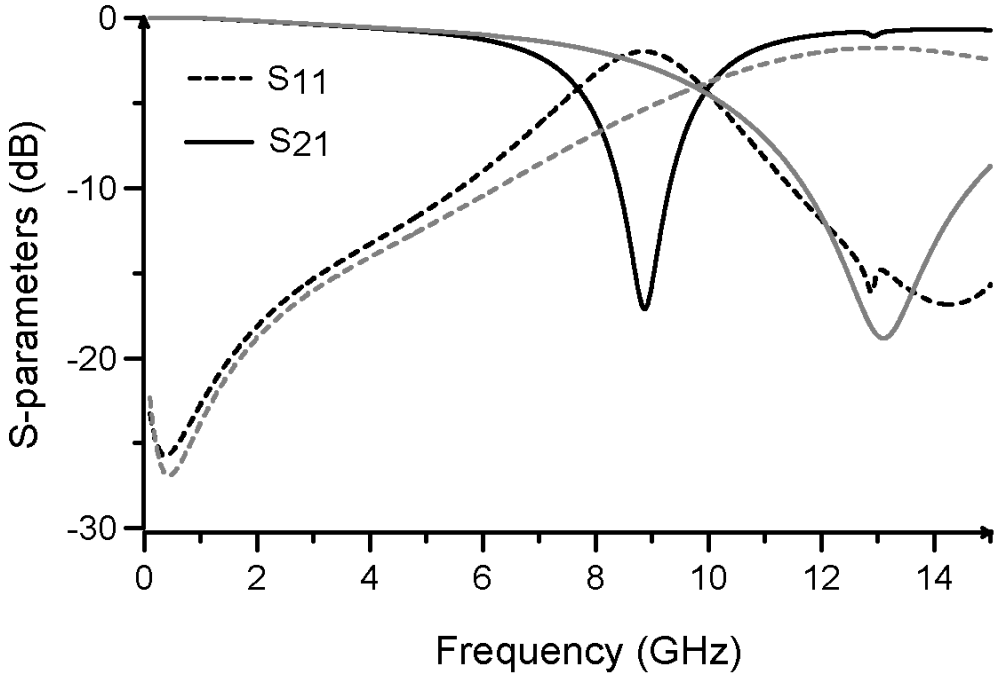

Figure 5-17: Simulated S-parameters of SSS (black lines) and DSS (grey lines).

5.4.5. Compact Pseudo-Interdigital SIR Bandpass Filters with Improved Stopband using DGS

The design of compact pseudo-interdigital bandpass filters with improved stopband performance is based on the addition of DGS structures etched under 50 Ω feeding lines at the input and output of filters. Spiral shaped slots DGS have been used and adjusted to have a bandstop at the spurious harmonics frequencies of bandpass filters. This method, proposed in [5-16] also discusses the addition of spur-line section embedded into feeding lines to suppress more harmonics. In this section the design of bandpass filters with suppression of harmonics using DGS only is presented.

The first step is the design of pseudo-interdigital bandpass filter with extended stopband using procedure described in 5.4.1. The bandpass filter with a center frequency 2.51 GHz, fractional bandwidth 38.2% has been designed using Rogers RT/Duroid 5880 substrate with dielectric constant $\varepsilon_r = 2.2$ and thickness $h = 0.867$ mm. The impedance ratio of SIR is equal to $R_Z = 0.657$ and the calculated spurious to fundamental resonance frequencies ratio is $f_S / f_0 = 3.61$. The filter has been simulated using HFSS. The simulated frequencies ratio is equal to $f_S / f_0 = 3.5$. To suppress the first spurious harmonics from 8.3 to 9.2 GHz, spiral shaped slots (SSS) etched below the feeding lines at input and output of filter have been implemented. The dimensions of SSS are the same used in previous section, $a = 1.8$ mm, $b = 1.6$ mm, $g = s = w_2 = 0.2$ mm, with the stopband centered at 8.91 GHz. The layout of proposed filter is shown in Figure 5-18, with the top layer conductors of filter shown with black colour filled shapes and SSS etched on the ground layer shown with black lines. The size of the filter is 32×6.8 mm or $0.41\lambda_g \times 0.09\lambda_g$ where λ_g is a wavelength at 2.5 GHz, which is the passband center frequency of filter.

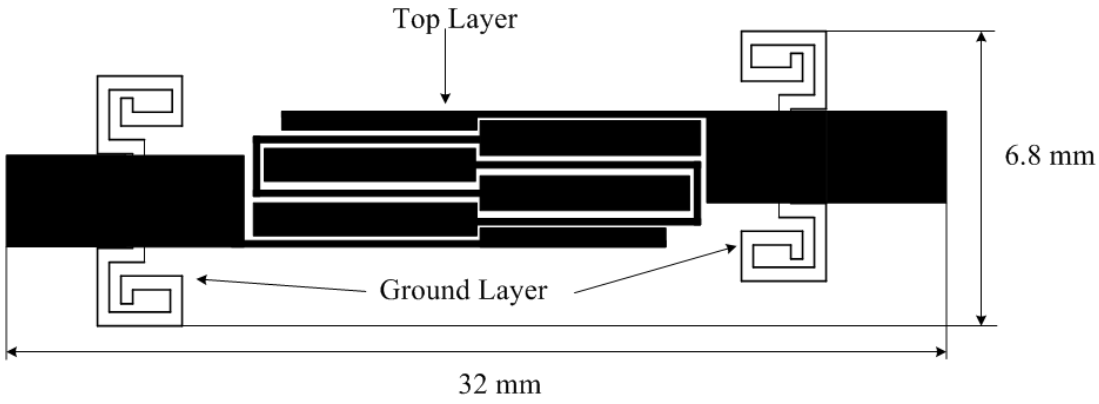

Figure 5-18: Layout of bandpass filter with one SSS.

The S-parameters of the proposed filter, simulated using Ansoft HFSS are shown in Figure 5-19. From simulation results, it can be seen that the filter has stopband with 15dB insertion loss till 13.4 GHz, which is $5.36 f_0$. For comparison with the stopband performance of bandpass filter without SSS, the simulated transmission coefficient of the filter without SSS was included and is noted in Figure 5-19 as S'_{21}. It is clear from this comparison that the addition of one SSS at the input and output of filter caused the suppression of first spurious harmonics to about 20 dB. The length of the filter with one SSS was increased by 3.5 mm on each side.

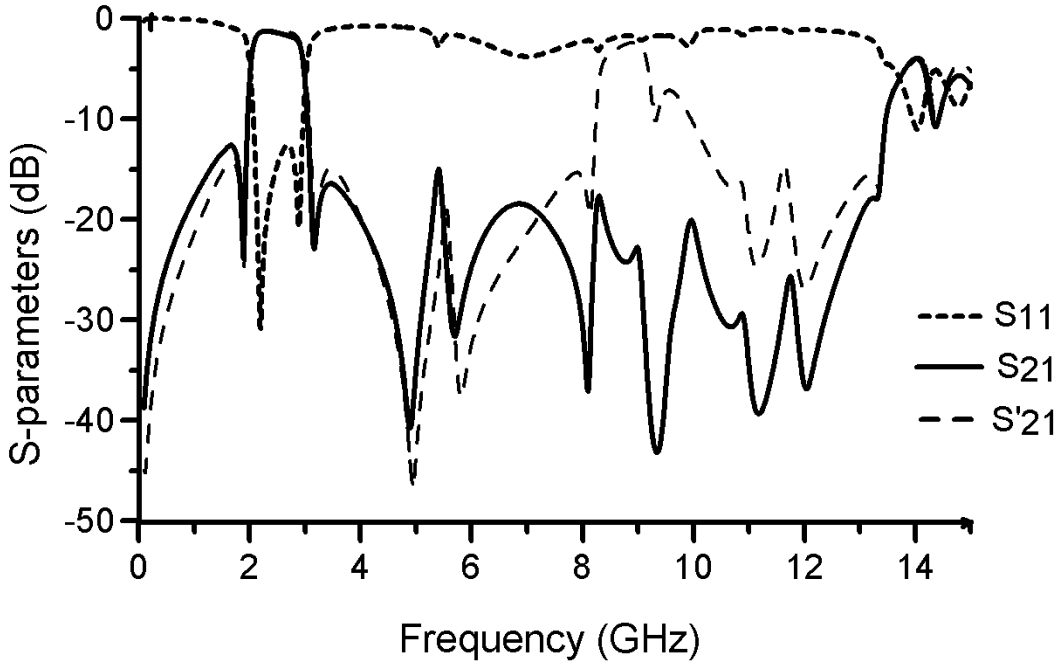

Figure 5-19: Simulated S-parameters of bandpass filter with one SSS.

To investigate the possibility of a further extension of the stopband of bandpass filter using DGS, a filter with two SSS etched below the feeding lines at the input and output has been designed. The layout of proposed filter is shown in Figure 5-20. The new filter structure consists of bandpass filter designed above with one more SSS etched below feeding line at the input and output and located between first SSS and port connection. The second SSS has smaller size with dimensions, noted as in Figure 5-16 (b), $a = b = 1.2$ mm, $g = s = w_2 = 0.2$, and width of 50Ω line $w = 2.6$ mm. The bandstop generated by small SSS is centered at 12.8 GHz. Figure 5-21 illustrates the simulated S-parameters of the two SSS located under 50Ω microstrip line. It can be seen that this structure has two bandstop peaks, low frequency peak generated by SSS of bigger size and high frequency peak, generated by SSS of smaller size.

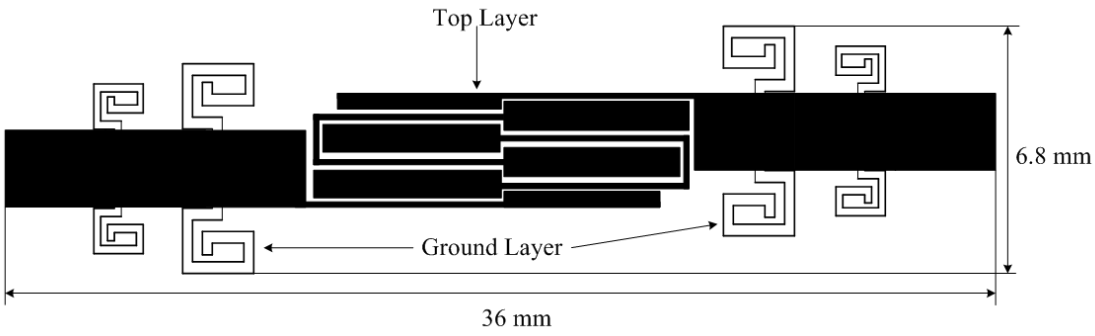

Figure 5-20: Layout of bandpass filter with two SSS.

Bandstop frequencies of both spiral shaped slots are controlled by adjusting the length of etched spiral slots. If the width of etched slot and the width of separation between them is constant, lengthening of spiral slots can be achieved by increasing the total area of DGS.

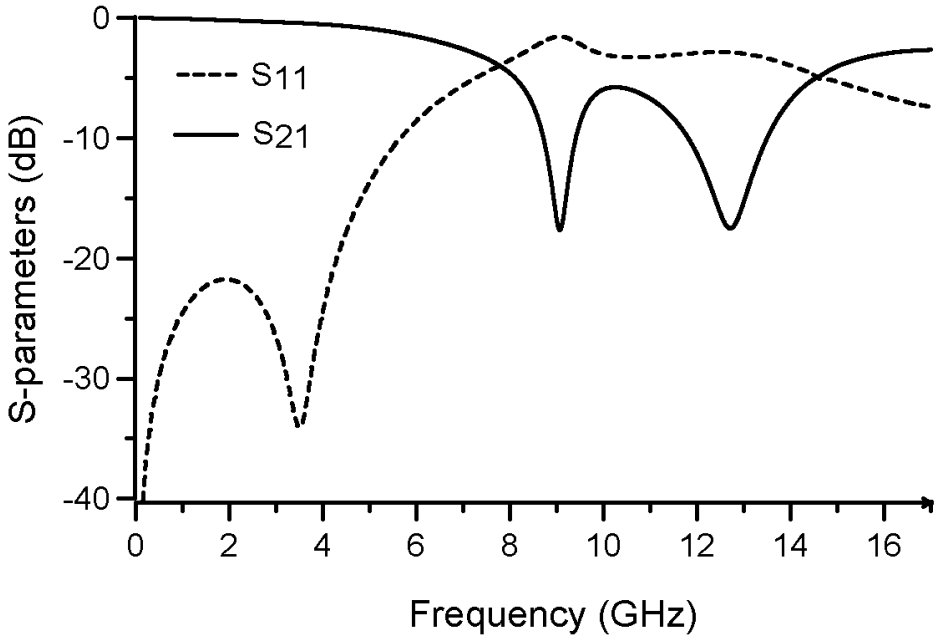

Figure 5-21: Simulated S-parameters of two SSS.

The S-parameters of proposed bandpass filter with two SSS etched under feeding lines were simulated using HFSS. Simulated S-parameters are shown in Figure 5-22. It can be seen that 15dB insertion loss stopband of the filter is extended to 16.5 GHz or to $6.6 f_0$. For comparison S_{21} of filter without DGS is included in Figure 5-22 and noted as S'_{21}. This comparison shows that the addition of the second small SSS caused the suppression of the second spurious harmonics of bandpass filter to 25-30 dB. The first spurious harmonics was suppressed to 14 dB by the use of SSS of bigger size. It also can be seen from Figure 5-22 that the second resonant frequency of small SSS, which resonates at 12.8 GHz, has shifted to higher frequency 13.4 GHz. This shift can occur due to additional coupling with bigger size SSS and stopband performance of small SSS can be further enhanced by the weak TZ of filter at 3.5 GHz.

The main drawback of the new filter is that now the lengths of both etched spiral slots should be adjusted to achieve the best stopband rejection. The total length of filter increased due to the addition of DGS by 6 mm on each side. The size of the filter is 36×6.8 mm or $0.46\lambda_g \times 0.09\lambda_g$ where λ_g is a guided wavelength at the center frequency of the fundamental passband of filter.

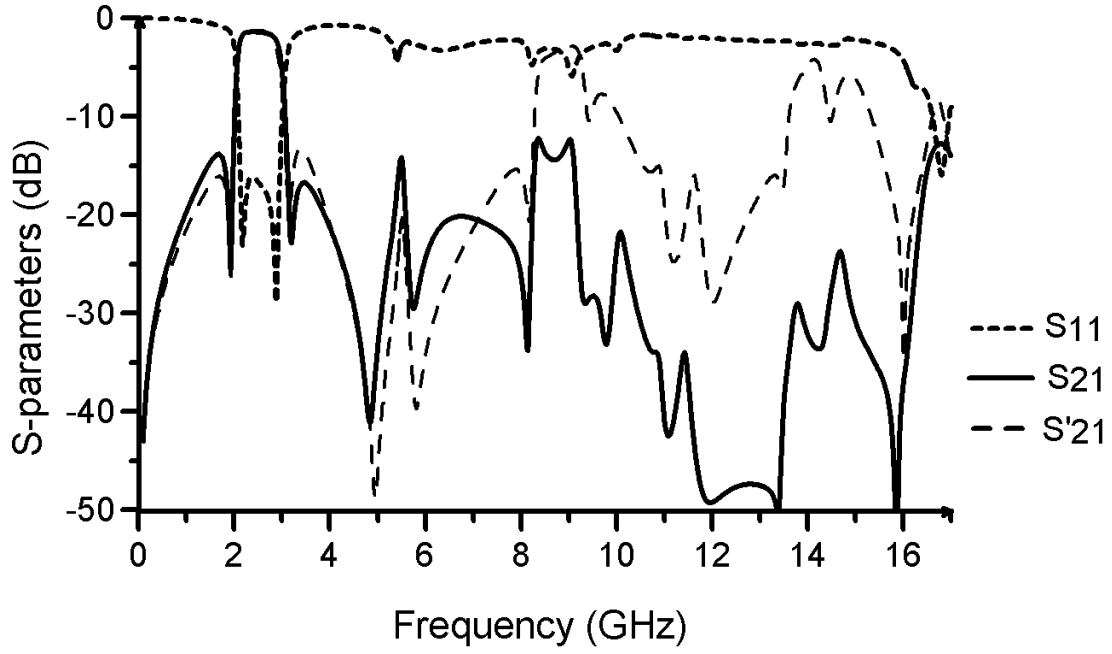

Figure 5-22: Simulated S-parameters of bandpass filter with two SSS.

5.5. Summary

In this chapter pseudo-interdigital bandpass filters with SIR are presented.

The fundamental characteristics of SIR are described in section 5.2. Section 5.3 presents the design of compact dual-band bandpass filter with passband centred at 2.03 and 4.62 GHz. In this filter SIRs with impedance ratio $R_Z = 2.27$ have been used to shift spurious resonance frequency to $2.27 f_0$.

The pseudo-interdigital bandpass filters with improved stopband are presented in section 5.4. In all these filters, SIRs with impedance ratio $R_Z = 0.66$ have been used to extend the stopband till $3.6 f_0$. A further improvement of the stopband has been investigated combining bandpass filters with elements that introduce bandstops tuned to the harmonic frequencies bandpass filter. The design of band pass filter with stopband extended to $5.5 f_0$ using spur-lines and open-circuited stubs is presented. the spiral shaped slots etched in the ground plane under the feeding line on each side of bandpass filters are employed to design filters with stopbands to $5.36 f_0$ and $6.6 f_0$ for filters with one and two slots respectively.

5.6. References

[5-1] M. Makimoto and S. Yamashita, "Compact bandpass filters using stepped impedance resonators," *Proceedings of the IEEE*, vol. 67, no. 1, pp. 16-19, January 1979

[5-2] C. Qing-Xin and C. Fu-Chang, "A Compact Dual-Band Bandpass Filter Using Meandering Stepped Impedance Resonators," *IEEE Microwave and Wireless Comp. Lett.,* vol. 18, no. 5, pp. 320-322, May 2008

[5-3] K. Jen-Tsai, Y. Tsung-Hsun, and Y. Chun-Cheng, "Design of microstrip bandpass filters with a dual-passband response," *IEEE Trans. on Microwave Theory and Tech.*, vol. 53, no. 4, pp. 1331-1337, April 2005

[5-4] J. T. Kuo and E. Shih, "Microstrip stepped impedance resonator bandpass filter with an extended optimal rejection bandwidth," *IEEE Trans. on Microwave Theory and Tech.,*, vol. 51, no. 15 pp. 1554-1559, May 2003

[5-5] L. Shih-Cheng, D. Pu-Hua, L. Yo-Shen, W. Chi-Hsueh, and C. Chun Hsiung, "Wide-stopband microstrip bandpass filters using dissimilar quarter-wavelength stepped-impedance resonators," *IEEE Trans. on Microwave Theory and Tech.,* vol. 54, no. 3, pp. 1011-1018, March 2006

[5-6] M. Sagawa, M. Makimoto, and S. Yamashita, "Geometrical structures and fundamental characteristics of microwave stepped-impedance resonators," *IEEE Trans. on Microwave Theory and Tech,* , vol. 45, no. 6, pp. 1078-1085, July 1997.

[5-7] M. Makimoto, S. Yamashita, *Microwave resonators and filters for wireless communication:theory, design and application.* New-York*:* Springer, 2001

[5-8] M. Makimoto and S. Yamashita, "Bandpass Filters Using Parallel Coupled Stripline Stepped Impedance Resonators," *IEEE Trans. on Microwave Theory and Tech.,* vol. 28, no. 12, pp. 1413-1417, December 1980.

[5-9] A. A. A. Apriyana and P. Zhang Yue, "A dual-band BPF for concurrent dual-band wireless transceiver," *5th Conf. Electronics Packaging Tech.,* Singapore December *2003,* pp. 145- 149

[5-10] J. S. Hong and M. J. Lancaster, "Development of new microstrip pseudo-interdigital bandpass filters," *IEEE Microwave and Guided Wave Lett.,* vol. 5, no. 8, pp. 261-263, August 1995

[5-11] Z. Yue Ping and S. Mei, "Dual-Band Microstrip Bandpass Filter Using Stepped-Impedance Resonators With New Coupling Schemes," *IEEE Trans. on Microwave Theory and Tech.,* vol. 54, no. 10, pp. 3779-3785, October 2006.

[5-12] C. Yi-Ming, C. Sheng-Fuh, C. Chia-Chan, and C. Cheng-Yu, "A dual-band bandpass filter by interleaving heterogeneous stepped-impedance resonators," *37th European Microwave Conf.*, Munich, Germany, October 2007, pp.854-857

[5-13] P. K. Singh, S. Basu, and W. Yeong-Her, "Miniature Dual-Band Filter Using Quarter Wavelength Stepped Impedance Resonators," *IEEE Microwave and Wireless Comp. Lett.*, vol. 18, no. 2, pp. 88-90, February 2008.

[5-14] D. Zayniyev and D. Budimir, "Compact microstrip dual-band pseudo-interdigital stepped impedance bandpass filters for wireless applications," *IEEE AP-S/URSI Int. Symp. Dig*., Charleston, USA, June 2009

[5-15] P. Hoi-Kai, H. Ka-Meng, T. Kam-Weng, and R. P. Martins, "A compact microstrip λg/4-SIR interdigital bandpass filter with extended stopband," *IEEE MTT-S, Int. Microwave Symp. Dig.,* June 2004, pp. 1621- 1624

[5-16] K. Chul-Soo, K. Duck-Hwan, S. In-Sang, K. M. K. H. Leong, T. Itoh, and A. Dal, "A design of a ring bandpass filters with wide rejection band using DGS and spur-line coupling structures," *IEEE MTT-S, Int. Microwave Symp. Dig., June 2005*, pp. 2183-2186

[5-17] A. Griol, J. Marti, and L. Sempere, "Microstrip multistage coupled ring bandpass filters using spur-line filters for harmonic suppression," *Electronics Letters*, vol. 37, no. 9, pp. 572-573, April 2001

[5-18] B. M. Schiffman and G. L. Matthaei, "Exact Design of Band-Stop Microwave Filters," *IEEE Trans. on Microwave Theory and Tech.,* vvol.63, no.1, pp. 69-74, May 1963

[5-19] D. M. Pozar, *Microwave engineering*. 3rd edition, New York: John Wiley & Sons, 2004

[5-20] C. Nguyen and C. Hsieh, "Millimeter Wave Printed Circuit Spurline Filters," *IEEE MTT-S, Int. Microwave Symp. Dig.*, vol.83, no.1, pp. 98- 100, May 1983

[5-21] Y. Z. Wang and M. L. Her, "Compact microstrip bandstop filters using stepped-impedance resonator (sir) and spur-line sections," *IEE Proceedings Microwaves, Antennas and Propagation,* vol. 153, no. 5 pp. 435-440, October 2006.

[5-22] I. N. Alvizuri Romani, A. J. M. Soares, and H. Abdalla, "Compact microstrip bandpass filter with enhanced stopband performances," *IEEE Microwave and Optoelectronics Conf.,* pp.950-953, October 2007

[5-23] D. Zayniyev and D. Budimir, "Compact microstrip pseudo-interdigital stepped impedance bandpass filters with improved stopband performance," *IEEE Wireless and Microwave Technology Conf.,* April 2009

[5-24] W. Duk-Jae and L. Taek-Kyung, "Suppression of harmonics in Wilkinson power divider using dual-band rejection by asymmetric DGS," *IEEE Trans. on Microwave Theory and Tech.*, vol. 53, no. 6, pp. 2139-2144, June 2005

[5-25] L. Jong-Sik, K. Ho-Sup, P. Jun-Seek, A. Dal, and N. Sangwook, "A power amplifier with efficiency improved using defected ground structure," *IEEE Microwave and Wireless Comp. Lett.,* vol. 11, no. 4, pp. 170-172, April 2001

[5-26] J. Dong-Jin and C. Kai, "Low-Pass Filter Design Through the Accurate Analysis of Electromagnetic-Bandgap Geometry on the Ground Plane," *IEEE Trans. on Microwave Theory and Tech.,* , vol. 57, no. 7, pp. 1798-1805, July 2009

[5-27] P. Jong-Im, K. Chul-Soo, K. Juno, P. Jun-Seok, Q. Yongxi, A. Dal, and T. Itoh, "Modeling of a photonic bandgap and its application for the low-pass filter design," *Asia-Pacific Microwave Conf.*, Singapore, November 1999, vol.2, pp.331-334

[5-28] K. Chul-Soo, L. Jong-Sik, N. Sangwook, K. Kwang-Yong, and A. Dal, "Equivalent circuit modelling of spiral defected ground structure for microstrip line," *Electronics Letters*, vol. 38, no.19, pp. 1109-1110, September 2002.

[5-29] K. Chul-Soo, L. Jong-Sik, N. Sangwook, K. Kwang-Yong, P. Jong-Im, K. Geun-Young, and A. Dal, "The equivalent circuit modeling of defected ground structure with spiral shape," *IEEE MTT-S, Int. Microwave Symp. Dig.,* vol.3, June 2002, pp.2125-2128

6. DESIGN OF COMPACT MICROSTRIP DIPLEXERS

6.1. Introduction

A diplexer is a three-port network which usually consists of two filters connected in a special way in order to provide the passband and stopband characteristics of each filter from the common connection [6-1]. Diplexers are two channel versions of multiplexers. These devices can be used to connect single antenna with several receivers or transmitters or to provide the coexistence of different wireless systems [6-2] in multiservice and multiband communication systems. Diplexers and triplexers are needed in these systems to possess the capabilities of high compactness, light weight and high isolation. A low voltage standing-wave ratio should be displayed at the common ports of multiplexers, whereas high isolation should be maintained between each of the filters.

A multiplexer is called contiguous if the passband of adjacent channels cross-over is at the 3dB level. All other multiplexers have a guardband, channel that separates adjacent passbands. To design a multiplexer, component filters should be connected in such a way that each filter appears as an open circuit to each other filter. For the design of diplexers only one open circuit condition should be satisfied and this can be done using optimisation of the T- or Y-junction. For the design of triplexers with two open circuit conditions, or multiplexer with four channels, more complex matching circuits using rings and impedance transformers can be used [6-3], [6-4].

In this chapter, designs of compact microstrip diplexers using miniaturized pseudo-interdigital bandpass filters, developed in the previous chapters, are presented. Section 6.2 presents a diplexer designed using modified Y-junction. In section 6.3, the design of a diplexer using common feeding techniques is presented. In both these diplexers, pseudo-interdigital bandpass filters with uniform impedance resonators are used. SIR dual-band bandpass filters are employed in the design of three-port four-channel diplexer, presented in section 6.4.

6.2. Microstrip Diplexers using Y-Junction

The design procedure for microstrip diplexer begins from the design of two pseudo-interdigital bandpass filters as described in 4.5. The bandpass filter with center frequency at 2.44 GHz and FBW 24.7% was designed for the first channel of diplexer. A bandpass filter with a center frequency at 3.5 GHz and FBW 24.9% was designed for the second channel of diplexer. The layout of filters is the same as in Figure 4-10 and for the dielectric substrate with dielectric constant 2.2 and thickness 0.78 mm, the length of the first and second filter is 30.7 mm and 23.4 mm respectively. Figure 6-1 illustrates the S-parameters of both filters simulated using ADS Momentum.

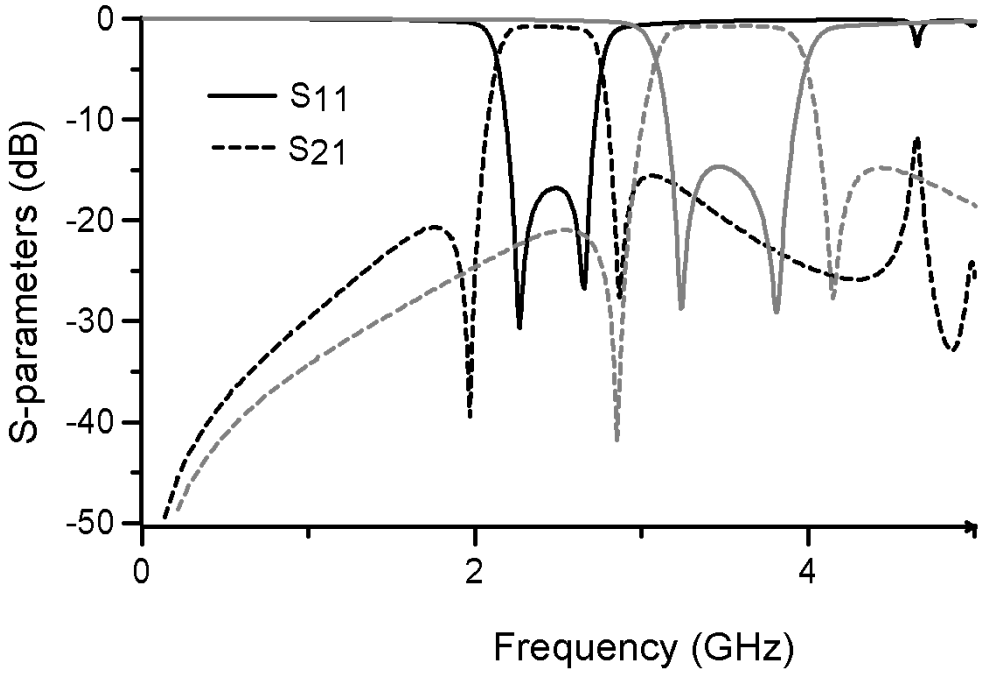

Figure 6-1: Simulated S-parameters of bandpass filters: with passband centered at 2.44 GHz (black lines); with passband centered at 3.5 GHz (grey lines).

From the simulation results the passband insertion loss of both filters is 0.75 and the return loss is about 15 dB. The first filter, with a center frequency 2.44 GHz, has TZs at 1.97 and 2.87 GHz. The second filter has TZs at 2.85 and 3.81 GHz. The passbands of filters are approximately 0.36 GHz apart from each other. Therefore, the designed diplexer should have a guardband or frequency separation channel of the same size.

To build a diplexer, both designed filters should be combined using some matching circuit. One port of this circuit should be matched at the center frequency of filter and the other port should be open-circuit. Thus, only one open condition is needed for diplexer design. For the design of diplexers the most popular option of combining circuits is the T-junction [6-5], [6-6], or one of its modification- the Y-junction [6-7]. T-junction or Y-junction is combined with the branch lines which are optimised and should be designed to meet the condition of no reflection at the center frequency of one passband and total reflection at the center frequency of the other passband. Thus, for example the branch line that connects filter 1 to the junction should be adjusted to meet the open-circuit condition at the center frequency of filter 2.

From the comparison of the simulated diplexer with T- and Y-junctions used to combine designed bandpass filters, it has been found that using the Y-junction introduces fewer losses than the T-junction. Therefore, the Y-junction was chosen for further optimisation. After a few optimisation steps, the Y-junction matching circuit has been chosen as it is shown in Figure 6-2. The length of the 50Ω line connecting the low passband filter is 5mm, the angle of slope of line connecting high passband filter is 43.26º. The size of the diplexer is 38.8×7.2 mm [6-8].

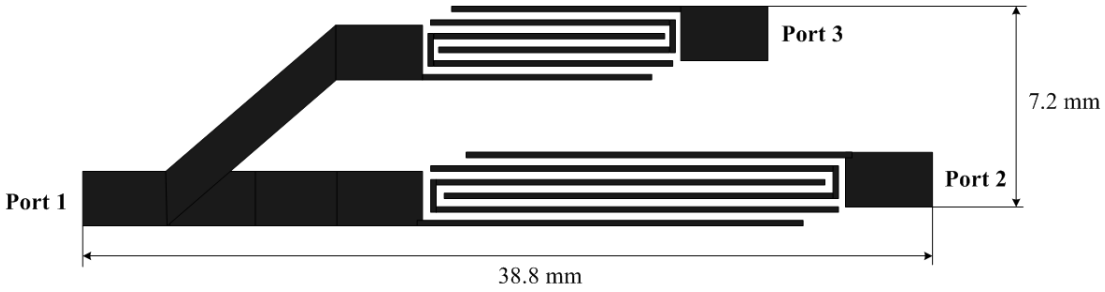

Figure 6-2: Layout of microstrip diplexer with Y-junction.

The simulated S-parameters of diplexer are shown in Figure 6-3. From simulation results it can be seen that the isolation between ports 2 and 3 at the low channel is 25-30 dB, at the high channel is 15-20 dB. The passband performance of the first filter is deteriorated and insertion loss has become 1.9 dB and return loss – 7dB. The width of the frequency separation channel has increased 0.6 GHz due to the decrease of fractional bandwidth of the first channel. The frequencies of TZs of the first filter have

shifted to 1.99 GHz and 2.74 GHz. The characteristics of the second channel filter have not changed much and only the passband return loss is decreased by 1dB.

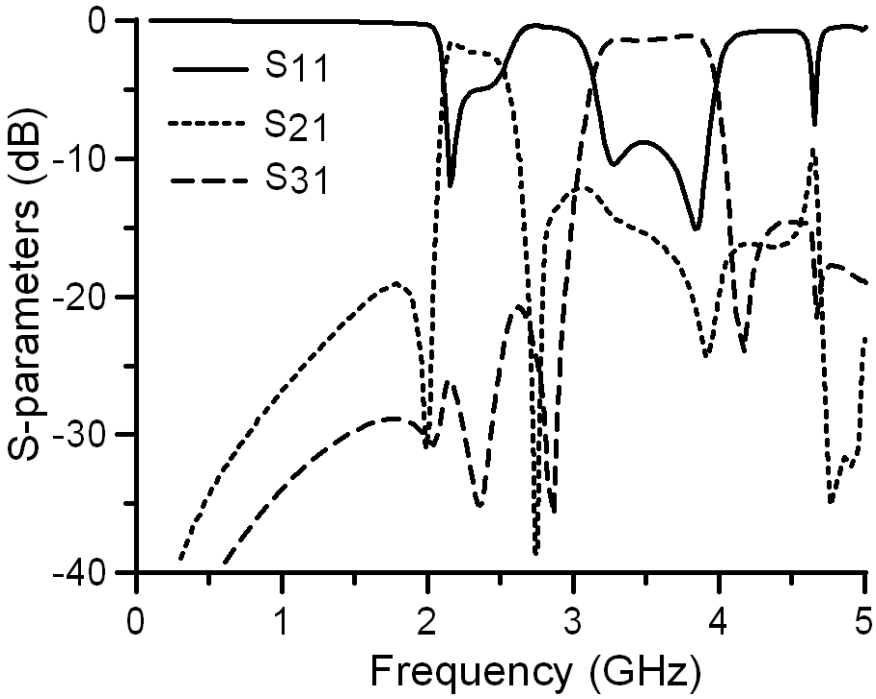

Figure 6-3: Simulated S-parameters of microstrip diplexer with Y-junction.

6.3. Miniaturised Microstrip Diplexers for Wireless Applications

The main problem of the diplexer discussed above was the degradation of filter's characteristics of one filter due to the combination with another. The design of the matching network can be time consuming and demands a lot of optimisation iterations. Using other multiplexing techniques, such as transformers and circulators increases the total size of diplexer substantially. In order to decrease the degradation of the passband of low channel filter and decrease the size of diplexer another diplexing technique is used. It is based on the common-transformer diplexer [6-9] which is common solution for diplexers based on combline or interdigital filters. In these diplexers combline or interdigital filters are coupled by means of the common transformer, as shown in Figure 6-4.

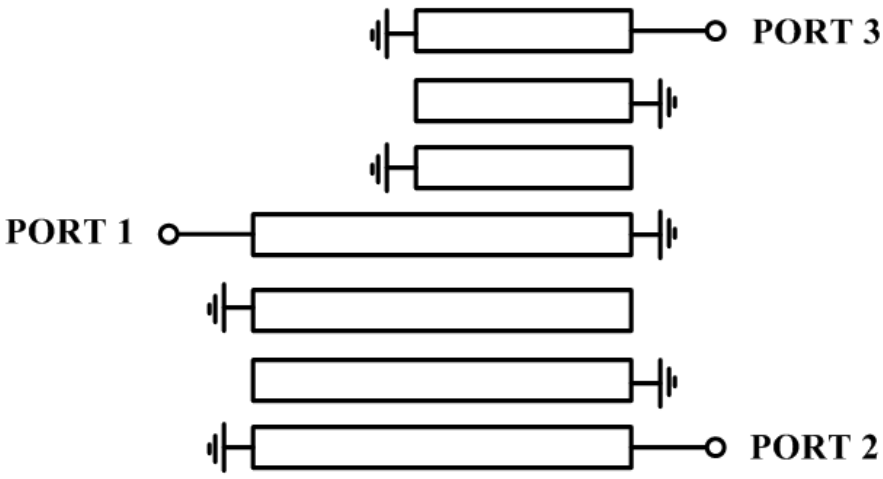

Figure 6-4: Common-transformer diplexer with interdigital filters.

As microstrip bandpass pseudo-interdigital filter has a lot in common with the microstrip interdigital bandpass filter, coupling of the two pseudo-interdigital filters using a common transformer has been studied. The feeding line of the pseudo-interdigital filter is much narrower than a 50Ω line and the length of coupled feeding line is shorter than the length of arms of pseudo-interdigital resonator. Therefore, the common-transformer line was divided in two high impedance feeding line with different lengths. The width of slot between the feeding lines is found using

optimisation. The application of common feeding reduces the total size of diplexer to 30.7 × 5.6 mm or to $0.25\lambda_g \times 0.08\lambda_g$ where λ_g is a wavelength at 2.7 GHz. The same diplexing technique was reported in the design of the diplexer using hairpin bandpass filters [6-10]. The layout of the proposed diplexer is shown in Figure 6-5.

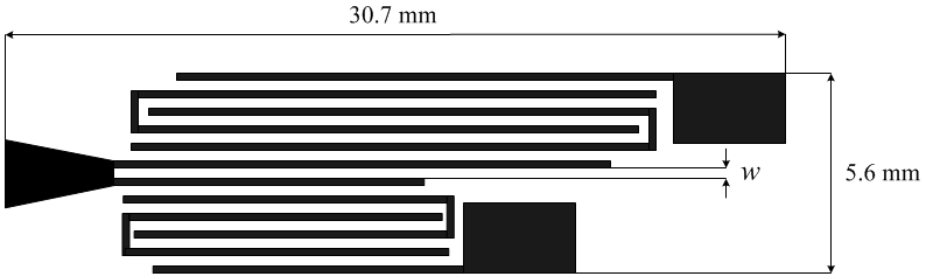

Figure 6-5: Layout of miniaturised microstrip diplexer.

The most optimal width between the two feeding lines of the common transformer has been found to be $w = 0.3$ mm. For the design of diplexer, two bandpass filters, analogues to the ones used in previous section, with center frequencies 2.7 and 3.8 GHz are used. The simulated S-parameters of diplexer are shown in Figure 6-6 by the dashed lines.

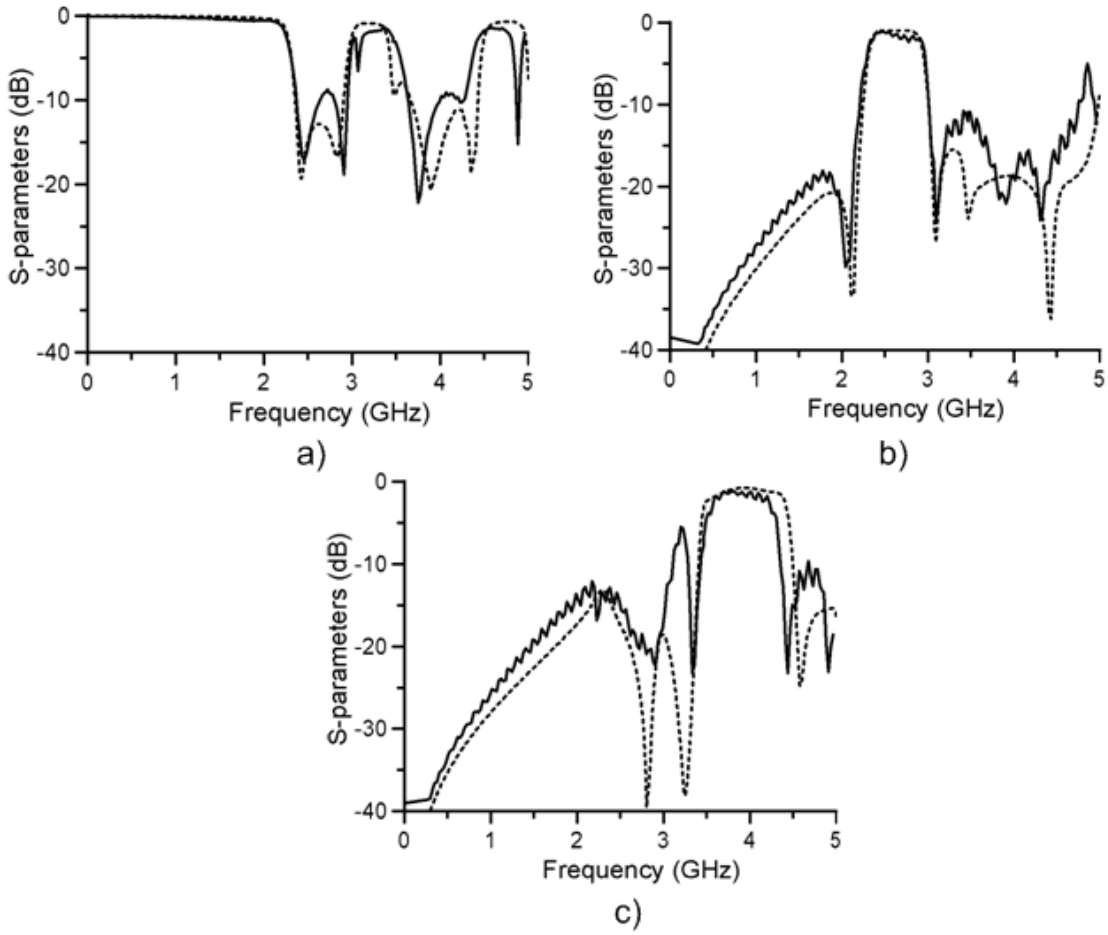

Figure 6-6: Simulated (dashed) and measured (solid) S-parameters of miniaturized microstrip diplexer: (a) S_{11} coefficients; (b) S_{21} coefficients; (b) S_{31} coefficients

From simulated performance of diplexer with common feeding, it can be seen that the passband characteristics of both channels of diplexer were not distorted much and that they are very similar to the passband characteristics of the filter. Compared to microstrip diplexer with the Y-junction, the common feeding diplexer has passband of the second channel altered, but not much. Both channels have a passband return loss of about 13dB and insertion loss 1dB for channel one and 2-2.5 dB for channel two. The TZs frequencies of both filters did not change and occurred at 2.3 and 3.09 GHz for channel one and 3.25 and 4.57 GHz for channel two. The isolation between ports two and three is 20 dB for both channels and the width of the guardband is 0.55 GHz. The miniaturized microstrip diplexer was fabricated on 0.762 mm thick Rogers RT/Duroid 5880 ($\varepsilon_r = 2.2$). The response of the fabricated diplexer was measured with Agilent

PNA (E8361A) network analyzer [6-11]. The measured S-parameters of diplexer are shown in Figure 6-6 by solid lines.

From Figure 6-6, the slight the frequency shift between simulated and measured S-parameters is observed. Poor manufacturing and additional radiation losses caused by it is the reason of increased insertion losses and decreased return losses at both channels of diplexer. Parasitic peak in at 3.3 GHz in the out-of-band region of the second filter is caused by the additional parasitic coupling between the two filters. The deterioration of the bandwidth of the bandpass filter of the second channel is also observed. This can be due to decreased coupling between resonators caused by roughness of milled slots between microstrip lines.

A photograph of fabricated diplexer is shown in Figure 6-7.

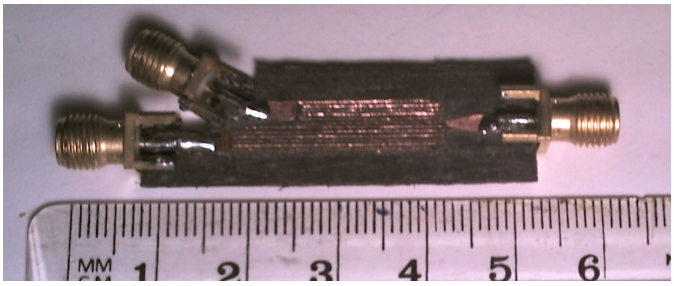

Figure 6-7: Photograph of fabricated miniaturized microstrip diplexer.

6.4. Microstrip Three-Port Four-Channel Diplexers

In previous section, designs of the microstrip diplexer using single band bandpass filters are presented. The possibility to use the same design procedure in order to develop the three-port four-channel diplexer using dual-band bandpass filter will be investigated in this section. The simplest way to build such a diplexer is to use four single band bandpass filters and connect them as shown in Figure 6-8 (a) [6-12]. In this scenario, due to the unwanted interaction between filters, the degradation of stopbands and passbands is possible. The size of such architecture is expected to be bigger than four times the size of filter as matching circuit should also be designed. Figure 6-8 (b) illustrates the architecture of diplexer which will be designed in this section. The main advantage of this architecture over the one with four single band filters is the size reduction. The implementation of this architecture with two dual-band bandstop filters instead of the bandpass filter was reported in [6-13].

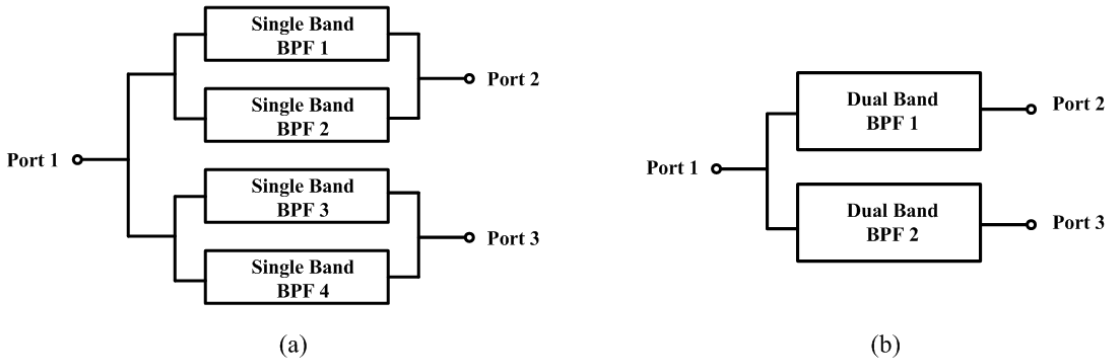

Figure 6-8: Architecture of diplexer: (a) using four single band filters; (b) using two dual-band filters.

Two dual-band pseudo-interdigital SIR bandpass filters were designed using the procedure described in 5.3. The first filter was designed to have passbands centred at 1.65 and 4.65 GHz, the second filter - at 2.5 and 6.9 GHz. Both filters were designed with impedance ratio of SIR $R_Z = 1.176$. Thus the spurious to fundamental passband frequency ratio should be $f_S / f_0 = 2.8$. This ratio for the first filter, obtained from simulation results, is equal to 2.81, and is equal to 2.76 for the second filter. The diplexer was designed for a Rogers RT/Duroid 5880 material with a substrate thickness

of 0.508 mm and a dielectric constant of 2.2. The layout of diplexer is shown in Figure 6-9.

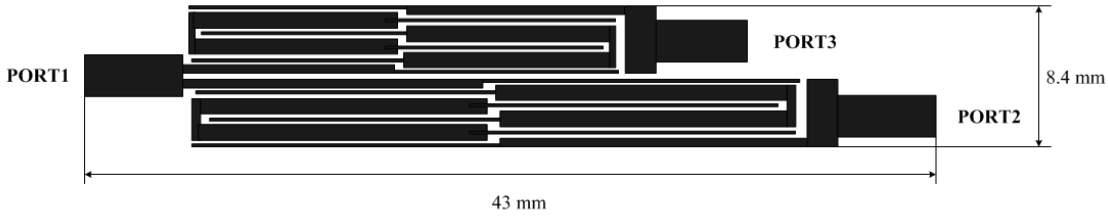

Figure 6-9: Layout of three-port four-channels diplexer.

A diplexer consists of two filters with a layout analogous to the filter shown in the Figure 5-5. Bandpass filters are combined with feeding lines connected to a common feeding 50Ω line. This combining technique can be considered as a modification of the common-transformer diplexing, as it was discussed in the previous section. The diplexer is designed to take 1.65, 2.5, 4.65 and 6.9 GHz into port one and to separate 2.65 GHz and 4.65 GHz to port two and 2.5 GHz and 6.9 GHz to port 3. Figure 6-10 shows the simulated S-parameters of port 1 to port 3 bandpass filter.

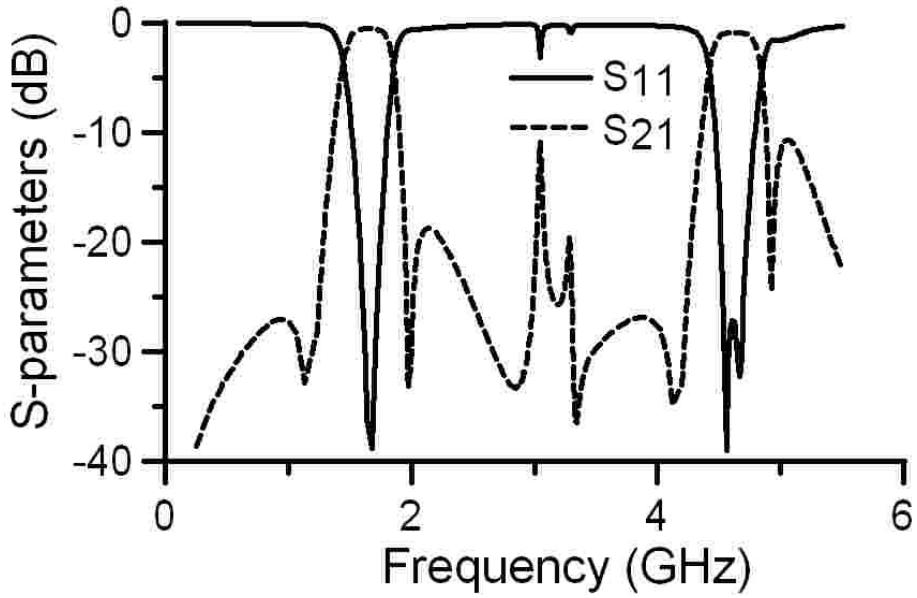

Figure 6-10: Simulated S-parameters of port 1 to port 3 bandpass filter.

The simulated S-parameters of diplexers are shown in Figure 6-11. The simulation diplexer has very good transmission and reflection characteristics on both channels of the first passbands of dual-band filters with minor distortions on the second passband of dual-band filters [6-14]. The insertion losses of the 1.65 GHz and the 4.65 GHz

passbands of the first channel are 0.6 dB and 1.3 dB respectively. For the second channels' passbands insertion losses are 0.9 dB and 1.9 dB for the first and second passbands respectively. The isolation between the channels is about 20 dB. The integration of two filters caused the distortion of characteristics and appearance of additional peaks at about 3 and 6 GHz.

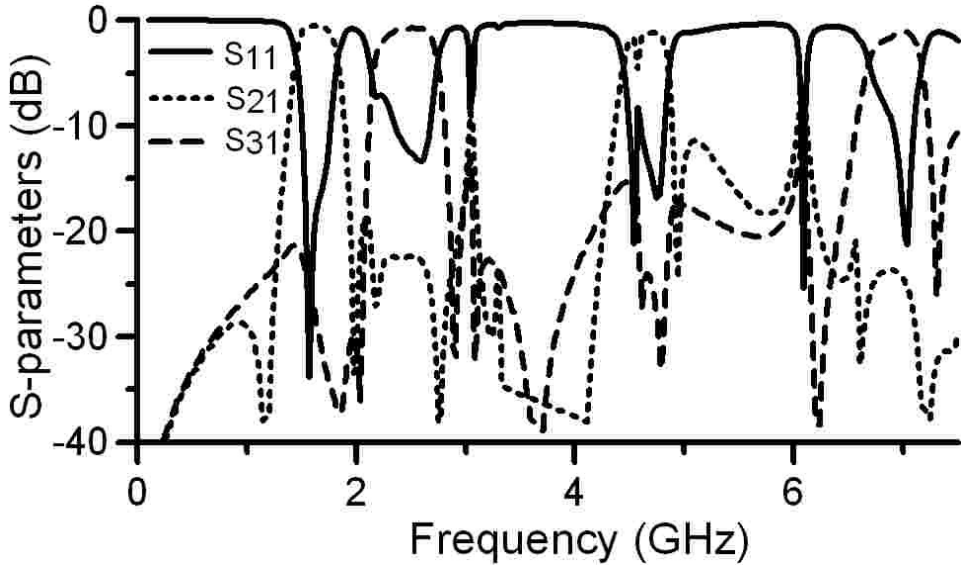

Figure 6-11: Simulated S-parameters of three-port four-channel diplexer.

6.5. Summary

In this chapter, the application of pseudo-interdigital bandpass filters in the design of compact microstrip diplexers is presented.

Section 6.2 presents microstrip diplexer built using bandpass filters with the passband centred at 2.44 GHz and 3.5 GHz. Optimized Y-junction is used to combine filters and connect them to the common port. The isolation between the channels of about 20 dB is achieved, but deterioration of the first channel is observed.

The miniaturised microstrip diplexer with combining circuit based on common transformer is presented in section 6.3. Using this combination technique, a compact size and 20 dB isolation of channels of diplexer are achieved without substantial increase of insertion and return loss of both filters.

Section 6.4 presents the design of three-port four-channel diplexer in which two SIR dual-band filters are combined using the same common transformer based technique. In this diplexer, four channels are separated in pairs to ports 2 and 3. The isolation between channels is 15-20 dB.

6.6. References

[6-1] R. Levy, R. V. Snyder, and G. Matthaei, "Design of microwave filters," *IEEE Trans. on Microwave Theory and Tech.,* vol. 50, pp. 783-793, March 2002

[6-2] L. Ming-Iu and J. Shyh-Kang, "A microstrip three-port and four-channel multiplexer for WLAN and UWB coexistence," *IEEE Trans. on Microwave Theory and Tech.,* vol. 53, no. 10 pp. 3244-3250, October 2005

[6-3] D. Pu-Hua, L. Ming-Iu, J. Shyh-Kang, and C. Chun Hsiung, "Design of Matching Circuits for Microstrip Triplexers Based on Stepped-Impedance Resonators," *IEEE Trans. on Microwave Theory and Tech.,* vol. 54, no. 12, pp. 4185-4192, December 2006

[6-4] M. Zewani and I. C. Hunter, "Design of Ring-Manifold Microwave Multiplexers," *IEEE MTT-S, Int. Microwave Symp. Dig.*, June 2006, pp.2019-2022

[6-5] A. F. Sheta, J. P. Coupez, G. Tanne, S. Toutain, and J. P. Blot, "Miniature microstrip stepped impedance resonator bandpass filters and diplexers for mobile communications," *IEEE MTT-S, Int. Microwave Symp. Dig.*, June 1996, pp. 607-610

[6-6] L. Yo-Shen, C. Po-Ying, and L. Chun-Lin, "Compact parallel-coupled microstrip diplexers with good stopband rejection," *Asia-Pacific Microwave Conf.,* Singapore, December 2009, pp.2621-2624

[6-7] G. Tudosie and R. Vahldieck, "An efficient design approach for planar microwave multiplexers," *34th European Microwave Conference,* Amsterdam, Netherlands, October 2004, pp. 1229- 1232

[6-8] D. Zayniyev, D. Budimir, and G. Zouganelis, "Microstrip filters and diplexers for WiMAX applications," *IEEE AP-S/URSI Int. Symp. Dig.*, June 2007, pp.1561-1564

[6-9] J. D. Rhodes and R. Levy, "A Generalized Multiplexer Theory," *IEEE Trans. on Microwave Theory and Tech.,* vol. 27, no. 2, pp. 99-111, February 1979.

[6-10] W. Min-Hang, H. Cheng-Yuan, and S. Yan-Kuin, "A Hairpin Line Diplexer for Direct Sequence Ultra-Wideband Wireless Communications," *IEEE Microwave and Wireless Comp. Lett.,* vol. 17, no. 7, pp. 519-521, July 2007

[6-11] D. Zayniyev, D. Budimir, and G. Zouganelis, "Miniaturized microstrip filters and diplexers for wireless communication systems," *Microwave and Optical Technology Lett.*, vol. 50, no. 10, pp. 2701-2702, February 2008

[6-12] Y. Tae-Yeoul, W. Chunlei, P. Zepeda, C. T. Rodenbeck, M. R. Coutant, L. Ming-yi, and C. Kai, "A 10- to 21-GHz, low-cost, multifrequency, and full-duplex phased-array antenna system," *IEEE Trans. on Antennas and Propagation,* , vol. 50, no. 5, pp. 641-650, May 2002

[6-13] B. Strassner and K. Chang, "Wide-band low-loss high-isolation microstrip periodic-stub diplexer for multiple-frequency applications," *IEEE Trans. on Microwave Theory and Tech.,* vol. 49, no. 10 pp. 1818-1820, October 2001

[6-14] D. Zayniyev and D. Budimir, "Microstrip three-port 4-channel multiplexers using dual-band bandpass filters for wireless applications," *IEEE AP-S/URSI Int. Symp. Dig*., July 2008.

7. INTEGRATED ANTENNA FILTERS AND ANTENNA DIPLEXERS FOR WIRELESS APPLICATIONS

7.1. Introduction

Microstrip patch antennas, proposed in 1950's, consist of a radiating patch on one side of dielectric with a ground plane on the other side [7-1]. These are low-profile, light weight antennas, which are used in a wide range of modern microwave systems, especially in aerospace and mobile applications. The main advantages of microstrip antennas are low cost of production and the possibility to integrate with microwave integrated circuits and to fabricate feed and matching circuits simultaneously with antenna structure. Dual-frequency and dual-polarization microstrip antennas can also be easily made [7-2]. The main disadvantages of microstrip antennas are low gain, narrow bandwidth, and poor efficiency especially for antennas built using high dielectric substrate for easy integration with MIC RF front-end circuitry. Although integration of patch antennas with filters can be used to improve bandwidth and gain [7-3], the main purposes of such an integration is the reduction of size of the microwave front-end [7-4], [7-5], suppression of higher order antenna's resonances [7-6] and the creation of wideband antennas with narrow band interferer rejection characteristics, for which band-stop filters are used [7-7]. Dual-band patch antennas can be integrated with diplexers to reduce component count in dual-band wireless systems, in which diplexers are used to separate high and low bands of antennas [7-8], [7- 9].

This chapter presents applications of filters and diplexers discussed in previous chapters in integrated antenna filters and antenna diplexers. The integration of inset-fed rectangular patch antenna with pseudo-interdigital bandpass filer is presented in section 7.2. As a result of this integration, suppression of the first and the second spurious harmonics of antenna has been achieved. Section 7.3 presents integration of multiband patch antenna with a diplexer. This integration was used to suppress the antenna's peaks that are out of the passbands of the diplexer's filters and to separate physically bands of antenna. The integration of the dual-band multi-resonators microstrip-fed patch antenna with microstrip diplexer and filter is presented in section 7.4. Improvement in performance of the antenna and the physical separation of channels has been achieved as a result of integration.

7.2. Integrated Antenna Filters with Harmonic Rejection

A rectangular microstrip patch antenna is a basic configuration of a microstrip antenna. The main disadvantages of this configuration are narrow band and spurious harmonics. Suppression of spurious harmonics of antenna can be achieved by, for example, etching a U-slot in the antenna's patch [7-10], or by designing special feeding technique using proximity coupling [7-11]. The most obvious solution to the spurious harmonics problem is an integration of the antenna with a lowpass or bandpass filter [7-4].

One of the main challenges of such an integration using a single layer microstrip is that for microstrip patch antennas the most preferable type of substrate is a thick substrate with a small dielectric constant. Using this substrate, better efficiency and larger bandwidth of the antenna can be achieved. For microstrip filter, on the contrary, thin substrates with high dielectric constant are preferable as employment of this type of substrate reduces radiation losses and size of filters. To address this issue composite substrates and multilayer solutions can be used [7-12]. Another challenge is the size of the integrated antenna filters. The necessity of using impedance matching in the feeding of antenna can increase the size of the circuit substantially [7-6]. The proposed integrated antenna-filter is a good solution for both of these challenges as compact pseudo-interdigital bandpass filter designed using low dielectric constant substrate will be used as a replacement of the impedance transformer employed as a feeding line of microstrip patch antenna.

The layout of inset-fed microstrip patch antenna is shown in Figure 7-1. The length of the patch is approximately equal to half the wavelength. The width and length of antenna can be found from formula [7-13]:

$$W = \frac{c}{2f_0}\left(\frac{\varepsilon_r + 1}{2}\right)^{-0.5} \tag{7-1}$$

$$L = \frac{c}{2f_0\sqrt{\varepsilon_{eff}}} - 2\Delta L \tag{7-2}$$

where f_0 is resonance frequency, ΔL is length extension due to the fringing capacitance with a value that can be found from (7-3). For a 0.867 mm thick substrate with dielectric constant 2.2, and the resonance frequency $f_0 = 2.4$ GHz, using Eq. (7-1) – (7-3) the width is equal to 49.2 mm and the length 41.5 mm. As the width of the patch does not affect the resonance frequency and affects only the gain of antenna, its value of 42 mm has been chosen in order to decrease the simulation time.

$$\Delta L = \frac{0.412h\left(\varepsilon_{eff}+0.3\right)\left(\frac{W}{h}+0.264\right)}{\left(\varepsilon_{eff}+0.258\right)\left(\frac{W}{h}+0.8\right)} \tag{7.3}$$

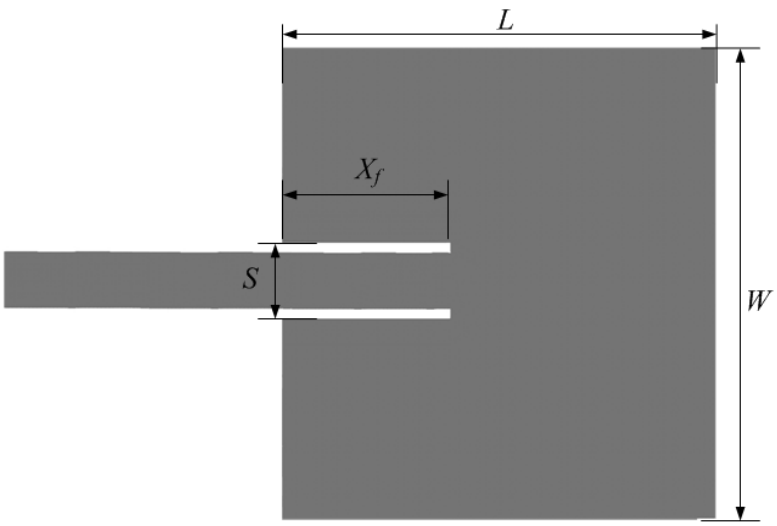

Figure 7-1: Layout of microstrip inset-fed patch antenna.

The length of inset distance X_f cannot be found using some closed form expression. It was reported that a shifted cosine-squared function describes the variation of the resonant input resistance with the feed location [7-14].

$$R_{in} = A\cos^2\left[\frac{\pi}{2}\left(X_n - B\right)\right] \tag{7-4}$$

where $X_n = 2X_f / L$ and parameters A and B depend on the notch width S and the geometry of the substrate. In order to obtain the initial approximate value of the X_f, parameters A and B given in [7-14] for the $\varepsilon_r = 2.42$ substrate with the width of notch S equal twice the width of feeding line, were used. After a few steps of tuning and iterations, the final dimensions of the antenna were chosen to be $L = 41.7\,\text{mm}$, $W = 41\,\text{mm}$, $S = 6\,\text{mm}$, $X_f = 11.8\,\text{mm}$, and the width of the 50Ω feeding line $w_f = 2.6\,\text{mm}$. From the simulation results, the fundamental resonant frequency of this antenna is 2.41 GHz, and the first spurious response is at 4.64 GHz.

For integration with the designed antenna pseudo-interdigital SIR bandpass filter discussed in section 5.4.1 has been used. The impedance ratio $R_Z = 0.6$ has been chosen and the filter is designed with a center frequency at 2.17 GHz and with $FBW = 30.5\%$. The first spurious passband of filter is centred at 8.13 GHz, thus the simulated the ratio of the first spurious resonance frequency to the fundamental resonance frequency is $f_S / f_0 = 3.75$, which is almost equal to the calculated value of 3.77. The layout of the designed filter is analogous to the one depicted in Figure 5-9, and the simulated performance of the filter is similar to the one shown in Figure 5-10.

As the next step, the feeding line of antenna has been replaced by the designed filter. The layout of the integrated antenna filter is shown in Figure 7-2. The additional transition section consisting of microstrip taper and meander line sections is used to improver impedance matching [7-15].

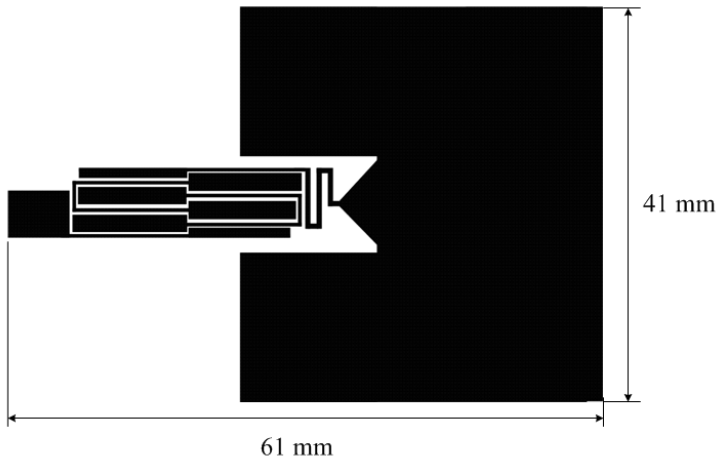

Figure 7-2: Layout of microstrip antenna filter.

The integrated antenna filter has been simulated using ADS Momentum and the simulated S_{11} coefficient of antenna-filter is shown in Figure 7-3 by the solid line. The simulated S_{11} coefficient of the inset-fed patch antenna is shown in the same figure by the dashed line for comparison.

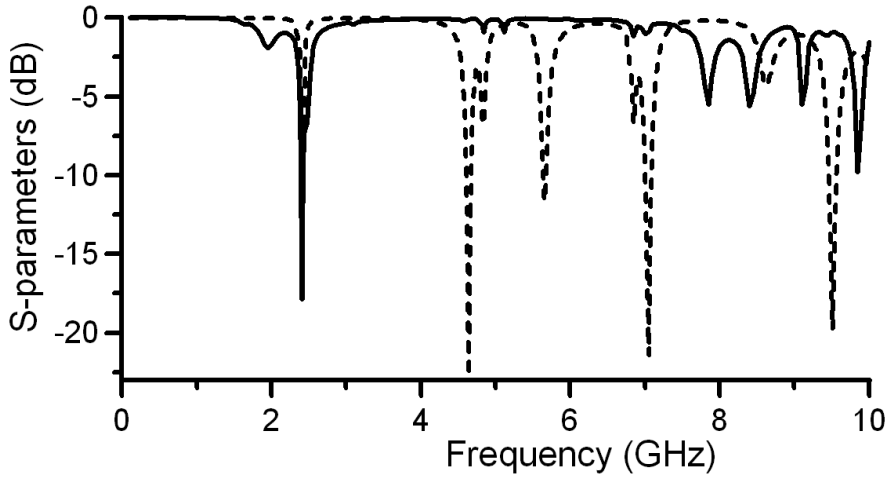

Figure 7-3: Simulated S_{11} of inset-fed antenna (dashed) and antenna filter (solid).

As it can be seen from Figure 7-3 the first and the second harmonics of the inset-fed antenna were suppressed in the antenna filter. The two peaks appearing in the antenna filter's response at 7.85 and 8.4 GHz are due to the second passband of bandpass filter. The simulated radiation patterns of both antenna and antenna filter at fundamental resonance are shown in Figure 7-4. It can be seen from this figure that integration of antenna with filter has not caused much alteration in radiation pattern but only decrease of gain from maximum 6.08 dB for antenna to 5.04 dB for antenna filter.

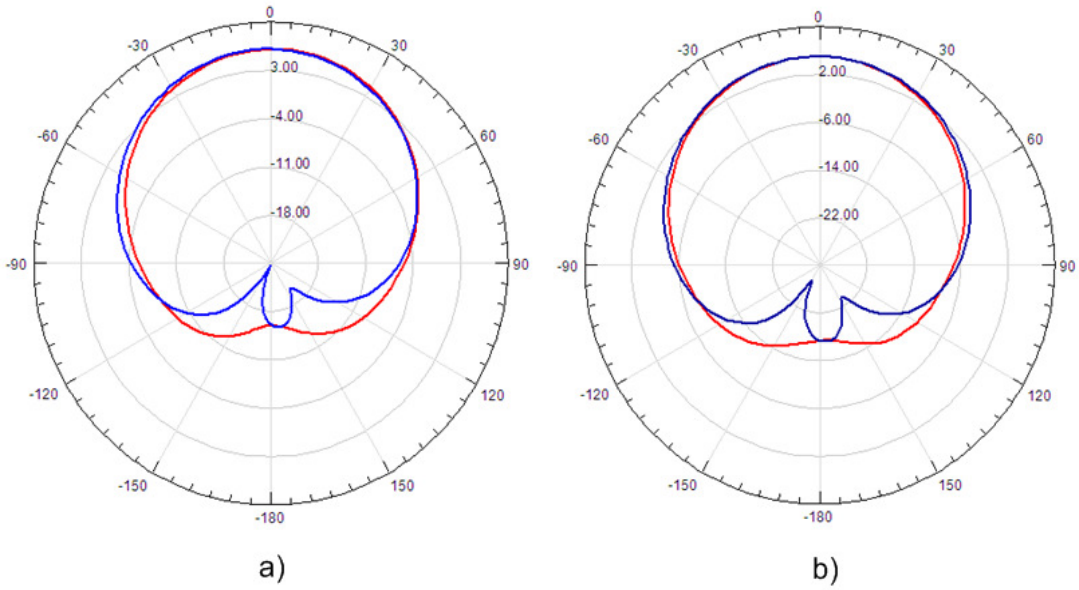

Figure 7-4: Simulated radiation patterns, E-plane (red) and H-plane (blue): (a) Patch antenna; (b) Integrated Antenna Filter.

7.3. Microstrip Antenna Diplexers for Wireless Communications

The integration of microstrip antennas with filters is used to suppress the spurious harmonics of antennas or to improve antenna's characteristics at the fundamental resonance. The integration of microstrip antennas with diplexers can be used to reduce the number of components in wireless system [7-8] and to separate physically the signal from the different antennas [7-9]. In this section, the integration of multiband antenna with diplexer for physical separation of antenna's bands is presented. The integrated antenna diplexers can be used in the design of wireless systems operating on multiple bands, such as for example WLAN IEEE 802.11 standard operating at 2.4-2.45 GHz and 5.15-5.85 GHz and WiMAX IEEE 802.16 standard, operating at 2.3-2.7 GHz, 3.3-3.9 GHz, and 5.15-5.85 GHz.

The layout of the proposed integrated antenna diplexer is shown in Figure 7-5.

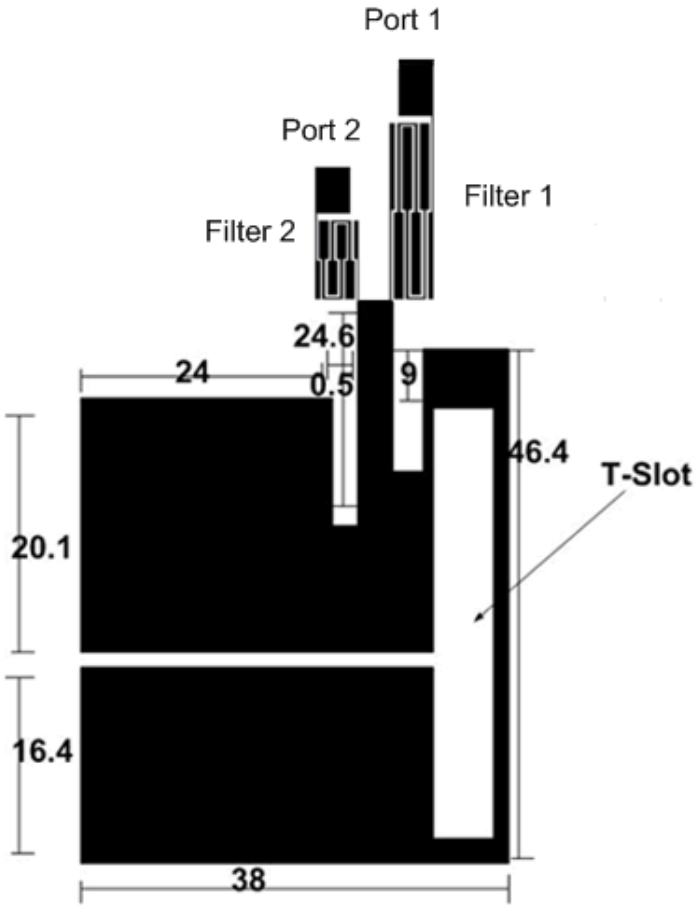

Figure 7-5: Layout of proposed microstrip antenna diplexer

The size of the whole subsystem is 38×69 mm; it consists of a compact diplexer, constructed from two filters, and a patch antenna. The integration of the antenna with diplexer has been arranged by connecting the common port of the diplexer with the microstrip line feeding antenna. As both lines are 50 Ohms lines, no additional impedance matching was applied. The design specifications for the proposed antenna are, the dielectric material selected for the design is FR4 which has a dielectric constant of 4.4 and a height of substrate $h = 1.57$ mm. The antenna is fed by a 50 Ω microstrip line. The main advantage of using a transmission line feeding is very easy to fabricate and simple to match by controlling the inset position and relatively simple to model.

The broadband characteristic of a microstrip patch antenna with different shapes has been confirmed by many published results and several designs of the broadband slots antenna has been reported [7-16], [7-17]. The T-slot has been applied on the patch antenna to let the current path travel longer than its usual way in order to achieve multi-band performance to be used in wireless applications. This is similar to the dual-band performance of microstrip patch antennas with dual U-slot in which surface-current path has a different length for different resonance frequencies. Thus, at 2.5 GHz surface current has a longer path and it has to go around T-slot. It has been found that, by inserting the T-Slot to the patch and optimising width and length of slot, the required resonant frequencies can be achieved. The proposed antenna has been simulated with commercially available package HFSS software which is based on the finite element method. The antenna was designed to operate in dual-band mode, mainly for the wireless applications standard 2.5 and 5.2 GHz. The simulated S_{11} of antenna is shown in Figure 7-6.

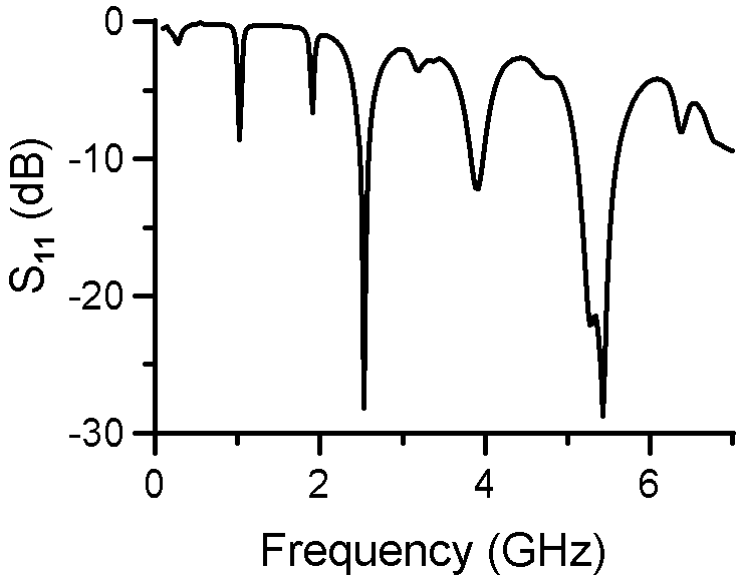

Figure 7-6: Simulated S_{11} of proposed antenna.

The microstrip diplexer is built using two compact pseudo-interdigital SIR bandpass filters with extended stopband which were discussed in 5.4.1. The filters are combined using a common feeding technique based on the common-transformer diplexer. This combining method was discussed in 6.3. The filters are designed for a 1.57 mm thick substrate with $\varepsilon_r = 4.4$. The impedance ratio of SIR in both filters is 0.7 and the calculated spurious to fundamental frequencies ratio is $f_S / f_0 = 3.5$. Both filters have $FBW = 31.4\%$ and the first filter has a passband centred at 2.42GHz, the second has a passband centred at 5 GHz. The layout of filters is similar to the one shown in Figure 5-9 and can be seen in Figure 7-5. The simulated S-parameters of the filters are similar to the response shown in Figure 5-10. Tthe simulated S-parameters of diplexer are shown in Figure 7-7.

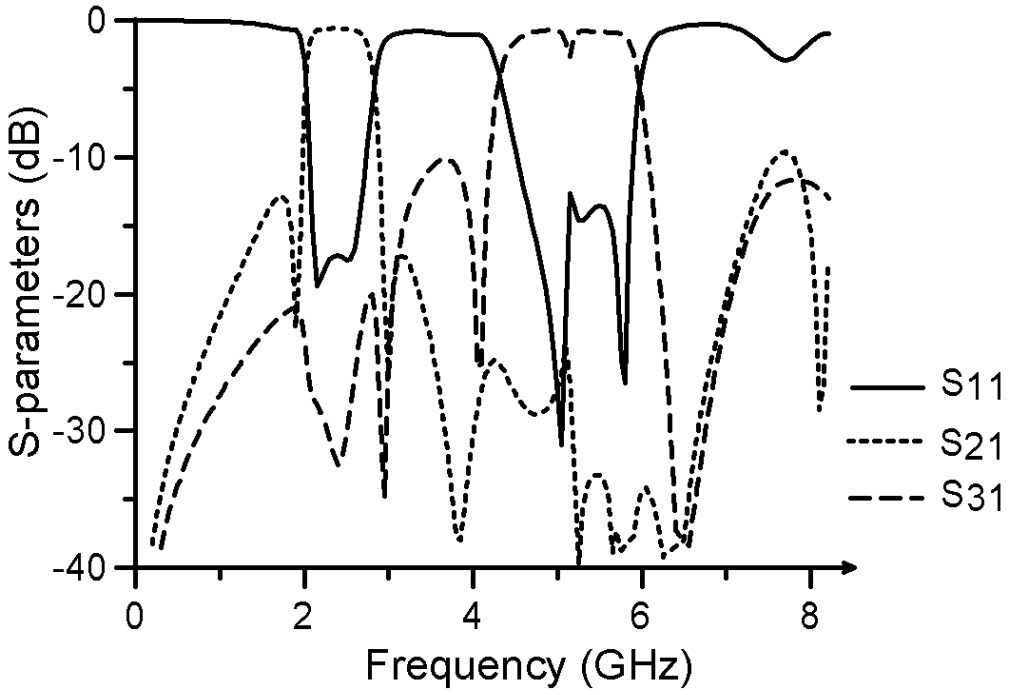

Figure 7-7: Simulated S-parameters of microstrip diplexer.

It can be seen from the simulation results that the diplexer has a channel isolation of about 25 dB [7-18]. The insertion loss of each channel is almost the same as the insertion loss of bandpass filter used in the corresponding channel, whereas the return loss in the passband is decreased to 15 dB.

The integrated antenna diplexer structure was simulated by the Agilent ADS electromagnetic simulator. The simulated S-parameters are presented in Figure 7-8.

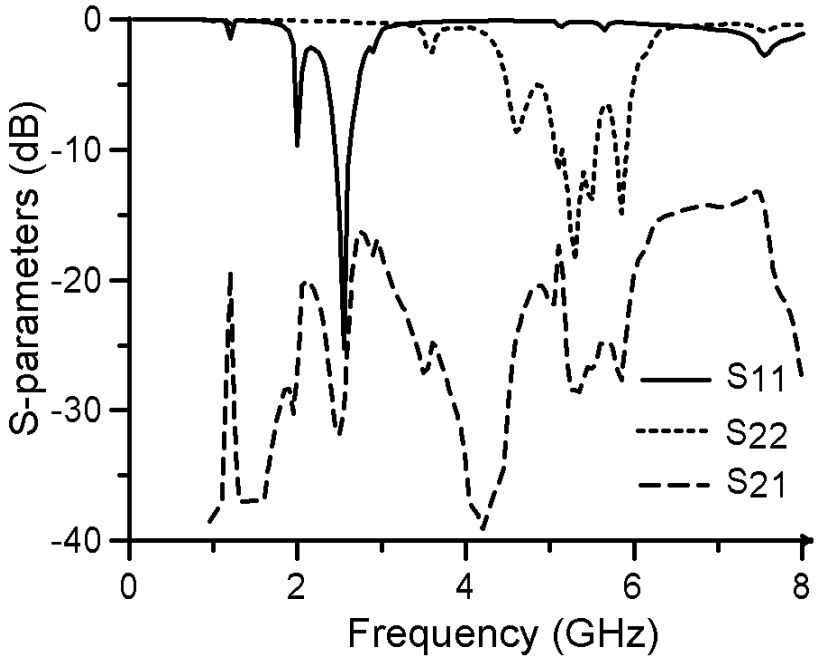

Figure 7-8: Simulated S-parameters of microstrip antenna diplexer.

As a result of the integration of the antenna with the diplexer, the high frequency band of antennas centered at 5.2 GHz is physically separated from the low frequency band of antenna centered at the 2.5 GHz. Unwanted spurious peaks of the antenna appearing at 1 GHz and 3.9 GHz were suppressed by the diplexer. The total structure demonstrates good isolation of channels from each other.

7.4. Integration of Microstrip Filters/Diplexers with Dual-band Multi-Resonator Microstrip-Fed Patch Antenna

In the following section, the integration of microstrip diplexers and filters with dual-band multi-resonators microstrip-fed patch antenna is presented. The integration with the diplexer is used to separate physically bands of antenna. The integration of antenna with dual-band filters is employed in order to improve the bandwidth of the antenna. The procedure used to develop integrated antenna diplexer is the same as the one described in the previous section with dual-band monopole patch antenna used instead of multiband microstrip patch antenna. The layout of the proposed structure is shown in Figure 7-9.

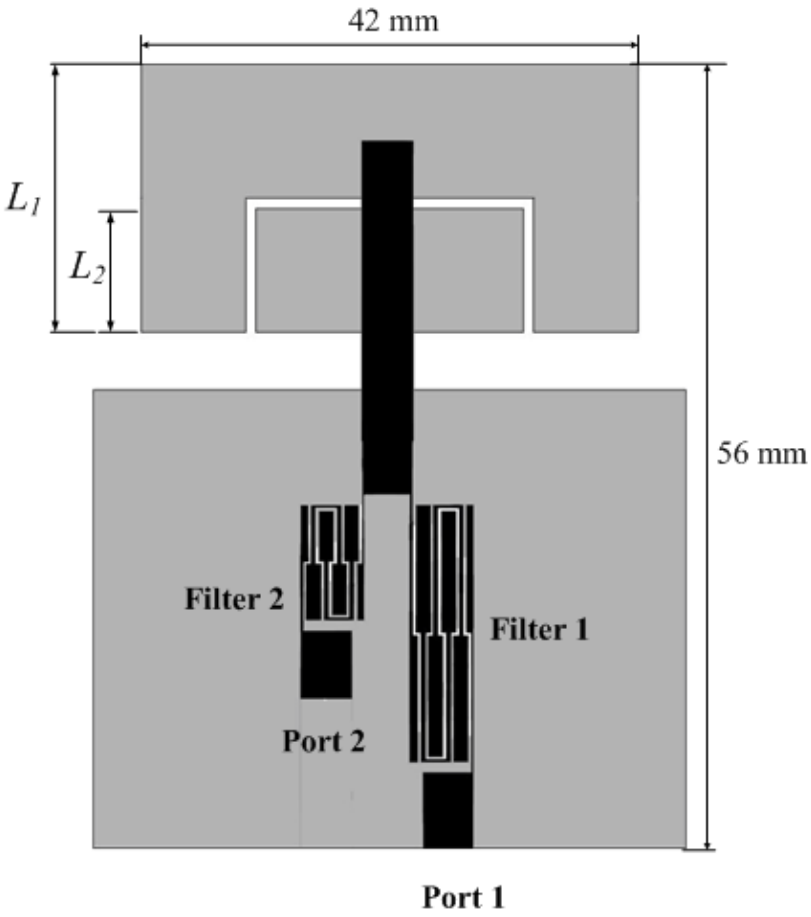

Figure 7-9: Layout of proposed antenna diplexer.

The multi-resonator microstrip-fed patch antenna proposed in [7-19] is used for a broadband dual-frequency operation. The antenna consists of two resonators separated by a U-shaped slit. The lengths of resonators L_1 and L_2 are around a quarter-wavelengths at the first and second resonant frequencies respectively. This antenna is the printed monopole antenna with feeding through proximity coupling. The operational principle of this antenna is equivalent to the operational principle of the conventional monopole antenna made of metallic wire or rod and which consists of one radiating arm. Very frequently monopole antennas are used above a full or partial ground plane and the reflection from this ground plane produces a virtual monopole below the ground. Thus, monopole antennas in this case can be evaluated in the same way as dipole antennas, which consist of two radiating arms with feed point at the center. The current distribution of these antennas is sinusoidal standing wave with current at the end of the radiating arms equal to zero and at the feeding point current is the maximum when dipole antenna is $\lambda/2$ long and monopole antenna is $\lambda/4$ long. The radiation pattern of dipole antenna is slightly flattened torus and it is rotationally symmetric around the axe along which radiating arms are positioned. For monopole antenna above ground plane, radiation pattern is the upper half of dipole antenna and the directivity of monopole antenna is twice of its dipole counterpart due to the power to the lower half space reflected to the upper space. One of the main reasons why the most popular size of dipole antenna is half wavelength and for monopole antenna is a quarter wavelength respectively is that in this case the input impedance of antenna can be easily matched with a standard transmission line. Moreover, antenna of these sizes is a good trade-off between the directivity and size.

The antenna shown in Figure 7-9 is fed by a 50 Ω transmission line printed on the opposite side of the substrate. The length of the feeding stub is tuned for impedance matching on both resonant frequencies. The antenna was designed for Rogers RT 5880 substrate with thickness 1.57 mm and dielectric constant 2.2. The designed antenna was simulated with the commercially available package HFSS software which is based on the finite element method. The simulated return loss of antenna is shown in Figure 7-10.

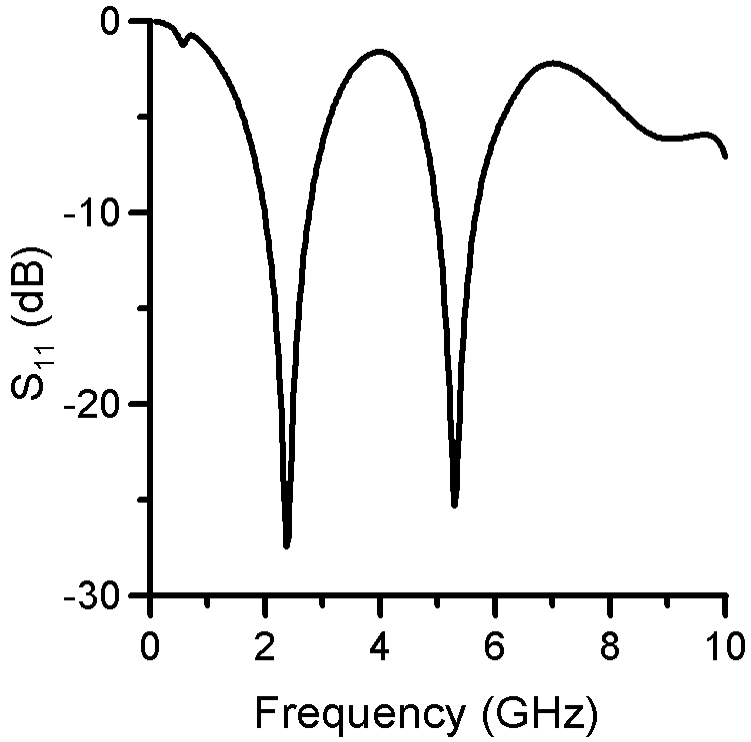

Figure 7-10: Simulated return loss of multi-resonator patch antenna.

The antenna was designed to resonate at the frequencies 2.37 and 5.3 GHz. The bandwidth, for return loss <-10 dB, of the first band of antenna is 31.5% and for second band is 12.6%.

The diplexer integrated with the antenna is equivalent to the diplexer used in the previous section, but designed for a substrate with dielectric constant 2.2. The impedance ratio of the SIR of the bandpass filters was chosen to be 0.5 with the ratio of spurious to fundamental harmonic frequencies calculated to be $f_S / f_0 \approx 4$. Such an impedance ratio was chosen to extend further the stopband of the first filter in order to diminish interaction with the passband of the second channel. Filters were designed to have center frequencies at 2.4 GHz and 5.3 GHz respectively. The S-parameters of the microstrip diplexer, simulated using EM Sonnet are shown in Figure 7-11. The isolation between the bands is 20 dB for channel one and 25 dB for channel two. The passband performance of the second filter was deteriorated by the losses introduced due to the big impedance step. To avoid this in future designs, a smaller impedance step for SIR of the second, high frequency band filter, will be used.

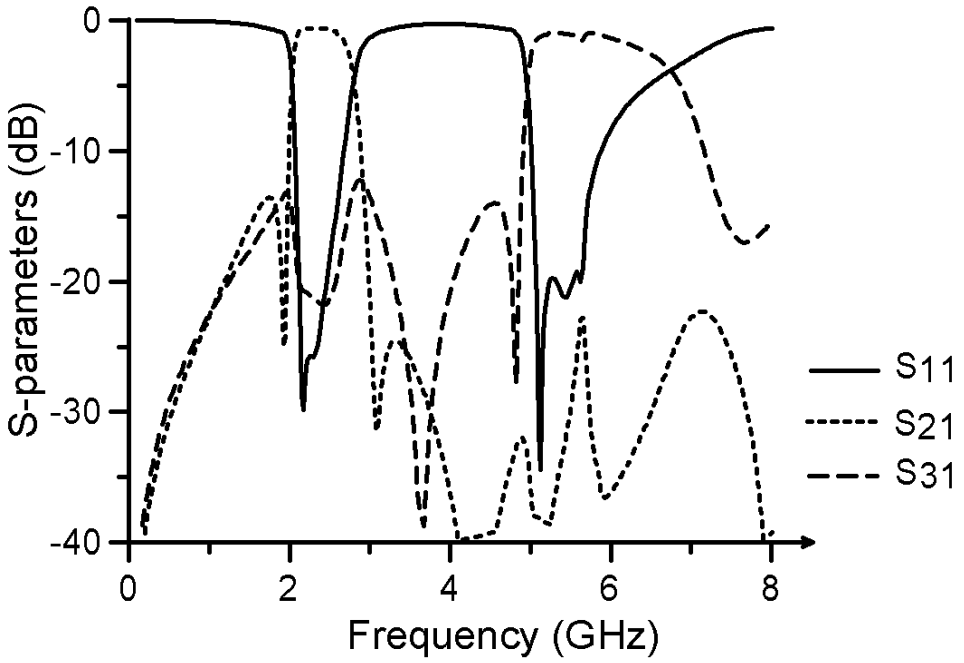

Figure 7-11: Simulated S-parameters of microstrip diplexer.

The integrated antenna diplexer was simulated using HFSS and simulated S-parameters are shown in Figure 7-12.

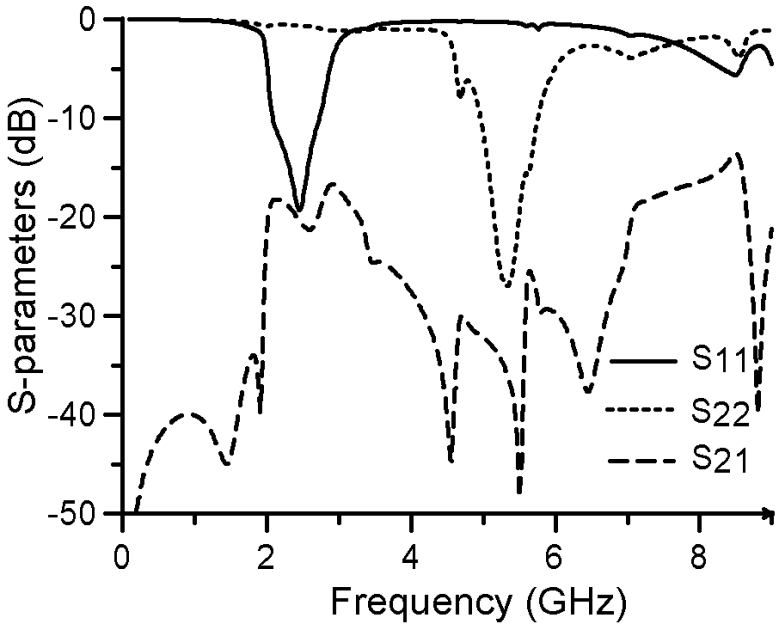

Figure 7-12: Simulated S-parameters of integrated antenna diplexer.

As a result of the integration of antenna with diplexer, different bands of antenna were physically separated. The total structure demonstrates good isolation of channels from

each other. An isolation of 20 dB was achieved for channel one and of 30 dB for channel two [7-20].

The integration of antennas with the bandpass filter can also be used to improve the performance of antenna [7-3]. The integration of dual-band antenna with the dual-band filter was investigated in order to find the effect and alteration of the performance of antenna due to the integration with the filter. The same multi-resonators microstrip-fed dual-band patch antenna, used for the integration with the diplexer, is employed for integration with the dual-band microstrip filter.

The dual-band bandpass filter equivalent to the filter discussed in section in 5.3 was designed for Rogers RT 5880 substrate with thickness 1.57 mm and dielectric constant 2.2. The passbands of filter are centred at 2.45 and 5.55 GHz and FBW is equal to 31.4% for band one and 13% for band two. The impedance ratio of SIR of filters was chosen to be equal to 2.24 with spurious to fundamental resonance frequencies' ratio calculated to be equal $f_S / f_0 = 2.2$. This ratio extracted from the simulation results is equal to 2.27. The performance of the designed filter is similar to the one depicted in Figure 5-6 with center frequencies of bands shifted to 2.45 and 5.55 GHz. The layout of the integrated dual-band antenna filter is shown in Figure 7-13. The dual-band filter was used to replace the microstrip feeding line [7-21].

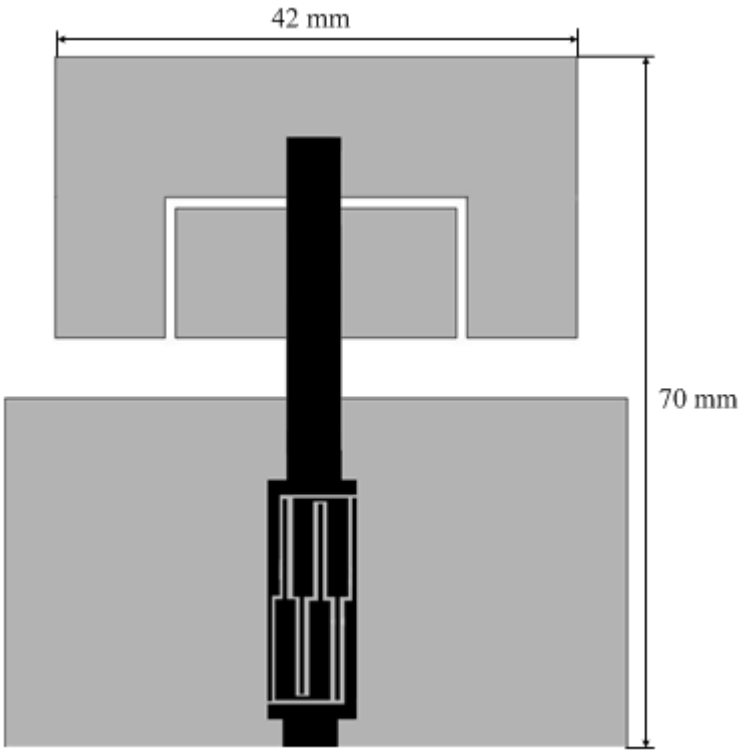

Figure 7-13: Layout of integrated dual-band antenna filter.

The integrated dual-band antenna filter was simulated with using Ansoft HFSS package. The simulated return loss is shown in Figure 7-14.

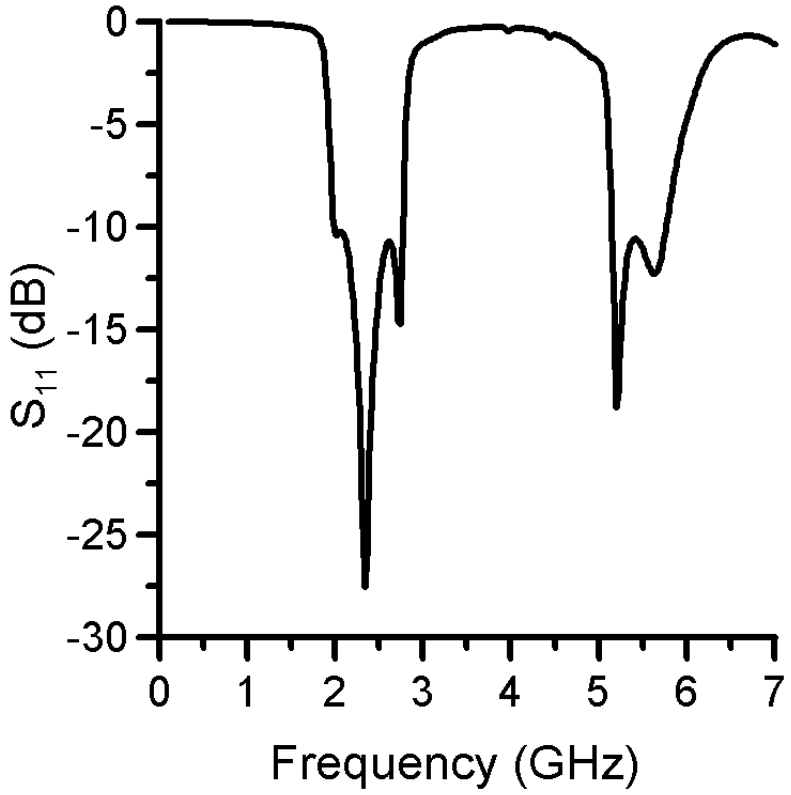

Figure 7-14: Simulated return loss of integrated dual-band antenna filter.

As it can be seen from Figure 7-14, a significant improvement of the bandwidth of the antenna was achieved. The antenna's reflection in the out-of-band regions of the dual-band filter was also suppressed. This suppression is possible due to the increased steepness in the insertion loss of the dual-band filter caused by the appearance of TZs at finite frequencies. Therefore, such an integration approach can be used for the suppression of the unwanted reflection of antennas as well as for the improvement of selectivity of wideband antennas used in the design of the dual-band systems.

7.5. Summary

In this chapter the integrated antenna filters and the antenna diplexers are presented. These subsystems are designed to demonstrate the application of filters and diplexers, proposed in the previous chapters, in the design of RF front-end.

Section 7.2 presents the integration of the single band bandpass filter with the inset-fed rectangular patch antenna. The suppression of the second and the third harmonics of the patch antenna was achieved. The whole subsystem has small size because a compact bandpass filter was employed as a replacement of the feeding line of antenna.

The integrated antenna diplexer is presented in section 7.3. The purpose of the integration of the multiband patch antenna with diplexer is a physical separation of the low and high bands of the antenna and the reduction of the number of components in wireless system. The resonant peaks of the antenna that occurred at the frequency outside the passbands of the diplexer were also suppressed.

Section 7.4 presents integration of dual-band multi-resonators microstrip-fed patch antenna with microstrip diplexer and filter. The integration with diplexer is used to reduce the components' count in wireless systems and to separate high and low bands of the antenna. The improvement of bandwidth and selectivity of the antenna resulted from the integration of antenna with the dual-band bandpass filter.

7.6. References.

[7-1] D. M. Pozar, "Microstrip antennas," *Proceedings of the IEEE*, vol. 80, no. 1 pp. 79-91, January 1992

[7-2] R. Garg, P.Bhartia, I. Bahl, A. Ittipiboon, *Microstrip Antenna Design Handbook*. Norwood: Artech House, 2001

[7-3] Z. Jianhong, C. Xinwei, H. Guorui, L. Li, and Z. Wenmei, "An Integrated Approach to RF Antenna-Filter Co-Design, "*Antennas and Wireless Propagation Letters, IEEE*, vol. 8, pp. 141-144, 2009.

[7-4] A. Abbaspour-Tamijani, J. Rizk, and G. Rebeiz, "Integration of filters and microstrip antennas," *IEEE AP-S/URSI Int. Symp. Dig*., June 2002, pp. 874–877.

[7-5] F. Queudet, I. Pele, B. Froppier, Y. Mahe, and S. Toutain, "Integration of pass-band filters in patch antennas," *32nd European Microwave Conf*., Milan September 2002, pp. 685 - 688

[7-6] B. Atallah, M. Jan, and O. Abbas, "Microstrip-CPW bandpass filter for antenna application," *Microwave and Optical Technology Lett.*, vol. 50, no. 1, pp. 51-55, June 2007

[7-7] L. Wang-Sang, K. Jin-Hyun, L. Won-Gyu, S. Kwang-Seop, L. Hyung-Sun, and Y. Jong-Won, "Capacitively Coupled Band-Stop Filter with an Integrated Antenna,"*IEEE MTT-S, Int. Microwave Symp. Dig.*, June 2006, pp.2019-2022

[7-8] C. Pei-Ling, W. Syu-Sheng, and L. Yu-De, "Integrated antennas and diplexers for dual-band wireless local area network (WLAN) system," *Asia-Pacific Microwave Conf.*, Suzhou, China, Dec. 2005, vol. 4 pp. 4-7

[7-9] D. Veysel, H. Chun-Wen Paul, and E. Atef, "Novel dual-band WLAN antennas with integrated band-select filter for 802.11 a/b/g WLAN radios in portable devices," *Microwave and Optical Technology Lett.*, vol. 49, no. 8, pp. 1868-1872, January 2007.

[7-10] R. Dehbashi, K. Forooraghi, and Z. Atlasbaf, "A Harmonic-Rejecting Inset-Fed U-Slot Antenna for Rectenna Application," *Sarnoff Symposium, IEEE*, March 2006

[7-11] L. Inclan-Sanchez, J. L. Vazquez-Roy, and E. Rajo-Iglesias, "Microstrip patch antenna with compact feed to reduce harmonics," *1st European Conf. Antennas and Propagation ,* Nice, France, November 2006

[7-12] T. Le Nadan, J. P. Coupez, and C. Person, "Optimization and miniaturization of a filter/antenna multi-function module using a composite ceramic-foam substrate," *IEEE MTT-S, Int. Microwave Symp. Dig.*,June 1999, pp.219-222

[7-13] Z. I. Dafalla, W. T. Y. Kuan, A. M. A. Rahman, and S. C. Shudakar, "Design of a rectangular microstrip patch antenna at 1 GHz," *RF and Microwave Conf.,* October 2004, pp. 145-149

[7-14] H. Ying, D. R. Jackson, J. T. Williams, S. A. Long, and V. R. Komanduri, "Characterization of the Input Impedance of the Inset-Fed Rectangular Microstrip Antenna," *IEEE Trans. on Antennas and Propagation,* vol. 56, no.10, pp. 3314-3318, October 2008

[7-15] D. Zayniyev and D. Budimir, "An integrated antenna-filter with harmonic rejection," *3rd European Conf. Antennas and Propagation,* Berlin, Germany, March 2009, pp.393-394

[7-16] H. F. AbuTarboush, H. S. Al-Raweshidy, and R. Nilavalan, "Triple band double U-slots patch antenna for WiMAX mobile applications," *14th Asia-Pacific Conf. on Communications,* Tokio*,* Japan, October 2008

[7-17] A. M. Hadian and H. R. Hassani, "Wideband Rectangular Microstrip Patch Antenna with U-Slot," *2nd European Conf. Antennas and Propagation,*, Edinburgh, UK, November 2007

[7-18] D. Zayniyev, H. F. AbuTarboush, and D. Budimir, "Microstrip antenna diplexers for wireless communications," *39th European Microwave Conference,* Rome, Italy, September 2009

[7-19] M. C. Mukandatimana and T. A. Denidni, "A multi-resonator microstrip-fed patch antenna for broadband dual-band operation," *IEEE AP-S/URSI Int. Symp. Dig*., Monterey, USA, June 2004, pp. 4292- 4295

[7-20] D. Zayniyev and D. Budimir, "Integrated Microstrip Antenna Diplexers," *4th European Conf. Antennas and Propagation,* Barcelona, Spain, April 2010.

[7-21] D. Zayniyev and D. Budimir, "Dual-band Microstrip Antenna Filter for Wireless Communications," *IEEE AP-S/URSI Int. Symp. Dig.,* Toronto, Canada, July 2010 (accepted)

8. CONCLUSION AND FUTURE WORK

8.1. Introduction

Microstrip filters are extensively used in various RF/microwave applications. The explosive growth and commercial interest in wireless communications, especially in personal and mobile communication systems, significantly increased the demand for low cost, compact size, and high performance bandpass filters, which are the key components used to confine signals. The reduction of the size of the filters and the need of more stringent specifications, such as high selectivity and low insertion loss, is very important in the design of new bandpass filters.

The object of the thesis was to develop compact microstrip bandpass filters and diplexers with high performance, which are easy to design and cheap to manufacture. The aim was also to investigate the limits in the achievable filters' characteristics and to develop a simple design procedure of bandpass filters that can also be applied for the design of compact dual-band bandpass filters and bandpass filters with improved stopband. This chapter evaluates the importance of this work with regard to the development of advanced microstrip filters and their applications.

This chapter summarises the contribution made in this thesis and offers recommendations for future work.

8.2. Contributions of the Thesis

The following contribution has been made in this thesis:

- Development of very compact microstrip bandpass filters and diplexers with advanced characteristics. Preliminary analysis of coupled pseudo-interdigital resonators has been carried out. A simple design procedure of pseudo-interdigital bandpass filters based on the image parameter method and results from the analysis of coupled resonators have been developed. A compact diplexer composed of the developed filters using optimized common-transformer feeding has been designed.

- Implementation of SIR in the design of pseudo-interdigital bandpass filters for the development of compact dual-band bandpass filters and single-band bandpass filters with extended stopband. Employment of bandstop generating structures for further improvement of the stopband performance of single-band bandpass filters.

- Application of developed filters and diplexers in the design of integrated antenna filters and antenna diplexers. A single-band bandpass filter has been integrated with patch antenna for harmonics suppression. The integration of dual-band bandpass filter with dual-band antenna has been used to improve of the antennas response. Dual-band and multi-band patch antennas were integrated with diplexers to reduce the number of components and to separate the bands of antennas.

8.2.1. Development of Compact Microstrip Bandpass Filters and Diplexers

A compact pseudo-interdigital bandpass filter with a centre frequency of 3.8 GHz and FBW 25%, designed using pair of coupled pseudo-interdigital resonators, has been presented. Analysis of these resonators has been carried out using an impedance matrix model of the coupled lines and the EM simulators in order to derive approximate TZ conditions and to investigate the nature of coupling between resonators. It was shown that TZ frequencies depend mainly on the length of coupled lines and also is affected by the strength of the feeding and gaps between resonators. It has been found that coupling between the resonators due to the different spacing slots is opposite in sign and that adjusting these slots can produce a wide range of coupling coefficients .

The design procedure of pseudo-interdigital bandpass filters is based on the second order parallel-coupled transmission-line-resonator filters, designed by applying IPM to coupled microstrip lines. The application of this method allowed the incorporation of technological constraints and the design of filters using microstrip lines with the smallest realizable width. The second order parallel-coupled transmission-line-resonator filter has been transformed into hairpin-line bandpass filter and, subsequently, into a pseudo-interdigital bandpass filter using coupling coefficient design curves. Minor optimization of the filter has been used to achieve the best passband performance and selectivity, as well as good suppression of the second harmonic of the filter. The size of the designed filter is approximately $0.25\lambda_g \times 0.04\lambda_g$ that makes it very attractive for the design of diplexers and integrated antenna filters. Two pseudo-interdigital filters with passbands centered at 2.7 and 3.8 GHz were used in the design of compact microstrip diplexer with size $0.25\lambda_g \times 0.08\lambda_g$. The common feeding technique, based on the modified common-transformer diplexer, was used to combine filters in the diplexer without degrading the performance of the filters. Both filter and diplexer were fabricated and measured. The experimental results are in good agreement with the simulations.

8.2.2. Design of Stepped Impedance Pseudo-Interdigital Bandpass Filters

The implementation of SIR in pseudo-interdigital bandpass filters, in order to control spurious harmonics, has been explored. An SIR with impedance ratio $R > 1$ were applied in the design of dual-band bandpass filter, in which spurious harmonics were shifted closer to the fundamental passband and was used as a second passband. The impedance ratio $R = 2.27$ was used to build a dual-band bandpass filter with passbands centered at 2.03 GHz and 4.623 GHz. The size of the filter is $0.3\lambda_g \times 0.1\lambda_g$ where λ_g is the wavelength at the first band. The compact filter was fabricated and measured. The measurement results showed good agreement with simulations. The application of SIR dual-band bandpass filters in the design of compact microstrip three-port four-channel diplexer was demonstrated.

The SIR with impedance ratio $R < 1$ was used in the design of single-band bandpass filter with the stopband extended by shifting spurious harmonics to higher frequencies. In both these types of filters, employing SIR, control over the frequency of spurious harmonics is limited by difficulties in the realization of small and big impedance ratio. Therefore, for further improvement of the stopband of single-band bandpass filters, the structures generating stopbands centered at the frequencies of spurious harmonics were used. The spur-lines and open-circuited stubs were employed in the design of the bandpass filter with the stopband extended to $5.5f_0$. The compact bandpass filters with the stopband extended to $5.36f_0$ and $6.6f_0$ were designed using spiral shaped slots etched in the ground plane of microstrip under the feeding lines of filters.

8.2.3. Integration of Filters and Diplexer with Patch Antennas

The application of developed filters and diplexer in the design of integrated antenna filters and antenna diplexer was proposed. The single-band SIR pseudo-interdigital bandpass filter with extended stopband was integrated with the inset-fed patch antenna to suppress the first the second spurious harmonics of the antenna. The compactness was achieved by replacing the feeding line of the antenna by the filter. The integration of dual-band bandpass filter with dual-band antenna was used to improve the performance of the antenna.

To reduce the number of components in dual-band systems the integration of duplexers with dual-band and multiband patch antennas was proposed. In order to achieve the compact size of the whole structures feeding lines of antennas were replaced by diplexers. The common port of diplexers was connected to the antennas. Thus the physical separation of the high and low bands of the antennas with 20 dB isolation was achieved.

8.3. Suggestions for Future Work

In this dissertation, pseudo-interdigital resonators were used in the design of moderate bandwidth bandpass filters. These resonators can also be used in the design of wide and ultra wideband (UWB) filters. The coupling of pseudo-interdigital lines can be utilized, as part of a bigger circuit, for the generation of transmission zeros in order to improve the stopband performance and selectivity of filters.

In this work dual-band bandpass filters were designed using SIR. Control over the frequency of the second band is limited by the realizable impedance ratio. Dual-band filter with bands centered at any required frequencies can be designed by the parallel combination of two pseudo-interdigital bandpass filters which can be diplexed at both the input and output. This filter will be compact as single-band filters are very narrow, and the only challenge is to design compact optimized diplexing circuit which will preserve passband characteristics of both filters.

The application of bandpass filters in the design of diplexers was presented in this work. The design of triplexers, composed of three bandpass filters is worthy of further investigation. A diplexer with improved stopband can be developed using single-band bandpass filters with improved stopband.

In integrated antenna filters and antenna diplexers, presented in this dissertation, dual- or multiband antennas were used. In many practical applications broadband antennas are employed. Therefore, it is worth investigating the integration of dual-band filters and diplexers with broadband antennas for channel separation and size reduction.

PUBLICATIONS

[1] D. Zayniyev, D. Budimir, and G. Zouganelis, "Microstrip filters and diplexers for WiMAX applications," *IEEE AP-S/URSI Int. Symp. Dig*., June 2007, pp.1561-1564

[2] D. Draskovic, D. Zayniyev, and D. Budimir, "Microstrip patch antennas with harmonic rejection using composite right-left handed transmission lines," ," *IEEE AP-S/URSI Int. Symp. Dig*., June 2007, pp.365-368

[3] D. Zayniyev, D. Budimir, and G. Zouganelis, "Super Compact Microstrip Pseudo Interdigital Bandpass Filters," *11th Int. Symp. on Microwave and Optical Tech.,* Monte Porzio Catone, Italy, December 2007

[4] D. Zayniyev, D. Budimir, and G. Zouganelis, "Miniaturized microstrip filters and diplexers for wireless communication systems," *Microwave and Optical Technology Lett.*, vol. 50, no. 10, pp. 2701-2702, February 2008

[5] D. Zayniyev and D. Budimir, "Microstrip three-port 4-channel multiplexers using dual-band bandpass filters for wireless applications," *IEEE AP-S/URSI Int. Symp. Dig*., July 2008.

[6] D. Zayniyev and D. Budimir, "An integrated antenna-filter with harmonic rejection," 3rd *European Conf. Antennas and Propagation,* Berlin, Germany, March 2009, pp.393-394

[7] D. Zayniyev and D. Budimir, "Compact microstrip pseudo-interdigital stepped impedance bandpass filters with improved stopband performance," *IEEE Wireless and Microwave Technology Conf.,* April 2009

[8] D. Zayniyev and D. Budimir, "Compact microstrip dual-band pseudo-interdigital stepped impedance bandpass filters for wireless applications," *IEEE AP-S/URSI Int. Symp. Dig*., Charleston, USA, June 2009

[9] D. Zayniyev, H. F. AbuTarboush, and D. Budimir, "Microstrip antenna diplexers for wireless communications," *39th European Microwave Conference,* Rome, Italy, September 2009

[10] D. Zayniyev and D. Budimir, "Integrated Microstrip Antenna Diplexers, 4th *European Conf. Antennas and Propagation,* Barcelona, Spain, April 2010.

[11] D. Zayniyev and D. Budimir, "Dual-band Microstrip Antenna Filter for Wireless Communications," *IEEE AP-S/URSI Int. Symp. Dig.,* Toronto, Canada, July 2010 (accepted)